REPUBLIQUE ALGERIENNE DEMOCRATIQUE ET POPULAIRE
MINISTERE DE L'ENSEIGNEMENT SUPERIEUR ET DE LA RECHERCHE SCIENTIFIQUE
UNIVERSITE DE MEDEA



FACULTE DE TECHNOLOGIE

THESE DE DOCTORAT

Présentée en vue de l'obtention du diplôme de

Docteur en : Génie des procédés

Spécialité : Génie des matériaux

Présentée par : CHERIFI Leila

Thème

Modélisation fractionnaire des colmatages dans les membranes

Présentée devant le jury composé de :

Nom & Prénom	Grade	Institution d'affiliation	Désignation
RAHAL Sofiane	Professeur	Université de Médéa	Président
Yamina Ammi	Professeur	Université de Médéa	Directrice de thèse
ALOUAOUI Redha	MCA	Université de Médéa	Examinateur 1
ALI AGHA Hamza	MCA	Université de Médéa	Examinateur 2
HENINI Ghania	Professeur	Université de Chlef	Examinateur 3
HANINI Salah	Professeur retraité	Université de Médéa	Invité

Année académique : 2025/2026

PEOPLE'S DEMOCRATIC REPUBLIC OF ALGERIA
MINISTRY OF HIGHER EDUCATION AND SCIENTIFIC RESEARCH
UNIVERSITY YAHIA FARES OF MEDEA

FACULTY OF TECHNOLOGY

THESIS

To obtain the degree of

DOCTOR in: Process Engineering

Specialty: Materials Engineering

Presented by: Leila Cherifi

Thesis title

Fractional Modeling of Membrane Clogging

Defended in front of a jury composed of:

Last and first name	Grade	Institution of affiliation	Designation
RAHAL Sofiane	Professor	University of Medea	President
Yamina Ammi	Professor	University of Medea	Supervisor
ALOUAOUI Redha	MCA	University of Medea	Examiner 1
ALI AGHA Hamza	MCA	University of Medea	Examiner 2
HENINI Ghania	Professor	University of Chelf	Examiner 3
HANINI Salah	Professor Retired	University of Medea	Invited

Academic year: 2025/2026

Acknowledgments

First and foremost, all praise and gratitude are due to Allah for His countless blessings, for granting me the strength, patience, and perseverance to complete this work. To him I raise my thanks, for He is the One who facilitates all good and guides to the right path.

My heartfelt gratitude goes to my supervisor, **Professor HANINI Salah**, for his invaluable guidance, advice, and encouragement. His words, "I consider you like my daughter," will remain engraved in my memory, as they gave me great moral support during the most challenging times.

I also extend my sincere thanks to **Professor AMMI Yamina**, who was a beacon at the beginning of my path. She guided me with wisdom and confidence when I felt lost, and her encouragement had a profound impact on my academic journey.

I am deeply grateful to **Professor HARMAND Jérôme**, who opened new horizons for me and offered valuable opportunities for scientific and professional growth. My thanks also go to **Professor BENYAHIA Boumediène** for his generous support and assistance.

I would like to thank the Faculty Administration and all the administrative and academic staff for providing a motivating academic environment. Special appreciation goes to **Professor BOUAZIZ Mohamed Nadjib**, laboratory director, and to all the professors who have accompanied us since the beginning, contributing through their knowledge and dedication to our education and development.

I would like to thank **Professor. Sofiane Rahal** for presiding over the defense jury. I also wish to express my gratitude to **Dr. ALOUAOUI Redha**, **Dr. ALI AGHA Hamza**, and **Professor HENINI Ghania** for kindly agreeing to serve as members of the jury for this thesis and for taking the time to review this work. I am truly grateful to them.

Special thanks go to **Mr. Salah Zine** for his remarkable support and encouragement, which greatly impacted my journey. I also express my gratitude to **Dr. Dahmani**

Abdennasser, Dr. Hantabli Mohamed and, **Dr Bouzidi Amel** for their support and encouragement.

Dedication

I dedicate this thesis to my dear parents, the source of my strength and pride, for their continuous support, heartfelt encouragement, and prayers that surrounded me every step of the way. I also thank my brothers, sisters, **Asmaa** and her husband **Abd Elrahmane**, **Abdelhadi**, **Ezzeddine**, **Majid**, **Ahmed**, **Mariya**, **Rahim**, and my little one, **Njoud Asinat**, for their constant love, support, and encouragement throughout this journey.

Special thanks go to my uncle **Bouzid Tahri**, my grandparents, whose love and support have been a true pillar throughout my journey. I also extend my gratitude to my friends and colleagues who shared this journey with me through challenges, moments of joy, and hard work.

To everyone who supported, guided, contributed, or encouraged me, whether near or far, I say thank you from the bottom of my heart. I will never forget your kindness, and I pray that God rewards you all abundantly.

This thesis and I owe you all so much.

من جدّ وجد، ومن زرع حصد

Whoever strives, succeeds; whoever plants, reaps

الملخص: النمذجة الكسرية لانْسِداد الأغشية

تُعدّ تقنية الترشيح الغشائي من بين أهم التقنيات المستخدمة في معالجة المياه، والبيوتكنولوجيا، والعديد من التطبيقات الصناعية، نظرًا لكفاءتها العالية، وانتقائيتها، وطبيعتها الصديقة للبيئة. غير أن أداء هذه التقنية يتأثر سلبًا بسبب ظاهرة انسداد الأغشية، التي تؤدي إلى انخفاض تدفق الراشح، وزيادة استهلاك الطاقة، وارتفاع التكاليف التشغيلية. ومن ثَمّ، فإن النمذجة الدقيقة والتنبؤ الموثوق بالانسداد يمثلان خطوة أساسية لتحسين فعالية واستدامة عمليات الترشيح.

تتناول هذه الأطروحة هذه الإشكالية من خلال مساهمتين علميتين مكملتين تستندان إلى الحساب الكسري. تركز المساهمة الأولى على تطوير وتقييم ثمانية نماذج كسرية تجريبية لوصف تطور حجم الراشح تحت ظروف تشغيل مختلفة. تم استخدام منهجية تحسين هجينة تجمع بين خوارزمية اليعسوب والانحدار غير الخطي لتقدير معاملات النماذج. وقد أظهرت هذه النماذج أداءً تنبؤيًا ممتازًا، حيث تراوحت معاملات التحديد بين 0.9896 و0.9997 ، في حين تراوحت الأخطاء النسبية بين 0.86% و 2.95% وقد وفّرت هذه النماذج أدوات دقيقة ومرنة لمحاكاة ديناميكيات الترشيح، مع الإشارة إلى أن تحديد آليات الانسداد تم بطريقة غير مباشرة عبر تحليل إضافي باستخدام معادلة Hermia.

أما المساهمة الثانية، فقد تمثلت في اقتراح نموذج كسري تفاضلي عام (EDF) يُعدّ تقدماً كبيرًا مقارنة بالنماذج الكلاسيكية المعتمدة على Hermia. يعتمد النموذج على ثلاث معاملات (n, k, α) ويُوحّد بين الصيغ الكلاسيكية والكسريّة؛ إذ يتحول إلى صيغ Hermia عندما $\alpha = 1$ ، ويتوسع لتمثيل ديناميكيات أكثر تعقيدًا عندما $\alpha \neq 1$.وقد تم التحقق من النموذج نظريًا وتجريبيًا باستخدام ثلاث قواعد بيانات تمثل آليات انسداد مختلفة، حيث حقق دقة عالية (nRMSE بين 0.93% و1.73% ، ومعامل تحديد R^2 أكبر من 0.995). كما يُمكّن هذا النموذج من تحديد آلية الانسداد المسيطرة مباشرة في خطوة واحدة، متجاوزًا بذلك القيود الرئيسية للنماذج التقليدية.

تؤكد نتائج هذا العمل على قوة الحساب الكسري ومرونته في نمذجة ظاهرة انسداد الأغشية، من خلال الجمع بين الدقة التجريبية والفهم الآلي للظاهرة. كما يقدم هذا العمل أدوات رياضية جديدة تُسهم في تحسين تحليل الانسداد، وتحسين تشغيل عمليات الترشيح، وتطوير نظم ترشيح غشائي أكثر كفاءة. وتشمل آفاق البحث المستقبلية توسيع نموذج EDF لدراسة سلوكيات الانسداد غير العادية، والسوائل غير النيوتونية، والانسداد البيولوجي.

الكلمات المفتاحية : الترشيح الغشائي, الحساب الكسري , الانسداد، النمذجة التجريبية، خوارزمية اليعسوب، نموذج EDF, التحسين

Abstract: Fractional Modeling of Membrane clogging

Membrane filtration has become a key technology in water treatment, biotechnology, and various industrial applications, thanks to its efficiency, selectivity, and environmentally friendly operation. However, its performance is often limited by clogging, which leads to reduced permeate flux, higher energy consumption, and increased operational costs. Accurately modeling and predicting membrane clogging remain essential for improving the sustainability and efficiency of filtration processes.

This thesis addresses this challenge through two complementary contributions based on fractional calculus. The first contribution focuses on developing and evaluating eight empirical fractional models to describe the evolution of permeate volume under different operating conditions. A hybrid optimization approach combining the Dragonfly Algorithm with nonlinear regression (DA–nlinfit) was used to estimate model parameters. The models achieved excellent predictive performance, with determination coefficients ranging from 0.9896 to 0.9997 and relative errors between 0.86% and 2.95%. These models offer accurate and flexible tools for simulating filtration dynamics, although they do not directly identify clogging mechanisms, which were inferred through additional analysis using Hermia's equation.

The second contribution introduces a new general fractional differential model (EDF), which represents a significant advance over classical Hermia-based models. Defined by three parameters (n, k, α), the EDF model unifies classical and fractional formulations, reducing to Hermia's models when $\alpha = 1$ and extending them for $\alpha \neq 1$ to capture more complex dynamics. Validated theoretically and experimentally using three datasets representing different clogging mechanisms, the EDF model achieved superior accuracy (nRMSE between 0.93% and 1.73% and $R^2 > 0.995$) and allows the direct identification of the dominant clogging mechanism in a single step, overcoming the main limitations of classical approaches.

Overall, this work demonstrates the power and versatility of fractional calculus for modeling membrane clogging. It bridges the gap between empirical accuracy and mechanistic insight, providing new mathematical tools to improve clogging analysis, process optimization, and the development of more efficient membrane filtration systems. Future perspectives include extending the EDF model to abnormal clogging behaviors, non-Newtonian fluids, and biological fouling phenomena.

Keywords: Membrane filtration, clogging, fractional calculus, empirical modeling, Dragonfly Algorithm, EDF model, optimization

Résumé : Modélisation fractionnaire des colmatages dans les membranes

La filtration membranaire est devenue une technologie essentielle dans le traitement de l'eau, la biotechnologie et de nombreuses applications industrielles, grâce à son efficacité, sa sélectivité et son caractère respectueux de l'environnement. Cependant, ses performances sont souvent limitées par le colmatage, qui réduit le flux de perméat, augmente la consommation énergétique et les coûts opérationnels. Une modélisation et une prédiction précises du colmatage sont donc essentielles pour améliorer la durabilité et l'efficacité des procédés de filtration.

Ce travail de thèse aborde cette problématique à travers deux contributions complémentaires fondées sur le calcul fractionnaire. La première contribution est axée sur le développement et l'évaluation de huit modèles fractionnaires empiriques pour décrire l'évolution du volume de perméat dans différentes conditions opératoires. Une approche d'optimisation hybride combinant l'algorithme de la libellule (Dragonfly Algorithme) et la régression non linéaire (DA–nlinfit) a été utilisée pour estimer les paramètres des modèles. Ces modèles ont montré d'excellentes performances prédictives, avec des coefficients de détermination compris entre 0,9896 et 0,9997 et des erreurs relatives entre 0,86 % et 2,95 %. Ils constituent des outils précis et flexibles pour simuler la dynamique de la filtration, même s'ils n'identifient pas directement les mécanismes de colmatage, qui ont été déterminés par une analyse complémentaire à l'aide de l'équation d'Hermia.

La deuxième contribution introduit un nouveau modèle général fractionnaire différentiel (EDF), qui représente une avancée majeure par rapport aux modèles classiques basés sur Hermia. Défini par trois paramètres (n, k, α), ce modèle unifie les formulations classiques et fractionnaires, se réduisant aux modèles d'Hermia pour $\alpha = 1$ et s'étendant à des dynamiques plus complexes lorsque $\alpha \neq 1$. Validé théoriquement et expérimentalement sur trois bases de données représentant différents mécanismes de colmatage, le modèle EDF a démontré une précision supérieure (nRMSE entre 0,93 % et 1,73 % et $R^2 > 0,995$) et permet d'identifier directement le mécanisme dominant en une seule étape, surmontant ainsi les principales limites des approches classiques.

Dans l'ensemble, ce travail met en évidence la puissance et la flexibilité du calcul fractionnaire pour modéliser le colmatage des membranes. Il établit un lien entre précision empirique et compréhension mécanistique, en proposant de nouveaux outils mathématiques pour améliorer l'analyse du colmatage, l'optimisation des procédés et le développement de systèmes de filtration membranaire plus efficaces. Des perspectives futures incluent l'extension du modèle EDF aux comportements de colmatage anormaux, aux fluides non newtoniens et aux phénomènes de colmatage biologique.

Mots-clés : Filtration membranaire, colmatage, calcul fractionnaire, modélisation empirique, algorithme Dragonfly, modèle EDF, optimisation.

Graphical abstract

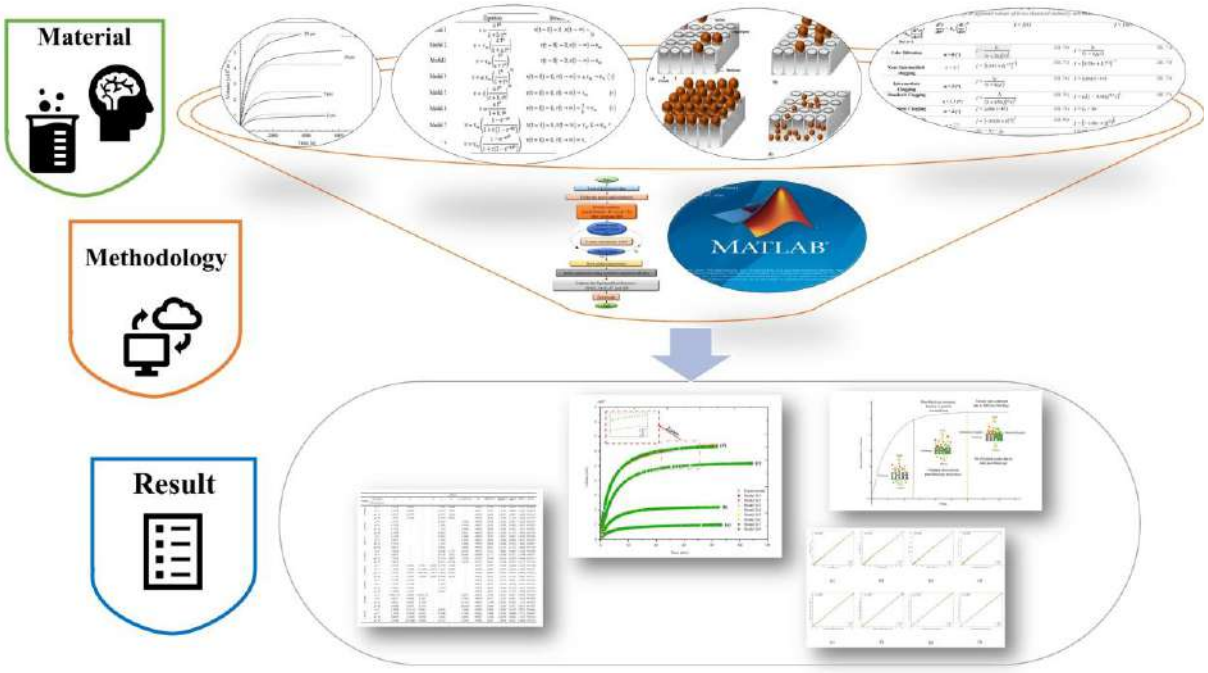


Table of contents

List of figures I
List of tables II
List of abbreviations III
Nomenclature III
General introduction 2
Chapiter I: 5
Literature review 5
Reader's guide 6
I.1. Membrane filtration and clogging phenomena 6
I.1.1. Membrane filtration 6
I.1.1.1. General background 6
I.1.1.2. Types of membrane filtration modes 8
I.1.1.2.1. Direct flow filtration (Frontal mode) 8
I.1.1.2.2. Parallel-flow filtration (Tangential mode) 9
I.1.2. The clogging phenomenon 11
I.1.2.1. Impacts of clogging 12
I.1.2.2. Clogging indicators: tools for monitoring membrane performance 12
I.1.2.3. Classification of clogging types 14
I.1.2.3.1. Based on the location of clogging 15
I.1.2.3.2. Based on the nature of clogging agents 16
I.1.2.3.3. Based on clogging reversibility 20
I.1.2.3.4. Based on type of interaction 21
I.1.2.4. Mechanisms of membrane clogging 23
I.1.2.4.1. Adsorption 23
I.1.2.4.2. Pore narrowing 24
I.1.2.4.3. Surface layer formation 25
I.1.2.5. Operational control and clogging prevention 26
I.2. Clogging modeling 28
I.2.1. Classical approaches to clogging mechanisms in membrane filtration 28
I.2.1.1. General background 28
I.2.1.2. Darcy 's law 28
I.2.1.3. Resistance in series model 29

I.2.1.4. Hermia's models 30
I.2.1.4.1. Complete clogging $n = 2$ 32
I.2.1.4.2. Standard clogging $n = 1.5$ 32
I.2.1.4.3. Intermediate clogging $n = 1$ 32
I.2.1.4.4. Cake filtration $n = 0$ 33
I.2.2. Limitation of classical models in membrane filtration clogging 35
I.2.3. Combined mechanisms in membrane fouling 36
I.3. Conclusion 39
Chapiter II: 40
Empirical fractional approaches for modeling membrane filtration clogging 40
Reader's guide 41
II.1. Materials and methods 41
II.1.1. Clogging of membrane filtration 41
II.1.2. The proposed empirical fractional estimation models 42
II.1.3. Building a database 44
II.1.4. Dragonfly algorithm coupled with nonlinear regression (DA_nlinfit) 46
II.1.5. Evaluation of the proposed models' performance 49
II.1.6. Parameter identifiability analysis 51
II.2. Results and discussion 51
II.2.1. Performance of the proposed model by statistical error analysis 51
II.2.2. Linear regression analysis of proposed model 55
II.2.3. Application of Hermia's model to clogging mechanisms 58
II.3. Conclusion 62
Chapiter III: 63
A new general fractional model for one-step calculation to identify membrane clogging mechanisms 63
Reader's guide 64
III.1. Background 64
III.2. Fractional approach to membrane clogging 66
III.3. Materials and methods 70
III.3.1. Fractional solution of the general clogging equation fractional order α with power n (where $n = n$) 70
III.3.2. Collection of the databases 76

III.3.3. Optimization algorithm 78
III.3.4. Evaluating the performance of proposed models 79
III.4. Results and discussion 81
III.4.1. Theoretical validation of the fractional model 81
III.4.1.1. Reduction to classical models (α = 1 Case) 81
III.4.2. Validation of the model using experimental data 83
III.4.2.1. Optimization of parameters (n, k, and α) for the general proposed clogging model (EDPO and EDF) 83
III.4.3. Comparison between the general EDF model and literature models 88
III.4.4. Summary of result 93
III.5. Conclusion 94
General conclusion and perspective 96
General conclusion 97
Perspective: 98
References 100
Annexes 110
Annex 1 111
Annex 2 117
Scientific production 126
Scientific production 127

List of figures

Figure I.1. 1: Classification of pressure-gradient-induced membrane separation processes, from GEA Process Engineering.... 8
Figure I.1. 2: Schematic representation of frontal filtration mode (Espinasse 2003) 9
Figure I.1. 3: Schematic representation of tangential filtration mode (Espinasse 2003) 11
Figure I.1. 4: Reverse Osmosis (RO) membrane before (A) and after (B) clogging. Adapted from Watertreatment Suppliers.... 12
Figure I.1. 5: Three types of clogging based on location.... 16
Figure I.1. 6: Organic clogging.... 17
Figure I.1. 7: Inorganic clogging 18
Figure I.1. 8: Biological clogging.... 19
Figure I.1. 9: Scanning electron microscopy (SEM) image of different fouling types: (a) organic fouling, (b) inorganic fouling, and (c) biofouling. Adapted from (Qrenawi and Abuhabib 2020).... 19
Figure I.1. 10: Schematic illustration of chemical fouling in a reverse osmosis (RO) membrane 22
Figure I.1. 11: Schematic representation of a deformed pore due to mechanical clogging 23
Figure I.1. 12: Schematic representation of clogging mechanisms in membrane filtration 26

Figure I.2. 1: Schematic representation of the four classical clogging mechanisms a) complete blocking, (b) intermediate blocking, (c) cake filtration, and (d) standard blocking 34

Figure II. 1: Procedure of the optimization algorithm (Dragonfly Algorithm Nonlinear Regression (DA_nlinfit)).... 49
Figure II. 2: Comparison between calculated and experimental volumes against time for eight models proposed at different pressures filtration of DB II. 1and DB II. 2.... 54
Figure II. 3: Regression plot comparison of the calculated vs. experimental volume values for eight models proposed at different pressures filtration: (a) P=2psi, (b) P=5psi, (c) P=10 psi and (d) P= 20 psi for DB II. 1 and (e) P=5 psi (pQR150), (f) P=8 psi (pQR150), (g) P=5 psi (pGEc47) and (h) P=5 psi (pGEc47) for DB II. 2.... 57
Figure II. 4: nRMSE plot comparison of the proposed models for different pressures and solutions.... 58

Figure III. 1: Structure of the DA coupled with nlinfit Optimization Algorithm.... 79
Figure III. 2: Regression plots comparing the calculated and experimental values using the proposed EDF and EDPO models under different clogging mechanisms, pressures, and solutions: for DB III. 1 (a–c), three tests with n = 0 at 1.5×10^5, 3.0×10^5, and 4.5×10^5 Pa; for DB III. 2 (d), test with n = 1 at $P = 2.76 \times 10^4$ Pa; and for DB II. 2 with n = 1.5: (e) $P = 3.447 \times 10^4$ Pa (pQR150), (f) $P = 5.516 \times 10^4$ Pa (pQR150), (g) $P = 3.447 \times 10^4$ Pa (pGEc47), and (h) $P = 5.516 \times 10^4$ Pa (pGEc47) 86
Figure III. 3: Evaluation results of EDF and model of reference using scale-dependent metrics. (A) Evaluation results using nRMSE. (B) Evaluation results using MAPE. 92

List of tables

Table I.1. 1: Summary of common strategies for membrane clogging prevention, mitigation, and cleaning 27

Table I.2. 1: Expressions of series resistance reported in the literature 29
Table I.2. 2 : Summary of classical membrane clogging models based on permeate volume over time under constant pressure 35
Table I.2. 3: Summary of combined membrane clogging models and corresponding mechanisms 38

Table II. 1: Statical analysis of the database variable (DB II. 1and DB II. 2) 46
Table II. 2: Validation result of the proposed empirical fractional estimation models for membrane filtration clogging at different pressures for database DB II. 1 52
Table II. 3: Validation result of the proposed empirical fractional estimation models for membrane filtration clogging at different pressures for database DB II. 2 53
Table II. 4: Linear regression vectors [Linear Equation:$\boldsymbol{y_{i,cal} = \alpha y_{i,exp} + \beta}$] and the performances of empirical fractional estimation models (R, R^2, and nRMSE). 57
Table II. 5: Equations of Model (II. 6), its derivatives, ... 59
Table II. 6: Adjustments parameters (a, b, and m) of model (II. 6), the clogging index (n), clogging constant (k), and coefficient of determination (R). 60
Table II. 7: Results of the comparative analysis of model accuracy 60

Table III. 1: Some useful Laplace transforms 70
Table III. 2: Proposed new fractional models EDF (n, k, α) for different values of n from Equation (I.2. 13) at constant pressure (cases of $\boldsymbol{v = f(t)}$ and $\boldsymbol{t = f(v)}$) 72
Table III. 3: Proposed new fractional models EDF (n, k, α) for different values of n from Equation (I.2. 13) at constant pressure ($\boldsymbol{cases\ of\ J = f(t)\ and\ J = f(v)}$) 74
Table III. 4: Summary of experimental data for different clogging mechanisms in membrane filtration 77
Table III. 5: Statistical analysis of experimental data 78
Table III. 6: Results of the first validation of the proposed new fractional sub-models $\boldsymbol{(n, k, \alpha)}$ for $\boldsymbol{\alpha = 1}$, $\boldsymbol{(v = f(t);\ v = f(v))}$, at different values of n via classical ordinary sub-models 82
Table III. 7: Results of the first validation of the proposed new fractional sub-models $\boldsymbol{(n, k, \alpha)}$ for $\boldsymbol{\alpha = 1}$, $\boldsymbol{(J = f(t);\ J = f(v))}$, at different values of n via classical ordinary sub-models 82
Table III. 8: Optimized values of $\boldsymbol{n}$, $\boldsymbol{k}$, and $\boldsymbol{\alpha}$ for different clogging types tested with the normal (EDPO) and fractional (EDF) models whit linear fitting parameters 86
Table III. 9: Reference model equations 88
Table III. 10: Comparative evaluation of the proposed fractional EDF model and literature-based clogging models 90

List of abbreviations

Abbreviation	Definition
Adj-R^2	Adjusted Coefficient of Determination
BSA	Bovine Serum Albumin
DA	Dragonfly Algorithm
EDF	Fractional Differential Equation
EDO	Ordinary Differential Equation
EDPO	Ordinary Partial Differential Equation
FI	Fouling Index
IgG	Immunoglobulin G (Human Plasma)
MF	Microfiltration
MFI	Modified Fouling Index
nChi	Normalized Chi-square Statistic
NF	Nanofiltration
nMAE	Normalized Mean Absolute Error
nRMSE	Normalized Root Mean Squared Error
PAN	Polyacrylonitrile
R	Coefficient of correlation
R^2	Coefficient of Determination
RO	Reverse Osmosis
SBR	Sequencing Batch Reactor
SDI	Silt Density Index
SEP	Standard Error of Prediction
SSR	Sum of Squares of Residuals
UF	Ultrafiltration
VAF	Variance Accounted For

Nomenclature

Latin symbols	Definition
A	Active membrane area (m^2)
a, b	Constants (units depend on specific equation)
A_0	Initial porous membrane surface area (m^2)
C	Particle concentration ($kg \cdot m^{-3}$)
J	Volumetric flux ($L \cdot m^{-2} \cdot h^{-1}$ or $m^3 \cdot m^{-2} \cdot s^{-1}$)
J_0	Initial permeate flux ($m \cdot s^{-1}$)
k, k_c, k_b, k_i, k_s, k_{ic}	Clogging constants (units depend on mechanism, e.g. m^{-1}, s^{-1}, $s \cdot m^{-2}$)
K_A	Membrane surface blocked per unit filtrate volume (m^2/m^3)
K_B	Pore cross-sectional area reduction per unit filtrate volume (m^{-1})
K_c	Resistance constant for complete pore blocking (m^{-1})
K_D	Cake layer area per unit permeates volume (m^{-1})
K_{gl}	Constant related to R_m, R_g, and KD ($s \cdot m^{-2}$)
L_p	Membrane permeability ($m \cdot s^{-1} \cdot Pa^{-1}$)
n	Clogging mechanism index (dimensionless)
P_c	Pressure at the concentrate (retentate) outlet (Pa)
P_f	Pressure at the feed inlet (Pa)
P_p	Pressure at the permeate (filtrate) outlet (Pa)
R_{a1}	Weakly adsorbed resistance (m^{-1})
R_{a2}	Irreversibly adsorbed resistance (m^{-1})

R_c	Cake resistance (m^{-1})
R_{cp}	Concentration polarization resistance (m^{-1})
R_{DS}	Cake layer formation resistance (m^{-1})
R_{ex}	External resistance due to cake layer (m^{-1})
R_f	Additional resistances due to fouling (m^{-1})
R_F	Resistance for other fouling phenomena (m^{-1})
R_g	Gel layer resistance (m^{-1})
R_h	Hydraulic resistance of membrane (m^{-1})
R_{in}	Internal resistance due to pore blockage (m^{-1})
R_{irrev}	Irreversible resistance (m^{-1})
R_m	Membrane resistance (m^{-1})
R_{rev}	Reversible resistance (m^{-1})
T	Elapsed time between measurements (s)
t_i, t_f	Initial and final times to collect a given volume (s)
TMP	Transmembrane Pressure (Pa or bar)
v	Permeate or cumulative filtrate volume (m^3)
v_∞	Asymptotic cumulative volume (m^3)
$\mathcal{D}^{\alpha}t$	Fractional derivative operator
Greek symbols	**Definition**
α	Fractional order of the derivative (dimensionless)
Γ (Gamma)	Gamma function (mathematical operator in fractional calculus)
μ	Water viscosity (Pa·s)

General introduction

General introduction

Membrane separation processes have become increasingly important in modern industry and environmental management due to their efficiency, selectivity, and wide-ranging applications in various fields. Ultrafiltration (UF), microfiltration (MF), nanofiltration (NF), and reverse osmosis (RO) systems are used extensively in water treatment, food processing, biotechnology, and the pharmaceutical industry. Between them, ultrafiltration and microfiltration seem to be particularly significant in the clarification, purification, and concentration of complex solutions consisting of macromolecules, colloids, and particles. Their advantages include low energy consumption, operating under mild conditions, and the ability to avoid chemical additives, which make them attractive alternatives to conventional methods of separation (Alborzi et al. 2022; Zydney and Ho 2002).

The challenge, however, for membrane processes is clogging (or fouling). The gradual accumulation of suspended particles, colloids, macromolecules, or biological material on or inside the membrane reduces the flow rate of permeate and negatively affects the performance over time. Clogging may take many forms, such as porous membrane blocking, intermediate deposition, or the formation of a cake layer, and these mechanisms can occur either sequentially or concurrently. The result is a shorter membrane lifetime, higher operating costs, and frequent cleaning or replacement of the membrane. For this reason, clogging is still considered one of the main obstacles to wider industrial utilization of membrane processes (Hermia 1985; C. C. Ho and Zydney 2000).

At the same time, understanding and predicting clogging behavior has been central to practice in membrane science. Original models, such as those first proposed by (Hermans and Bredée 1935) and later generalized by (Hermia 1982, 1985), provide empirical descriptions of flux decline under constant pressure. Hermia's framework characterizes filtration as consisting of four main mechanisms: complete pore blocking, intermediate pore blocking, standard blocking, and cake filtration. These models continue to be widely used, although they are limited by the assumption of a single mechanism, which is common because more realistic clogging (e.g., real filtration processes) represents a transition between several mechanisms. In order to overcome these constraints, later studies have introduced combined models and variants that

allow for simultaneous or sequential mechanisms (Mondal and De 2010). However, these models remain constrained by classical integer-order formulations.

In recent years, fractional calculus has emerged as a promising tool for modeling complex physical processes. Fractional derivatives, which generalize differentiation and integration to non-integer orders, can describe memory effects and long-term dependencies in a wide variety of systems, such as viscoelasticity, anomalous diffusion, and biological dynamics (Atangana and Owolabi 2017; Podlubny 1999). Fractional differential equations extend classical models and offer a richer framework to capture such dynamics. Although fractional calculus has been applied in many scientific and engineering fields, its use in membrane filtration remains very limited (Giusti et al. 2020; Abouda 2024).

This thesis builds on this research gap and develops two complementary approaches to improve the modeling and understanding of membrane clogging.

The first approach proposes a set of empirical fractional models designed to represent the accumulation of filtrate volume as a function of time under different operating conditions. These models, optimized using statistical criteria, demonstrate strong performance in capturing the dynamics of volume accumulation. However, they do not directly identify the specific clogging mechanisms. Their contribution lies in providing accurate empirical tools to describe the evolution of filtration behavior with improved flexibility compared to classical empirical models.

The second approach introduces and validates a general fractional model (EDF) derived from fractional calculus, which can determine the clogging mechanisms in a single step. This formulation integrates the fractional order α alongside parameters n and k, enabling a unified framework capable of reproducing classical Hermia models when $\alpha = 1$, while also extending them to capture more complex clogging dynamics when $\alpha \neq 1$. This approach provides greater flexibility and robustness, allowing for both theoretical validation (reduction to classical cases) and experimental validation using literature databases under different operating conditions. The methodology integrates the Dragonfly Algorithm (DA) with nonlinear regression (nlinfit) to achieve stable and accurate parameter estimation, and the model's performance is evaluated using multiple statistical indicators (R^2, Adj-R^2, RMSE, MAE, nRMSE, and MAPE).

The thesis is organized as follows. The first chapter reviews the theoretical foundations of membrane filtration, clogging phenomena, their types and mechanisms, and modeling approaches, with a focus on Hermia's models and their modifications (classical approach their limitation, and combined model). The second chapter presents the first contribution, namely the empirical fractional models for accumulative volume, along with their optimization, evaluation, and analytical analysis to identify the underlying mechanisms. The results are compared with literature models, and the chapter concludes with the main findings and perspectives for future work. The third chapter presents the second contribution, the fractional differential equation (EDF) general model with parameter n, and its sub-models for specific cases (n = 0, 1, 1.5, 2), which correspond to the classical mechanisms identified by Hermia (cake filtration, intermediate clogging, standard clogging, and complete clogging, respectively). In addition, the cases n = 0.5 and n = 2.5 are introduced as new approaches, referred to as Near-Intermediate Clogging and Standard Clogging (second type), respectively. This chapter also describes the databases used for validation and the methodology applied. The validation was carried out in two stages: first, by showing that when α = 1, the EDF reduces to the classical Hermia models; and second, by testing the model against literature databases, where it demonstrated strong predictive performance. Finally, the chapter compares the EDF model with existing models, and concludes with the main findings and perspectives for future work. The thesis closes with a general conclusion that synthesizes the main findings, highlights the advantages of fractional modeling approaches, and outlines perspectives for future research, particularly the extension of EDF to abnormal clogging, non-Newtonian fluids, and biological fouling phenomena.

Through these two approaches, the thesis contributes to bridging the gap between fractional calculus and membrane filtration science, by providing new models that enhance the predictive capacity of clogging analysis and by offering a robust framework for both theoretical research and industrial applications.

Chapiter I:
Literature review

Reader's guide

The first chapter includes a literature review organized as follows: in the first section, the filtration membrane and clogging phenomenon are discussed, covering their effects, indicators, classification of clogging, and mechanisms. The second section focuses on clogging modeling, presenting first the classical models, their limitations, and a literature review about the combined model for membrane filtration, and then we conclude with the necessity of developing new and hybrid modeling approaches that better capture the complexity of membrane clogging. This conclusion sets the foundation for the following chapters, where we present our contributions to improved modeling frameworks.

I.1. Membrane filtration and clogging phenomena

I.1.1. Membrane filtration

I.1.1.1. General background

Membranes and membrane technology were initially classified as analytical tools for chemical and biological assays in laboratories; however, they have rapidly evolved into industrial technologies and products with significant technical and commercial impact (Uragami 2017). Today, membrane technology is widely used in industrial applications and is generally categorized into three main types: membrane filtration, gas separation and pervaporation, and dialysis and electrodialysis (Collet 2013; Rouquié 2018; Uragami 2017). The differences depend on the membranes used and the driving force applied, such as pressure, concentration, and electrical potential (Charfi 2014). Membrane filtration is a highly evolved separation process that uses a selective method for separating substances in a fluid. This selective barrier, called a membrane, enables membrane filtration to partition a species based on molecular size, solubility, charge, or pressure sensitivity. A membrane provides a physical barrier (removal of the particular substance) and also grants selectivity (removal of unwanted substances). Water and a few dissolved substances pass by the membrane, but suspended solids, bacteria, and macromolecules cannot pass through the membrane (Bacchin 2005; Collet 2013; Romdhane 2014).

Typically, the separation is accomplished using a semi-permeable membrane. A semi-permeable membrane allows passage of some smaller molecules, while excluding the passage of larger molecules, depending on the size and character of the molecule. Separation using membrane usually relies on applied pressure on one side of the membrane, and allowing the fluid

in the separating membrane to pass through the tiny pores in the membrane (Bacchin 2005; Collet 2013).

The solution that passes through the membrane is called the permeate, and the liquid retained is called the retentate or concentrate (Collet 2013).

Membrane filtration is widely used for the treatment of water and wastewater (Bacchin 2005; Collet 2013; Emmanuel et al. 2024; Ounifi et al. 2022), processing of food and beverages (Castro-Muñoz et al. 2022), production of pharmaceuticals (Hentabli et al. 2021; de Morais Coutinho et al. 2009), and various biotechnology applications, to produce accurate and efficient separations without the application of heat and/or direct chemicals (Mehrabi and Vatanpour 2024), membrane reactors (Emmanuel et al. 2024). We can classify the membrane filtration into four types according to the pore size and separation capacity (Romdhane 2014). There are:

- Microfiltration (MF): Particle removal of suspended solids, as well as the removal of bacteria
- Ultrafiltration (UF): Removal of viruses, proteins, and colloids
- Nanofiltration (NF): Removal of small organic molecules and divalent ions
- Reverse Osmosis (RO): Removal of salts and pretty much everything else that is dissolved

Each of these methods brings an important contribution depending on its application and the fluid being treated. The classification of membrane filtration is shown in Figure I.1. 1.

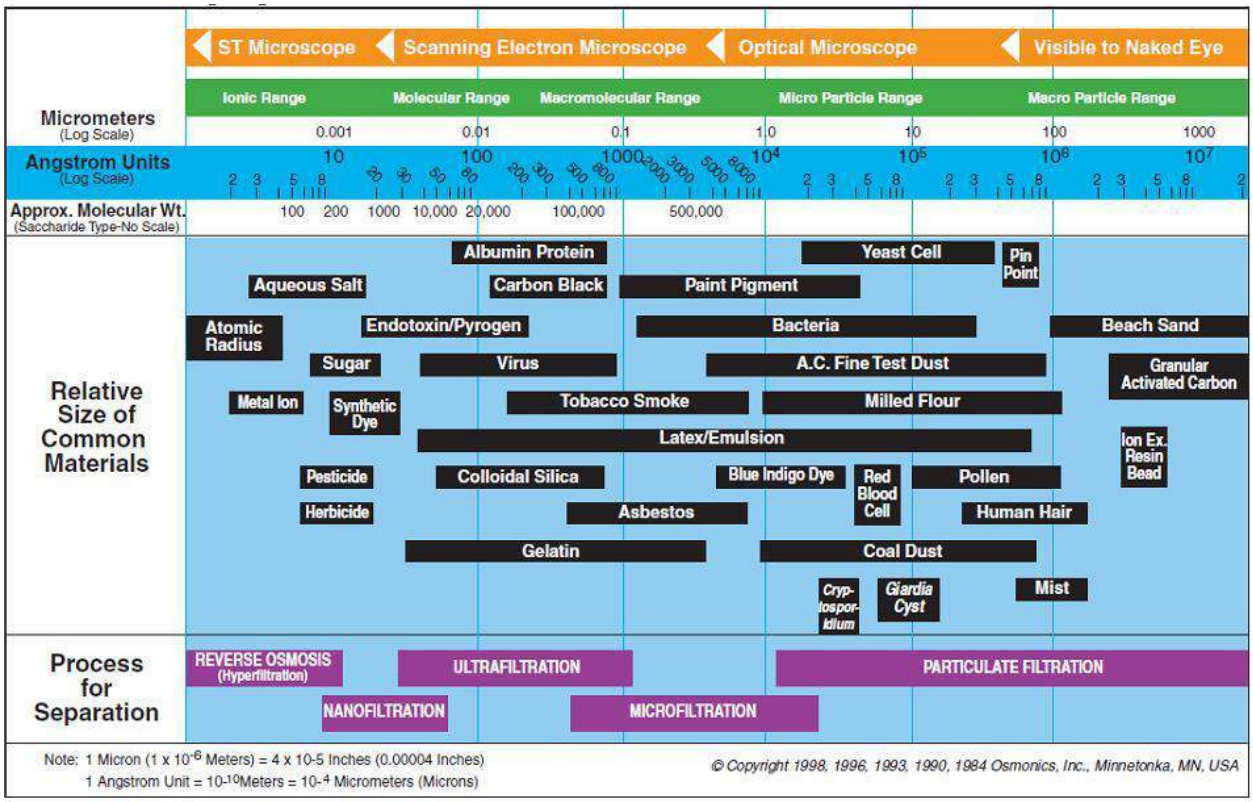


Figure I.1. 1: Classification of pressure-gradient-induced membrane separation processes, from (Romdhane 2014).

I.1.1.2. Types of membrane filtration modes

I.1.1.2.1. Direct flow filtration (Frontal mode)

Direct flow filtration also known as dead-end filtration is a membrane filtration configuration in which the feed fluid is introduced directly and perpendicularly to the membrane. The design of a direct flow filtration configuration allows the entire liquid volume to be pushed through the membrane under the effect of the pressure gradient, which also retains particles (organic, inorganic, or biological) from the feed solution so that over time a layer of retained material or an accumulated residue develops on the separation interface, leading to an increase in filtration resistance and a corresponding decrease in permeate flux. Because there is no crossflow or retentate circulation through the membrane, the system never reaches steady state, and clogging of the membrane surface is inevitable unless rinsing or stopping filtration is a

frequent step in the process. Dead-end filtration has been described as a simple, low-cost method in terms of process and energy. It is particularly appropriate in some applications, such as drinking water treatment or sterilization processes, for low-turbidity fluids, as the response to an increase in clogging after initial foulant characteristics can be poor. In addition, dead-end filtration is not efficient in processing highly loaded or fouling fluids, as clogging of the membrane will be rapid and require driving forces that will not be met without frequent operator intervention (Benavente 2016; Bessiere 2005; Charfi 2014; Espinasse 2003; Habibi 2014; Michel Jaffrin 2015; Morgane 2017; Romdhane 2014; Sophie 2024; Touffet 2014). The frontal filtration mode, as shown in Figure I.1. 2, is characterized by a perpendicular feed flow through the membrane.

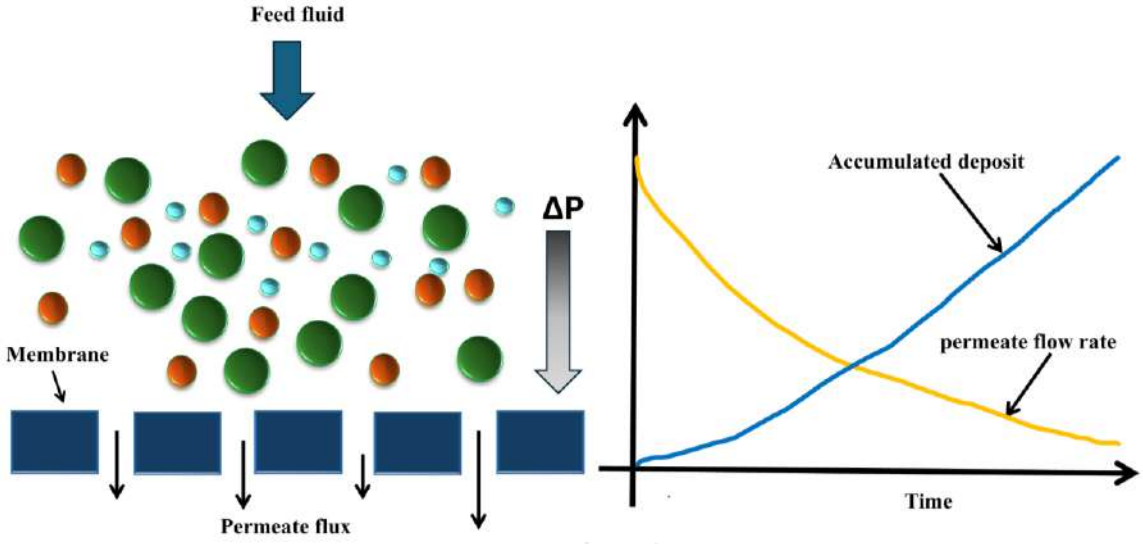


Figure I.1. 2: Schematic representation of frontal filtration mode (Espinasse 2003).

I.1.1.2.2. Parallel-flow filtration (Tangential mode)

Parallel-flow filtration or crossflow is a type of membrane filtration where the feed fluid runs parallel to or across the separation interface, instead of perpendicular to it. When set up in this manner, the feed is separated into two streams: permeate that travels through the membrane, and retentate, which travels along the membrane surface. Tangential flow has the advantage of shear stress from being tangential, which limits particle accumulation and lessens membrane fouling potential.

In comparison to frontal filtration systems, tangential systems have more components and are more complicated and will often require additional auxiliary equipment, such as recirculation pumps. However, tangential systems provide exceptional stability while operational stability maximizes membrane service life, especially if filtering fluids that heavily foul or have high particle loads. When the retentate continuously moves/liquid moves across the membrane surface in the flow path, this reduces the accumulation of a dense cake layer. This enables the system to reach a more stable quasi-steady state condition in terms of the filtration flux over time.

Crossflow filtration is well established with industrial applications in wastewater treatment, biotechnology, and food processing (e.g., dairy concentration) where the feed contains high concentrations of suspended solids. Energy consumption is higher, but longer filtration cycles or reduced cleaning frequency will often outweigh energy costs on demanding processes where crossflow filtration is desired. Many systems are designed to alternate between dead-end filtration and a crossflow configuration, depending on water quality or filtration objectives (Benavente 2016; Espinasse 2003; Habibi 2014; Michel Jaffrin 2015; Morgane 2017; Sophie 2024; Touffet 2014). The tangential mode of filtration, as shown in Figure I.1. 3, is characterized by a feed stream parallel to the membrane surface, combined with a transmembrane pressure that causes permeation.

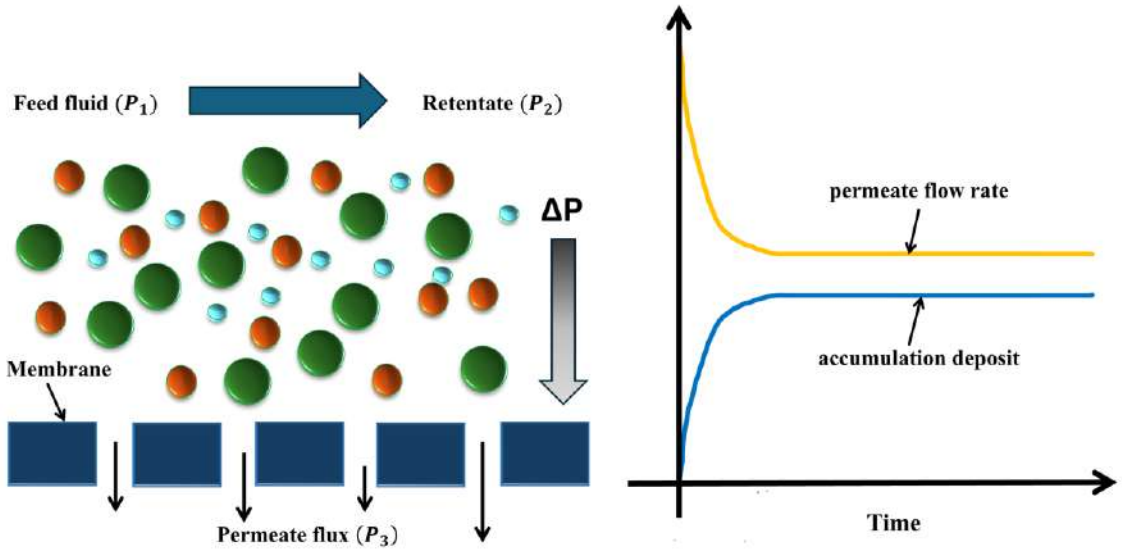
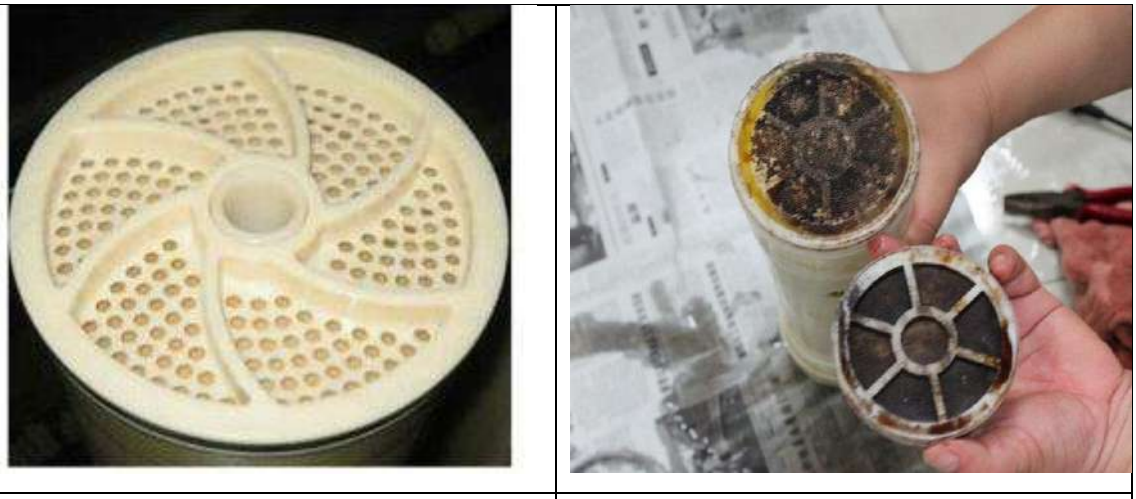


Figure I.1. 3: Schematic representation of tangential filtration mode (Espinasse 2003).

I.1.2. The clogging phenomenon

Membrane filtration is playing an increasingly important role. However, this process faces a number of operational limitations, not least clogging, a frequent problem in many production plants (Romdhane 2014). This phenomenon considerably limits the performance of membrane filtration units. Clogging is when particles, solutes, or microorganisms accumulate on the surface or in the pores of a membrane over time due to filtration, and this accumulation reduces permeability. Generally, clogging results in a decrease of permeate flow, an increase of transmembrane pressure (TMP), or a decrease of separation quality (Kalboussi 2018) . Clogging has been the subject of extensive research into clogging modeling, indicators, and mechanisms. Figure I.1. 4 shows clearly the difference between a clean reverse osmosis (RO) membrane and one affected by clogging.



(A) (B)

Figure I.1. 4: Reverse Osmosis (RO) membrane before (A) and after (B) clogging. Adapted from Water Treatment Suppliers (2023).

I.1.2.1. Impacts of clogging

The effects of clogging on membrane operation are severe and multi-faceted, as discussed below. Clogging has a profound negative impact on filtration system costs and performance. Serious loss of permeate flux takes place, and therefore, very little filtered water can be produced, and it is generally required to increase the pressure, which has implications for energy requirements. Clogging also results in unplanned system shutdowns (in cases where systems are designed for membrane cleaning) and, therefore, a loss in productivity. For instance, in membrane bioreactors, clogging can result in greater energy demand due to the energy required for air injection. In the long term, clogging damages membranes and has cost consequences and decreases lifespan. In any case, clogging hurts performance and energy requirements, incurs additional costs, and can cause a system to be decommissioned if an appropriate solution cannot be found (Abdelrasoul, Doan, and Lohi 2013; Alsawaftah et al. 2021; Fortunato, Lipnizki, and Dumée 2021; Hee-deung, N-soung, and Kwang-jin 2015; Kalboussi 2018; Morgane 2017).

I.1.2.2. Clogging indicators: tools for monitoring membrane performance

Clogging indicators are a crucial part of assessing membrane performance and problematic fouling issues in filtration systems. Clogging indicators are used to help operators quantify fouling occurrence, tailored cleaning processes and are used to maximize long term efficiency.

One of the most popular operational indicators that is used is transmembrane pressure (*TMP*), which is the difference in pressure between the feed side and the permeate side of a membrane (Habibi 2014; Kalboussi 2018). It is calculated as Equation (I.1. 1):

$$TMP = \frac{P_f + P_c}{2} - P_p \quad \text{(I.1. 1)}$$

P_f =Pressure at the feed inlet [Pa]

P_c= Pressure at the concentrate (retentate) outlet [Pa]

P_p=Pressure at the permeate (filtrate) outlet [Pa]

Continuous increases in transmembrane pressure (TMP) with time at set flow rate are a clear signal of clogging. A declining permeate flux at set TMP is indicative of the continued presence of fouling in the membrane system (Kalboussi 2018).

Measurement of TMP is fairly simple and provides real time data, however; TMP as an indicator is limited because it does not differentiate between different types of fouling or report fouling prior to the occurrence of clogging (Kalboussi 2018).

Besides TMP and flux, a good measure is the permeability of membranes, or L_p $[m.s^{-1}.Pa^{-1}]$ as determined by the ratio of permeate flux (J) to TMP (Kalboussi 2018; Romdhane 2014): The mathematical expression of L_p, as shown in Equation (I.1. 2):

$$L_p = \frac{J}{PTM} \quad \text{(I.1. 2)}$$

A decrease in L_p over time provides a reliable indication that membrane resistance, due to fouling, is increasing (Kalboussi 2018; Romdhane 2014).

To address this issue, several indicators have been developed to evaluate clogging for specific operational functions—many focusing on reverse osmosis (RO) and nanofiltration (NF). The silt density index (SDI) is one of the most common clogging indicators and is widely used to evaluate particulate clogging in RO, as it is based on filtration through a 0.45 µm membrane. Another tool is the fouling index (FI), which can be applied when particle size and membrane porosity conditions are met. For finer particulates and colloids posing a clogging threat, indicators such as modified fouling index MFI or MFI-UF provide a more comprehensive

evaluation, whit the latter being particularly suited for ultrafiltration systems due to its improved accuracy and sensitivity. However, they do provide more clarity and understanding of clogging potential (Alsawaftah et al. 2021; Collet 2013). Consequently, the SDI can be calculated using Equation (I.1. 3):

$$SDI = \frac{1 - \frac{t_i}{t_f}}{T} . 100 \quad \text{(I.1. 3)}$$

Where t_i and t_f are the initial and final times required for the collection of a specific volume *V*, and *T* is the elapsed time between measurements. An SDI value of up to 5 is generally acceptable, although a value below 3 is preferable (Alsawaftah et al. 2021).

The modified fouling index (MFI), also referred to as $(MFI_{0.45})$, quantifies the ease with which particulate and colloidal matter in water or feed solution can obstruct a membrane under constant pressure conditions. It is based on the physical principles of cake filtration and provides a corrected formulation. The equation gives a linear relationship between the index and the particle concentration in the tested sample and is expressed as follows: (Alsawaftah et al. 2021).

$$MFI = \frac{\mu \, \alpha \, C}{2 \, \Delta P \, A^2} \quad \text{(I.1. 4)}$$

Where: μ is the water viscosity, α the specific cake resistance, C the particle concentration, ΔP the transmembrane pressure, and A the active membrane area.

I.1.2.3. Classification of clogging types

Clogging in membrane filtration processes is a complex phenomenon. It occurs either on the membrane surface or within it due to the influence of several factors, including membrane properties such as composition, porosity, permeability, hydrophilicity, and surface roughness, or even hydrodynamic operating conditions such as flow velocity, transmembrane pressure, and temperature. It is also affected by physicochemical characteristics such as ionic strength and solute concentration. Therefore, understanding these factors is essential for classifying the types of clogging and identifying its mechanisms. Based on previous studies, we have classified

clogging types according to different criteria, such as the location of deposition, the nature of the foulant, the reversibility of clogging, or its origin.

I.1.2.3.1. Based on the location of clogging

This category focuses on where clogging occurs in the filtration membrane.

a) Concentration polarization

Concentration polarization is a physical phenomenon that occurs in pressure-driven membrane processes when rejected fluid or particles accumulate on the membrane surface as a result of convective transport (Bessiere 2005; Kalboussi 2018). This results in a layer with solute concentrations that are greater than those of the bulk solution. At relatively low concentrations, particles or solutes may remain dispersed if there are repulsive forces or the interactions are not strong enough. At higher concentrations, they may interact with one another, or with the surface of the membrane, and a more structured deposit (i.e., a cake layer) may form. Some of these deposits are reversible, i.e., they may be removed by increasing the hydrodynamic force of the feed solution, while some can only be removed by chemical cleaning (Bacchin 2005; Bessiere 2005; Collet 2013; Günther 2009; Kalboussi 2018; Sophie 2024; Touffet 2014). While concentration polarization is not technically a clogging type, it is a precursor or enabler to additional forms of clogging that may occur in membrane processes like scaling, organic catching, or biofouling.

b) Clogging by surface fouling

Clogging by surface fouling, also known as surface deposition or external fouling, is a type of membrane clogging when the feed fluid being treated retains and builds up particles, colloids, or macromolecules directly on the membrane surface, creating a layer referred to as the cake layer. This builds up hydraulic resistance during operation, causing a decline in permeate flux. The deposited layer can change in composition and may consist of organic material, colloidal particles, microbial cells, or a combination of all three. Surface fouling can be reversible, where the deposit is removed via physical cleaning or the system is backwashed, or irreversible, requiring chemical cleaning, to enable the membrane to return to its original performance. The degree of external clogging depends on various factors, including feed water quality, membrane characteristics, transmembrane pressure, and crossflow velocity (Bessiere 2005; Hee-deung, N-soung, and Kwang-jin 2015; Kalboussi 2018; Morgane 2017).

c) Clogging by pore fouling

Internal fouling, also known as pore clogging, is a kind of clogging in filtration processes. As the name suggests, this type of clogging occurs when particles, large particles, or colloids penetrate into the pores and block them completely or partially, which leads to a reduction in permeability flow. This type of clogging is considered more difficult to remove compared to external clogging, as it often requires intensive chemical cleaning or membrane replacement. Internal clogging is common in microfiltration and ultrafiltration processes, especially when treating water or liquids that contain high levels of fine suspended matter, colloids, or biopolymers (Bessiere 2005; Hee-deung, N-soung, and Kwang-jin 2015; Kalboussi 2018; Morgane 2017).

The Figure I.1. 5, illustrates the three types of clogging based on location (concentration polarization, surface fouling, and pore fouling).

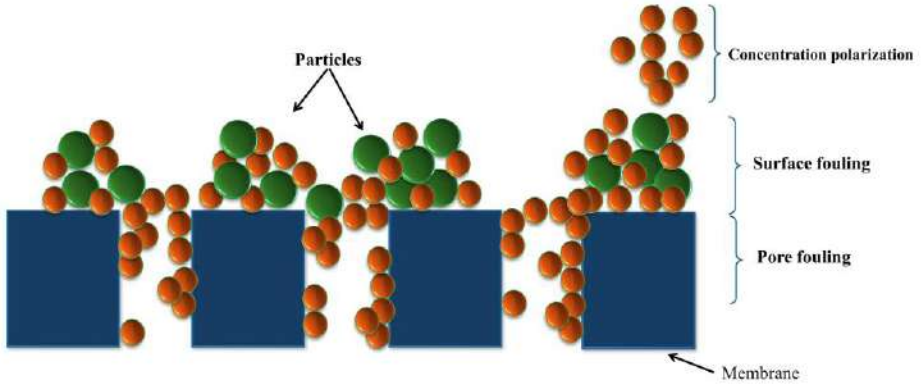


Figure I.1. 5: Three types of clogging based on location.

I.1.2.3.2. Based on the nature of clogging agents

This type classifies clogging according to the chemical or biological properties of the substances causing it.

a) Organic clogging

Organic clogging happens when organic substance(s)—in solution or colloidal form—deposit or accumulate on the surface of the membrane, or within its pores. Typical organic

foulants include proteins, polysaccharides, humic and fulvic acids, nucleic acids, lipids, and amino acids. Such materials may come from natural organic matter (NOM), algal organic matter, or soluble microbial products (SMPs). Additionally, synthetic organic materials produced by industries or generated through water disinfection may be referred to as responsible parties associated with clogging events. Organic matter may accumulate via adsorption and/or form gel layers or react with metal ions to form complex deposits, reducing the membrane's efficiency. The impact of organic foulants is dependent on water chemistry, the properties of the membrane, operational conditions, and the interactions of the foulant; removal can be challenging even with sophisticated pretreatment (Alsawaftah et al. 2021; Guo, Ngo, and Li 2012; Kalboussi 2018; Wang et al. 2014). The Figure I.1. 6, as shown the organic clogging.

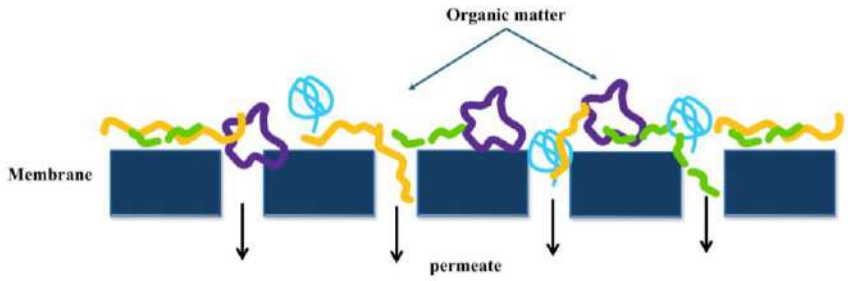


Figure I.1. 6: Organic clogging.

b) Inorganic clogging (Scaling)

Inorganic clogging (scaling), also called mineral clogging, is the formation of mineral deposits or inorganic compounds with low solubility or present in high concentrations in the feed fluid on the membrane surface or inside the pores of a salt-rejecting membrane system such as those used for NF, RO, leading to their crystallization, such as hydroxides, sulfates, carbonates, calcium, magnesium, iron, phosphates, silicic acids, and silica. This type of clogging can happen in water treatment processes (Alsawaftah et al. 2021; Sim et al. 2018; Wang et al. 2014). The inorganic clogging as schematized in Figure I.1. 7.

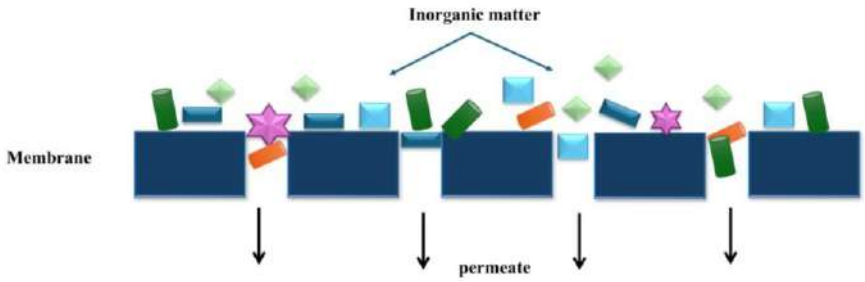


Figure I.1. 7: Inorganic clogging.

c) Biological clogging

Biological clogging, or biofouling, occurs when microorganisms settle on the membrane surface and begin to grow, forming what is known as a biofilm. Some researchers indicate that biofouling can also result from the adsorption of organic substances produced by microorganisms, such as soluble microbial products (SMP) and extracellular polymeric substances (EPS) (Malaeb et al. 2013). When , other researchers, such as Wang (Wang et al. 2014), classify the clogging caused by SMP and EPS as organic clogging .

The biofilm is considered one of the oldest and most resilient forms of life on Earth, owing to its robust structure, which results from the ability of microorganisms to develop layers of polymer-like substances (EPS) that protect them from toxic compounds and biocides (Al-Juboori and Yusaf 2012; Guo, Ngo, and Li 2012; Mafirad et al. 2011).

Moreover, microorganisms within the biofilm matrix can obtain the nutrients necessary for survival by adsorbing organic or inorganic substances from the surrounding environment. as illustrated in Figure I.1. 8.

In Figure I.1. 9, which shows scanning electron microscopy (SEM) image of different fouling types: (a) organic fouling, (b) inorganic fouling, and (c) biofouling. Adapted from (Qrenawi and Abuhabib 2020).

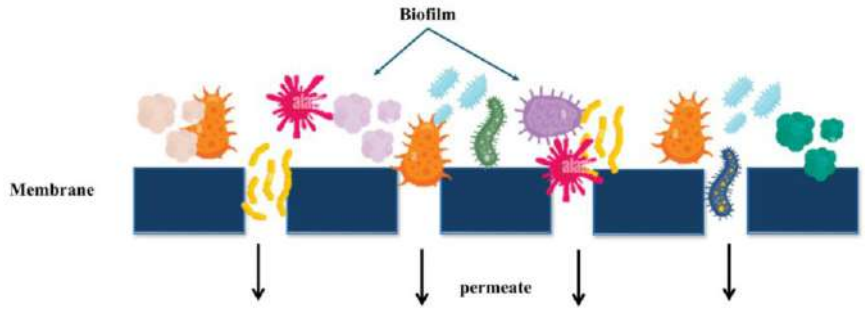


Figure I.1. 8: Biological clogging.

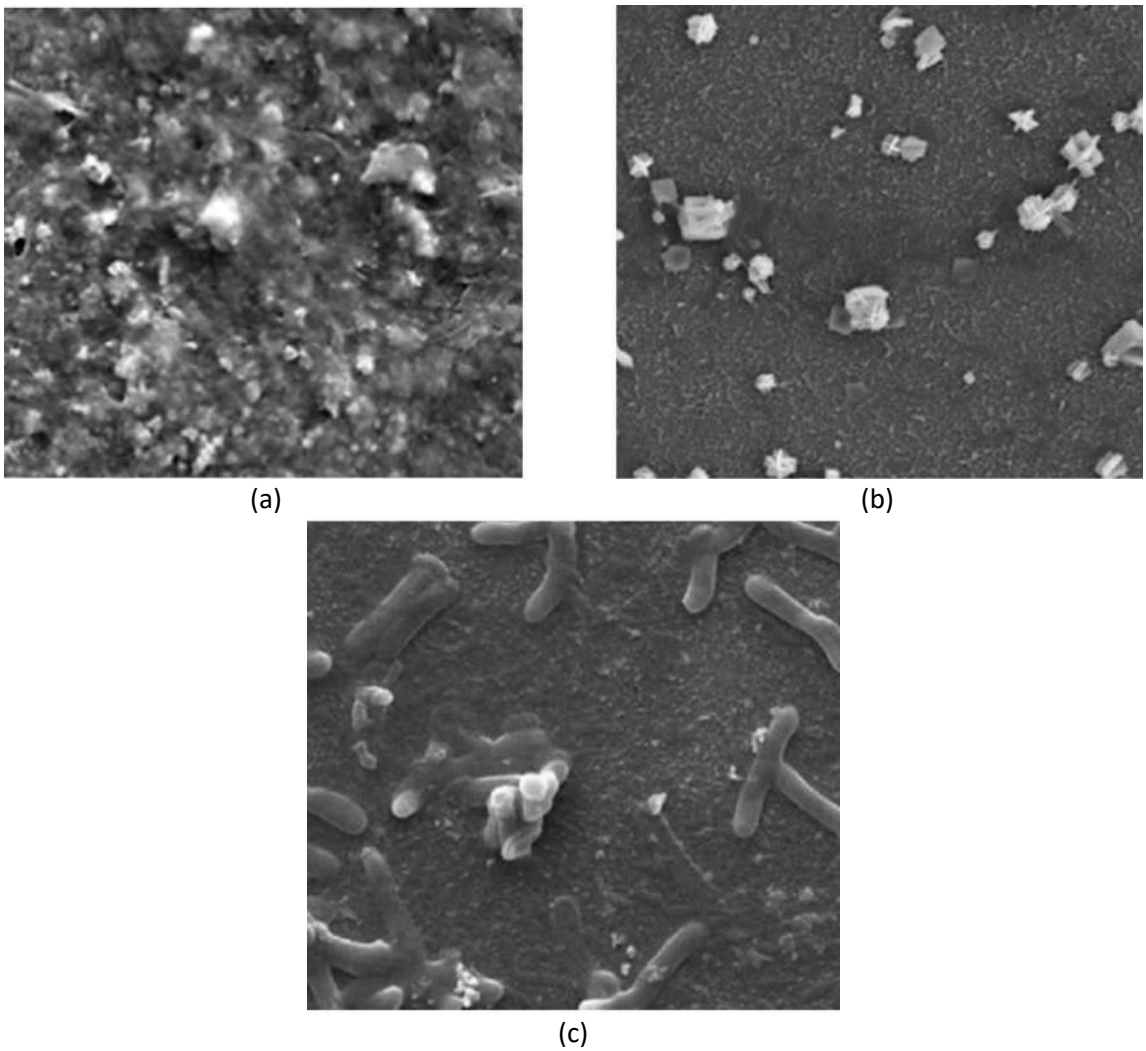


Figure I.1. 9: Scanning electron microscopy (SEM) image of different fouling types: (a) organic fouling, (b) inorganic fouling, and (c) biofouling. Adapted from (Qrenawi and Abuhabib 2020).

I.1.2.3.3. Based on clogging reversibility

This type is determined by whether clogging can be easily removed (reversible) or is difficult to eliminate (irreversible).

a) Reversible clogging

Reversible clogging refers to a situation in which particles or solutes are deposited on the membrane surface or at the opening to the pores of the membrane and can be removed by relatively simple means. Reversible clogging is primarily driven by weak physical interactions, such as loosely deposited suspended solids, weak adsorption forces, or a weakly compacted cake layer adjacent to the membrane. The cleaning methods used to remove this type of clogging are typically physical methods (backwashing, hydraulic flushing, air scouring, or just rinsing) and often result in almost complete recovery of the original membrane permeability with little chemical use. Reversible clogging normally occurs early in the filtration process or under moderate operating conditions, where the foulant–membrane interaction is weak and not permanent (Benyahia 2020; Kalboussi 2018; Rouquié 2018; Sophie 2024; Touffet 2014).

b) Irreversible clogging

Irreversible clogging is characterized by foulants establishing a strong interaction with the membrane surface, reaching deeply into its pore structure. In reversible clogging, the membrane can be cleaned and reused; however, irreversible clogging is based on strong and/or stable interactions and cannot be cleaned by simple physical cleaning. Strong adhesion mechanisms include hydrogen bonding, hydrophobic interaction, electrostatic attraction, and the development of biofilms. To remove an irreversibly clogged membrane, cleaning agents, such as acids, bases, oxidants, or detergents, will be used to break these strong, stable bonds and are generally effective at partially restoring the membrane's performance; however, achieving full original permeability is not always possible. Irreversible clogging is considered more important since it consistently accumulates and is also detrimental in reducing membrane performance and useful life and increasing cost (operational expense). It usually develops after prolonged operation, particularly under high transmembrane pressures, elevated foulant concentrations, or in the presence of sticky organic and biological matter(Benyahia 2020; Kalboussi 2018; Rouquié 2018; Sophie 2024; Touffet 2014).

c) Irrecoverable clogging

Irrecoverable clogging or permanent clogging is the most serious category of membrane deterioration. In this case, the foulants irreversibly adhere, resulting in structural damage and

irreversible modification to the membrane's inherent properties, such as pore collapsing, pore deformation, and chemical changes to the membrane's surface. At this point, neither physical cleaning methods nor chemical cleaning will restore the original performance; it is now considered permanently damaged, with only membrane replacement as a viable solution. Irrecoverable clogging is typically the result of prolonged exposure to extreme operating conditions, accumulation of irreversible foulants that were insufficiently controlled, or aggressive chemical cleaning that alters the membrane material itself.

I.1.2.3.4. Based on type of interaction

Clogging can also be classified according to the type of interaction between foulants and the membrane material (Morgane 2017). Within this framework. Each category is governed by different mechanisms and requires specific cleaning or control strategies, as discussed below.

a) Physical clogging

Physical clogging is the result of deposition of suspended solids or colloids onto the membrane surface or into the membrane pores. This type of clogging is typically associated with feedwater properties (particle size, concentration, nature of particle size distribution) and operational conditions (transmembrane pressure, flow velocity) (Habibi 2014). Since these deposits are usually weakly attached, they can often be removed through simple physical cleaning methods. For this reason, physical clogging is generally considered reversible.

Example: Once it has been initially separated in the ultrafiltration of surface water, natural colloids (e.g., clay particles and silica) allowed to separate at the membrane surface have the potential to develop, causing a cake layer to form. This layer can often be removed by backwash (or air sill scouring, if provided to slots in the membrane).

b) Chemical clogging

Chemical clogging happens when membrane materials undergo chemical reactions that cause changes in their structure, surface charge, or both. Often, this occurs through oxidation-reduction reactions or by precipitating onto the membrane surface due to the combination of operating conditions and constituent concentrations. This type of chemical clogging is considered irreversible by physical methods but can potentially be reversed through chemical cleaning.

Scaling is common in reverse osmosis desalination when low concentrations of extraction cause the formation of precipitated, poorly soluble salts like calcium carbonate, calcium sulfate, or barium sulfate. Simple methods cannot remove this clogging, which typically creates a dense, compacted layer on the membrane surface. Chemical cleaning with acidic or anti-scaling agents is usually necessary. Figure I.1. 10, illustrates an example from wastewater treatment using reverse osmosis (RO), showing how chemical clogging occurs through particle and molecule deposition that blocks the membrane pores.

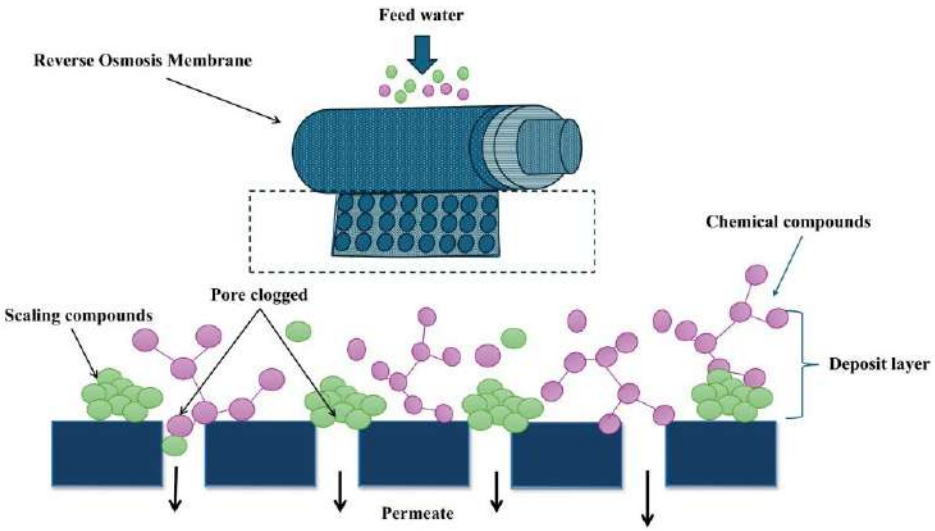


Figure I.1. 10: Schematic illustration of chemical fouling in a reverse osmosis (RO) membrane.

c) Mechanical clogging

Mechanical clogging is the result of big debris, particles, or fibers compressing or clogging the membrane surfaces (Bacchin 2005), deforming or compacting the membrane layers. This reduces the effective flow path for liquid flow and, unlike the other types of clogging, tends to inflict irreversible damage. While cleaning operations can remove deposited debris, they cannot reverse structural deformation of the membrane material. Mechanical clogging intensity is very much a function of treatment system operation and design, and in particular, how well the pretreatment units, such as coarse screens, sedimentation, or cartridge filters, operate as a primary barrier before the water reaches the membrane, are operating.

In wastewater treatment applications of hollow fiber membranes, fibrous material such as hair, textile fibers, or cellulosic residue tends to entrap and compress against the membrane

surface. Entanglement and compression reduce permeability and may cause localized, irreversible membrane damage.

Illustration of pore deformation in the membrane structure caused by mechanical clogging in Figure I.1. 11.

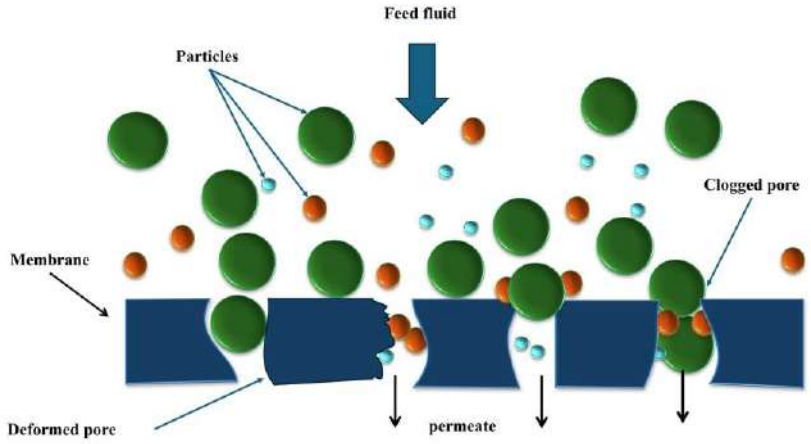


Figure I.1. 11: Schematic representation of a deformed pore due to mechanical clogging.

I.1.2.4. Mechanisms of membrane clogging

To understand how each type of clogging affects membrane performance, it is necessary to identify the chemical and physical mechanisms through which clogging occurs. Clogging may result from one or more mechanisms. In this part, the classifications proposed in previous studies have been compiled, including adsorption, pore narrowing, and surface layer formation. These mechanisms represent the fundamental processes that govern the onset and development of membrane clogging.

I.1.2.4.1. Adsorption

In membrane processes, adsorption occurs when solute molecules from a fluid phase adhere to the surface or within the pore structure of a membrane. This interaction can happen under a variety of conditions due to a range of physicochemical forces sustaining interactions, including van der Waals forces, electrostatic attraction, hydrogen bonding, or hydrophobic interactions between the membrane material and the solute constituents in suspension. Unlike other clogging mechanisms that also require flow or permeation to facilitate further solute attachment, adsorption can begin once a suspension is introduced to a membrane surface. The overall effect of adsorption is a slow and continuous narrowing of the pore channels and

additional hydraulic resistance created by the adsorbed layer, reducing permeate flux and filtration efficiency. In some cases, adsorption will be partially reversible via physical or chemical cleaning, though extended exposure may result in some of the adsorbed layer being rendered permanent (Benyahia 2020; Bessiere 2005; Günther 2009; Habibi 2014; Monnot 2015; Rouquié 2018; Touffet 2014).

One highly specific and particularly crucial form of adsorption is macromolecular adsorption, which is performed by large molecules such as proteins (Bacchin 2005), polysaccharides, and synthetic polymers. Large molecules like these typically possess complex conformations and various functional groups that strongly interact with the membrane surface. Under such circumstances, macromolecular adsorption typically occurs not only on the surface of the membrane but also in the interior pore structure, leading not only to considerable structural changes but also, at times, to complete blockage of the pores. On adsorption, proteins can alter their conformation upon adsorption, and this results in a denser adsorbed layer, and desorption becomes more difficult, while polysaccharides or extracellular polymers formed due to microbial metabolism can precipitate as gelatinous masses. Owing to their volume and strength of interactions, macromolecules are one of the most important contributors to irreversible clogging and, therefore, in general require site-specific chemical cleaning techniques.

I.1.2.4.2. Pore narrowing

Clogging by pore narrowing occurs as suspended particles or macromolecules partially gain entry and deposit themselves into membrane pores. in pore narrowing, the pore diameter decreases progressively, whereas in clogging, pores close off completely. Progressive constriction of pore diameters occurs throughout the duration of filtration, resulting in decreased permeability and selectivity. Pore narrowing is an important clogging mechanism in ultrafiltration because the size of the membrane pores is similar in size to the suspended particles; thus, pore narrowing in high concentrations can significantly reduce pore diameters. While pore narrowing is not as common as surface deposition, it is an important clogging mechanism because it changes the intrinsic structure of the membrane and can be more difficult to back-purge than other clogging mechanisms (De Bruijn, Salazar, and Bórquez 2005; Hee-deung, N-soung, and Kwang-jin 2015).

I.1.2.4.3. Surface layer formation

One of the most important membranes clogging mechanisms is the formation of a surface layer. A surface layer can form when suspended particles, colloidal or polymeric material, accumulate at or close to the surface of the membrane, rather than passing through pores. This mechanism is uncommon in conventional processes that use a grit chamber and clarifiers, but can be observed at large-scale membrane installations when treating water from rivers, lakes, or industrial effluents. Upon initial deposit, the surface layer would appear to be heterogeneous, thin, and relatively non-resistant to hydraulic flow until it thickens through continued filtration, which creates greater hydraulic resistance and ultimately decreases the permeate flux through the membrane. The surface layer formed may be easily removed by backwashing or cleaning operations if it is loose and amorphous; however, in some moments and whilst interstitial space and other physicochemical forces are weakly bonded through deposition of material, it will be possible to develop a cohesive mass that would be bound to the membrane and require higher flow rates or chemicals to remove it. The formation of surface layers by suspended solids or colloids in water treatments by ultra- and microfiltration is a relatively common clogging mechanism. The layer will act as an added barrier against passing contaminants, but will also affect the long-term effectiveness of the membrane (Cirillo, Tomaiuolo, and Guido 2021).

The Figure I.1. 12, shows the main clogging mechanisms in membrane filtration: adsorption, pore narrowing, and surface layer formation.

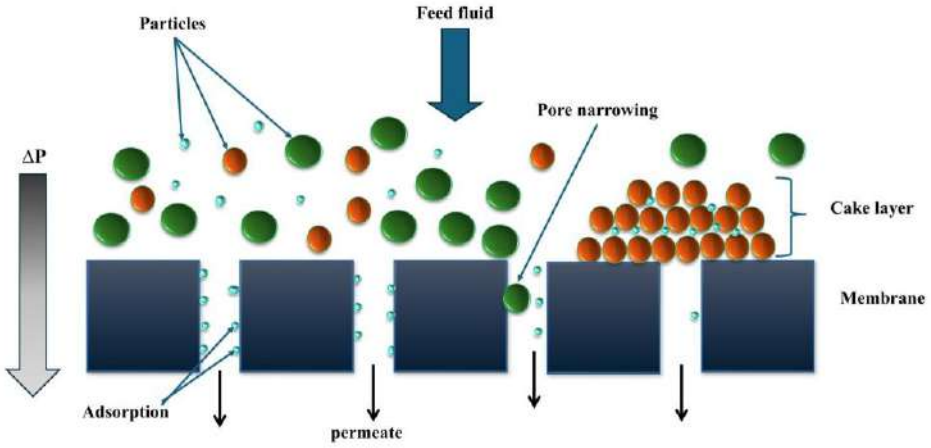


Figure I.1. 12: Schematic representation of clogging mechanisms in membrane filtration.

I.1.2.5. Operational control and clogging prevention

In the field of membrane filtration, several strategies are employed to prevent, mitigate, or remove clogging. These include adjusting operating conditions (e.g., reducing surface flux and transmembrane pressure, TMP), applying feed pretreatment (such as sedimentation, coagulation, or flocculation) (Abdelrasoul, Doan, and Lohi 2013), and implementing periodic cleaning techniques (backwashing, chemical cleaning-in-place, CIP). Table I.1. 1, summarizes these approaches.

Table I.1. 1: Summary of common strategies for membrane clogging prevention, mitigation, and cleaning.

Technique	Category	Underlying Principle	Application / Advantages	Limitations / Remarks
Pretreatment (sedimentation / coagulation / filtration)	Prevention	Removal or modification of suspended matter prior to membrane entry	Efficient in reducing particle load and delaying clogging onset	Requires additional infrastructure and operational costs
Crossflow operation	Mitigation	Tangential flow removes deposited matter on membrane surface	Limits cake layer formation and surface clogging	Higher energy demand
Flux / TMP regulation	Mitigation	Operating at sub-critical flux to minimize particle deposition	Simple and cost-effective clogging control strategy	May reduce short-term productivity
Backwashing	Physical cleaning	Reversing flow direction to detach accumulated particles	Rapid and effective for loosely attached deposits	Ineffective against strongly adhered layers
Air scouring	Physical cleaning	Shear forces from air bubbles dislodge surface deposits	Particularly effective for tubular or hollow-fiber membranes	Limited applicability to certain configurations
Chemical cleaning (CIP)	Chemical cleaning	Application of caustic/acidic agents to dissolve foulants	Essential for irreversible clogging and biofilm removal	Frequent use shortens membrane lifespan and increases costs
Biological control / biofilm management	Prevention/Cleaning	Environmental or chemical strategies to inhibit biofilm growth	Important in raw water rich in organic matter	May require biocides or system adjustments
Membrane surface modification (hydrophilicity / coating)	Prevention	Engineering membranes to resist adhesion and clogging	Enhances clogging resistance and operational longevity	Higher cost of advanced membranes
Pre-coating / controlled cake layer	Prevention/Control	Formation of a protective pre-layer or use of pre-filters	Effective in specific industrial applications	Adds hydraulic resistance; requires optimization
Process monitoring and automation (sensors, TMP tracking)	Prevention/Diagnosis	Real-time tracking of clogging indicators for proactive interventions	Improves system reliability and maintenance scheduling	Increased complexity and capital investment

Despite the wide range of techniques available to reduce or eliminate clogging—such as backwashing, chemical cleaning, or operating condition control—their effectiveness is often limited or temporary. Moreover, they may lead to increased operating costs or a reduction in membrane lifespan. In this context, mathematical modeling emerges as a complementary tool, enabling an accurate description of clogging mechanisms, the prediction of flux decline over time, and the identification of optimal operating conditions or the appropriate timing for cleaning interventions.

I.2. Clogging modeling

I.2.1. Classical approaches to clogging mechanisms in membrane filtration

I.2.1.1. General background

It is essential to distinguish between the physical and chemical mechanisms of clogging and the mathematical models. The mechanisms refer to the actual phenomena that lead to membrane clogging, such as adsorption, pore narrowing, and the formation of a surface layer. These mechanisms explain how clogging occurs at the material level and within the porous structure of the membrane. In contrast, mathematical models were developed to express the increase in hydraulic resistance, which represents the cumulative effect of the underlying physical and chemical mechanisms, or to describe and simplify the behavior of flux decline (i.e. is the practical indicator of clogging, since resistance growth reduces permeate flux) resulting from these mechanisms. The theoretical description has gradually evolved over more than a century, beginning with Darcy's fundamental law and later developed and adapted by several researchers who introduced mathematical models of clogging mechanisms as well as the concept of resistance.

I.2.1.2. Darcy 's law

The fundamental law of flow in porous media proposed by Henry Darcy (1856) is regarded as the theoretical basis of filtration. Darcy's law was derived from Darcy's field studies of groundwater flow, and he found an empirical relationship between volumetric flux, pressure, and hydraulic resistance. More specifically, he showed that volumetric flux through a porous medium is directly proportional to the applied pressure gradient and inversely proportional to hydraulic resistance. This empirical correlation between flow and pressure, came to be known as Darcy's law. The law proposed by Darcy provided the basis of nearly all subsequent models of filtration and membrane clogging because it provides the necessary mathematical framework to relate pressure, viscosity, and resistance to flow behavior.

Darcy's law can be mathematically expressed as Equation (I.2. 1) (Piry et al. 2012; Rayess 2023; Romdhane 2014).

$$J = \frac{\Delta P}{\mu R_h} \qquad \text{(I.2. 1)}$$

Where J is the volumetric flux $(L.m^{-2}.h^{-1})$, ΔP is the pressure difference across the medium (Pa), μ is the fluid viscosity $(Pa.s)$, and R_h is the hydraulic resistance of the membrane (m^{-1}).

I.2.1.3. Resistance in series model

The resistance-in-series model is one of the fundamental models used to describe clogging in membrane filtration processes. It assumes that the flow of the solution through the membrane, before clogging occurs, characterized by the intrinsic membrane resistance (R_m, m^{-1}), is directly proportional to the applied pressure, as previously explained in Darcy's law (I.2. 1). However, when clogging occurs, it is assumed that additional resistances (R_f, m^{-1}) are formed by clogging, hindering the passage of the liquid, such as the formation of a cake layer on the membrane surface or pore blocking. These resistances are therefore represented as hydraulic resistances and are added together, in the same way as electrical resistances connected in series. Consequently, Darcy's law takes the following form Equation (I.2. *2*).

$$J = \frac{\Delta P}{\mu(R_m + R_f)} \quad \text{(I.2. 2)}$$

Several studies have proposed different definitions of resistance hydraulic total $(R_t = R_m + R_f)$, depending on the type of clogging phenomenon considered. For example, some researchers include only the intrinsic membrane resistance and cake resistance, while others also account for pore blocking, adsorption, or concentration polarization. Table I.2. 1. summarizes the main approaches found in the literature for defining resistance hydraulic total (R_t, m^{-1}).

Table I.2. 1: Expressions of series resistance reported in the literature.

Resistance-in-series equations (for R_t)	Reference
$\boldsymbol{R_t = R_m + R_c}$	(Morgane 2017)
$\boldsymbol{R_t = R_m + R_{in} + R_{ex}}$	(Romdhane 2014)
$\boldsymbol{R_t = R_m + R_{irrev} + R_{rev}}$	(Rayess 2023)
$\boldsymbol{R_t = R_m + R_{cp} + R_g + R_{a1} + R_{a2}}$	(Cho, Amy, and Pellegrino 1999)
$\boldsymbol{R_t = R_m + R_c + R_{block} + R_{irrev}}$	(Broeckmann et al. 2006)
$\boldsymbol{R_t = R_m + R_{DS} + R_F}$	(Ludwig et al. 2012)

(Morgane 2017), reported that the intrinsic resistance of the membrane depends on its structural properties, such as thickness and pore size. In addition, suspended solutes can be retained within the pores and accumulate on the membrane surface, thereby hindering the liquid

flow through the membrane and altering its resistance. Therefore, in the resistance-in-series model, this resistance is represented as cake resistance (R_c, m^{-1}), A more detailed formulation was later adopted by (Romdhane 2014), in which the total resistance is expressed as the sum of the intrinsic membrane resistance (R_m, m^{-1}), the internal resistance due to pore blockage (R_{in}, m^{-1}), and the external resistance associated with cake layer formation (R_{ex}, m^{-1}). As highlighted by (Rayess 2023) , subsequent developments in clogging models express the formed resistance (R_f) as the sum of reversible (R_{rev}, m^{-1}) and irreversible (R_{irrev}, m^{-1}) contributions.

(Cho, Amy, and Pellegrino 1999) , investigated the filtration of water containing natural organic foulants using different types of membranes. The resistance-in-series model was used to interpret the flux decline, where the total resistance was considered as the sum of several components: the clean membrane resistance (R_m, m^{-1}), concentration polarization resistance (R_{cp}, m^{-1}), gel layer resistance (R_g, m^{-1}), and adsorption resistances (both weakly (R_{a1}, m^{-1}) and irreversibly adsorbed (R_{a2}, m^{-1})).

(Broeckmann et al. 2006) modeled formed fouling resistance (R_f) as the sum of cake layer (R_c, m^{-1}), pore blocking (R_{block}, m^{-1}), and irreversible resistances (R_{irrev}, m^{-1}), incorporating adhesion forces and pore/particle size distribution. Despite good prediction of filtration trends, a systematic bias remained due to unmodeled effects such as biofilm and concentration polarization.

(Ludwig et al. 2012) defined the formed fouling resistance (R_f) as consisting of two components: a reversible resistance due to cake layer formation (R_{DS}, m^{-1}) and a resistance accounting for other fouling phenomena (R_F, m^{-1}). This model was then applied to different membrane filtration modules and validated.

I.2.1.4. Hermia's models

It has been suggested that deposition processes can follow various patterns. The theoretical basis was established by (Hermans and Bredée 1935), who introduced the original mathematical formulations describing membrane blocking mechanisms (complete blocking, standard blocking, intermediate blocking, and cake filtration). Later, (Gonsalves 1950) reviewed the

physical models used to derive these laws, examining their assumptions and applicability. Subsequently, (Grace 1956) provided a comprehensive analysis linking blocking mechanisms to filter media performance, with a focus on the standard blocking mechanism.

A major breakthrough occurred when (Hermia 1966) developed a semi-empirical, unified mathematical model for constant-pressure dead-end filtration. He integrated the previously empirical intermediate blocking mechanism into a common framework alongside complete blocking, standard blocking, and cake filtration. Prior to that, (Shirato, Aragaki, and Iritani 1979) extended blocking models to power-law non-Newtonian fluids—initially excluding the intermediate blocking case. In a later study, (Hermia 1982) revisited all blocking mechanisms and reformulated them within a unified model applicable to power-law non-Newtonian fluids under constant-pressure filtration.

The general law of clogging under constant pressure filtration for non-Newtonian fluid is give from: (Hermia 1982).

$$\left(\frac{d^2t}{dv^2}\right) = k\left(\frac{dt}{dv}\right)^n \qquad \text{(I.2. 3)}$$

Here, t indicates the filtration time (s), v is the permeate volume (m^3), k is a constant of clogging, and n varies depending on the specific clogging mechanism.

The general law can be reformulated in terms of permeate flux J, defined as :(Ghalami Choobar et al. 2019).

$$J = \frac{dv}{A\,dt} \qquad \text{(I.2. 4)}$$

A: is membrane aera (m^2).

Which leads to the following differential equation: (Jelemenský et al. 2016).

$$\frac{dJ}{dt} = -K\,A^{2-n}J^{3-n} \qquad \text{(I.2. 5)}$$

Classical clogging models reported in the literature appear in several functional forms. Among them, the model presented in (Hermia 1982; Vela et al. 2008) for the four mechanisms is distinguished by the fact that its parameters have clear physical significance, being directly related to the filtration process characteristics.

I.2.1.4.1. Complete clogging $n = 2$

This type occurs when particles fill up the pores and block them fully, i.e., there is no more passage through them. Such a phenomenon is typically observed under the condition that the particle diameter is equal to or greater than the pore diameter. For $n = 2$ Hermia's model can be linearized and expressed in terms of permeate flux $(J, m\ s^{-1})$ as function of time: (Hermia 1982; Vela et al. 2008).

$$lnJ = lnJ_0 - K_c t \tag{I.2. 6}$$

The parameter K_c can be defined in relation to the membrane surface area blocked per unit of permeate volume, (K_A, m^{-1}), and the initial permeate flux, $(J_0, m\ s^{-1})$, as described in Equation (I.2. 7). Consequently, the effective membrane surface available for filtration decreases progressively due to complete pore blockage.

$$K_c = K_A J_0 \tag{I.2. 7}$$

I.2.1.4.2. Standard clogging $n = 1.5$

When this occurs, particles enter the pore of the membrane and increasingly deposit along the inner wall. This effect narrows the effective pore radius with time, so permeate flux decreases progressively rather than suddenly. For standard clogging model can be expressed by the following linearized equation: (Hermia 1982; Vela et al. 2008).

$$\frac{1}{\sqrt{J}} = \frac{1}{\sqrt{J_0}} + K_s t \tag{I.2. 8}$$

The parameter, K_s, is defined from:

$$K_s = 2\frac{K_B}{A_0} A\sqrt{J_0} \tag{I.2. 9}$$

Where K_B represents the reduction of pore cross-sectional area per unit permeated volume (m^{-1}), and A_0 is the membrane porous surface area (m^2).

I.2.1.4.3. Intermediate clogging $n = 1$

It is an intermediate condition between standard and complete clogging. Some pores become fully clogged, while in others, particles are deposited inside and progressively reduce

their effective cross-section. It is generally considered a semi-empirical model with more realistic clogging in laboratory experiments. The intermediate blocking model is represented by the following linearized equation (Hermia 1982; Vela et al. 2008):

$$\frac{1}{J} = \frac{1}{J_0} + K_i t \quad \text{(I.2. 10)}$$

The parameter, K_i, can be expressed as:

$$K_i = K_A \quad \text{(I.2. 11)}$$

I.2.1.4.4. Cake filtration $n = 0$

In this instance, particles do not penetrate pores but deposit on the surface of the membrane and, eventually, form a porous layer called a "cake." The deposited layer, with time, is the primary flow resistance and governs the overall decline in filtration efficiency. The cake filtration model is formulated by the following linearized equation (Hermia 1982; Vela et al. 2008):

$$\frac{1}{J^2} = \frac{1}{J_0^2} + K_{gl} t \quad \text{(I.2. 12)}$$

The constant $\left(K_{gl}, s\, m^{-2}\right)$ can be defined in relation to intrinsic membrane resistance (R_m, m^{-1}), the cake layer resistance $\left(R_g, m^{-1}\right)$, and the cake layer area formed per unit of permeated volume (K_D, m^{-1}), together with the initial permeate flux $(J_0,\ m\, s^{-1})$, according to Equation (I.2. 13). This relation highlights the contribution of both the membrane intrinsic properties and the additional resistance caused by cake deposition.

$$K_{gl} = \frac{2 R_g K_D}{J_0 R_m} \quad \text{(I.2. 13)}$$

The Figure I.2. 1, illustrates the four main clogging mechanisms.

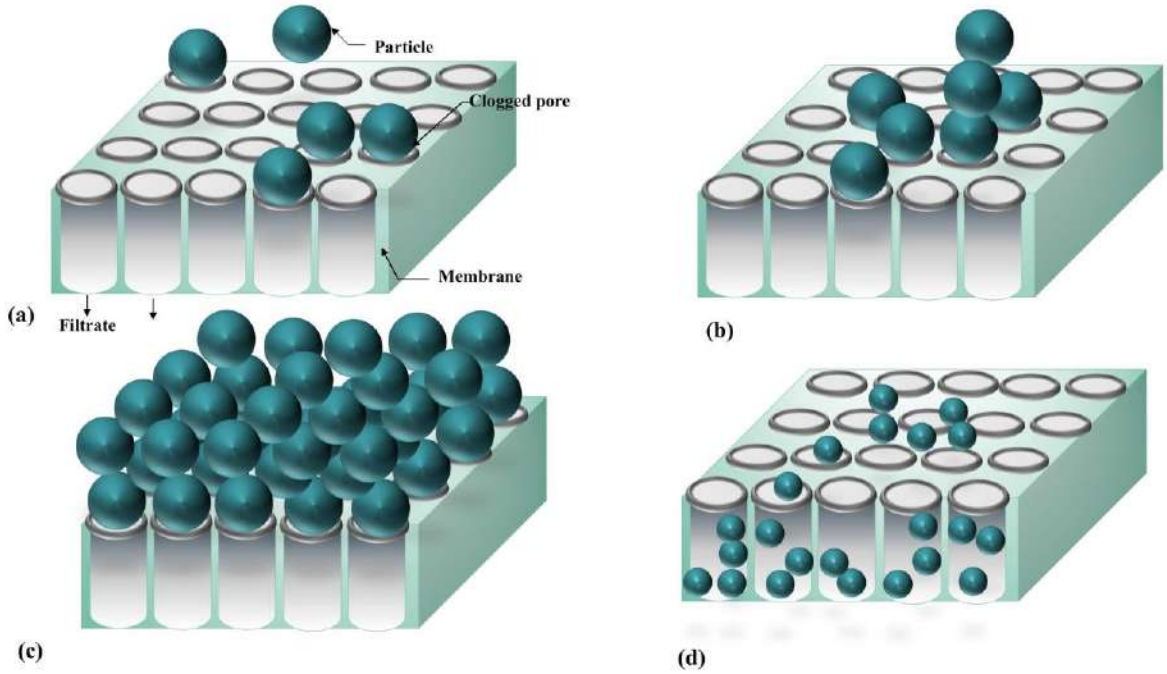


Figure I.2. 1: Schematic representation of the four classical clogging mechanisms a) complete blocking, (b) intermediate blocking, (c) cake filtration, and (d) standard blocking adopt from (Cherifi et al. 2025).

In addition to these classical models, which are usually expressed as flux–time relationships, other formulations have also been reported in the literature. These models describe the same clogging mechanisms but in terms of cumulative filtrate volume, offering an alternative perspective that may be more suitable for certain analyses. Table I.2. 2, summarizes the classical clogging models under constant transmembrane pressure filtration, presenting the permeate volume as a function of time.

Table I.2. 2: Summary of classical membrane clogging models based on permeate volume over time under constant pressure.

Model	Equation	Clogging parameters	Reference
Complete clogging (Eq. I.2. 14)	$V = \frac{V_0}{k_b}[1 - exp(-k_b t)]$	$k_b\ (s^{-1})$	(Affandy, Keshavarz-Moore, and Versteeg 2013; Laska et al. 2005)
Standard clogging (Eq. I.2. 15)	$V = (V_0 t)\left(1 + \frac{k_s V_0}{A_0} t\right)^{-1}$	$k_s\ (m^{-1})$	(Affandy, Keshavarz-Moore, and Versteeg 2013; Laska et al. 2005)
Intermediate clogging (Eq. I.2. 16)	$V = \frac{1}{k_i} ln(1 + k_i V_0 t)$	$k_i\ (m^{-3})$	(Affandy, Keshavarz-Moore, and Versteeg 2013; Laska et al. 2005)
Cake filtration (Eq. I.2. 17)	$V = \frac{1}{V_0 k_c}\left(\sqrt{1 + (2k_c V_0^2 t)} - 1\right)$	$k_c\ (s\ m^{-6})$	(Affandy, Keshavarz-Moore, and Versteeg 2013; Laska et al. 2005)

I.2.2. Limitation of classical models in membrane filtration clogging

Classical clogging models—such as Hermia's models (complete blocking, standard blocking, intermediate blocking, and cake layer formation)—are widely used to describe flux decline and predict filtration behavior. However, they suffer from fundamental limitations that must be considered when applied to real systems:

Classical models of membrane clogging, while widely applied, suffer from several inherent limitations. First, they rely on simplified assumptions regarding both membrane structure and particle characteristics. For instance, membranes are often idealized as assemblies of cylindrical pores, whereas in reality they exhibit highly interconnected, tortuous flow channels. Similarly, the feed suspension is typically assumed to consist of rigid, spherical particles, yet many real contaminants, such as plasmid DNA molecules, are flexible, coiled structures whose conformation and orientation dynamically change under fluid flow. These discrepancies reduce the ability of classical models to accurately describe the complex clogging mechanisms observed in practical systems, especially when dealing with large biomolecules(Affandy, Keshavarz-Moore, and Versteeg 2013; Haber et al. 2004; Larson et al. 2006; Zydney and Ho 2002) .

A second limitation lies in their inability to account for differences between operational modes. Capacities determined under constant-pressure conditions may vary significantly from those measured in constant-flow mode due to the influence of flow rate. This mismatch is

particularly problematic in biotechnological applications, where small-scale membrane tests are usually performed in pressure vessels under constant pressure, whereas large-scale operations rely on pumps under constant flow. At present, no predictive tool is available to translate data between these two modes, which hampers the scalability of filtration processes from laboratory to industrial levels (G. R. Bolton, Boesch, and Lazzara 2006).

These models inherently depend on constant operating conditions. They generally assume either constant pressure or constant flux, without providing a unified framework that enables transferability between the two. Consequently, results obtained under one operating mode often fail to predict performance under the other, further limiting the practical applicability of these models.

While classical models may fit specific laboratory datasets, they often fail to accurately describe industrial water treatment processes due to complex feed compositions and multi-fouling interactions (Pan et al. 2007; Xu et al. 2020).

Among the limitations of modeling is that a clear limitation still exists, namely the incomplete understanding of the mechanisms and conditions leading to clogging. The individual role of colloidal compounds (such as polysaccharides, polyphenols, and proteins) and particles (such as yeasts, bacteria, and colloidal aggregates) contributing to this phenomenon is still not precisely defined, which makes interpreting these phenomena and mitigating their adverse effects a challenging task (Rayess 2023).

I.2.3. Combined mechanisms in membrane fouling

In certain experimental cases, the decline in flux does not correspond to any of the classical clogging models when applied individually (Bowen, Calvo, and Hernández 1995; Charfi 2014). This can be attributed to the fact that clogging rarely consequences from a single mechanism; rather, it usually arises from the simultaneous action or coupling of two or more mechanisms, occurring either sequentially or concurrently.

Building on this observation, (De Bruijn, Salazar, and Bórquez 2005) proposed an approach that explicitly accounts for the concurrent nature of clogging mechanisms. In their framework, each mechanism is assigned a participation degree, expressed by a coefficient

ranging between 0 and 1, thereby allowing the relative contribution of each mechanism to the overall clogging thus quantifying (Charfi 2014).

The Ho and Zydney combined model for complete pore blocking and cake filtration has been particularly successful in describing flux decay for protein solutions, with multiple studies confirming its effectiveness for bovine serum albumin (BSA) filtration(C.-C. Ho and Zydney 2000; Hu et al. 2021). which was later used by (Mondal and De 2010; Slimane et al. 2018). Standard clogging was extended to include a second type of standard clogging (2nd type), considering internal clogging of membranes where n can take the value of 2.5 (Mokarizadeh and Raisi 2021; Xiao et al. 2019; Xu et al. 2020), for sufficiently slow adsorption (such as the adsorption of hydrophilic materials) (Li, Xia, and Mei 2016). Subsequently, (Duclos-Orsello, Li, and Ho 2006) developed a new model capable of accurately predicts not only cases of pure external or internal fouling, but also scenarios where both external and internal fouling occur simultaneously (Hou, Wang, and Song 2017a).

Similarly, (G. Bolton, Lacasse, and Kuriyel 2006) developed a combined models that integrate the classical clogging laws, resulting in explicit equations describing the cumulative permeate volume as a function of time under constant-pressure conditions. These combined models have the advantage of reducing to the individual classical models in the absence of additional clogging mechanisms, making them versatile and realistic tools for characterizing membrane clogging.

Table I.2. 3, summarizes the classical combined clogging models under constant transmembrane pressure filtration,

Table I.2. 3 Summary of combined membrane clogging models and corresponding mechanisms.

Model	Equation	Clogging parameters	Reference
Intermediate-standard (Eq. I.2. 18)	$V = \frac{A_0}{k_{ic}} ln\left(1 + \frac{2k_{ic}\left(\frac{V_0}{A_0}\right)t}{2 + k_s\left(\frac{V_0}{A_0}\right)t}\right)$	$k_{ic}(m^{-1})$ and $k_s(m^{-1})$	(Affandy, Keshavarz-Moore, and Versteeg 2013; G. Bolton, Lacasse, and Kuriyel 2006)
Complete-standard (Eq. I.2. 19)	$V = \frac{V_0}{k_b}\left(1 - exp\left(\frac{-2k_b t}{2 + k_s\left(\frac{V_0}{A_0}\right)t}\right)\right)$	$k_b(m^{-1})$ and $k_s(m^{-1})$	(Affandy, Keshavarz-Moore, and Versteeg 2013; G. Bolton, Lacasse, and Kuriyel 2006)
Cake-complete (Eq. I.2. 20)	$V = \frac{J_0}{k_b}\left(1 - exp\left(\frac{-k_b}{k_c J_0^2}\left(\sqrt{1 + 2k_c J_0^2 t} - 1\right)\right)\right)$	$k_c(s\, m^{-2})$ and $k_b(s^{-1})$	(G. Bolton, Lacasse, and Kuriyel 2006)
Cake-intermediate (Eq. I.2. 21)	$V = \frac{1}{k_i} ln\left(1 + \frac{k_i}{k_c J_0}((1 + 2k_c J_0^2 t)^{0.5} - 1)\right)$	$k_c(s\, m^{-2})$ and $k_i(m^{-1})$	(G. Bolton, Lacasse, and Kuriyel 2006)
Cake-standard (Eq. I.2. 22)	$V = \frac{2}{k_s}\left(\beta cos\left(\frac{2\pi}{3} - \frac{1}{3}arccos(\alpha)\right) + \frac{1}{1}\right)$, $\alpha = \frac{8}{27\beta^3} + \frac{4k_s}{3\beta^3 k_c J_0} - \frac{4k_s^2 t}{3\beta^3 k_c}$ and $\beta = \sqrt{\frac{4}{9} + \frac{4k_s}{3k_c J_0} + \frac{2k_s^2 t}{3k_c}}$	$k_c(s\, m^{-2})$ and $k_s(m^{-1})$	(G. Bolton, Lacasse, and Kuriyel 2006)

More sophisticated approaches have expanded beyond dual combinations to incorporate three or even four mechanisms. (Duclos-Orsello, Li, and Ho 2006). developed a notable flux decline model that combined three fouling mechanisms (standard blocking, complete blocking, and cake filtration) to describe microfiltration processes (Alsawaftah et al. 2021; Xu et al. 2020). This comprehensive model accounts for the theoretical basis that primitive fouling starts when pores are constricted and eventually become blocked, driving the accumulation of cake layers on the membrane surface. Some researchers have even combined all four classical fouling modes into one mechanistic model to explain the effect of coexisting fouling mechanisms (Xu et al. 2020).

Combined models stemming from the blocking filtration laws have been developed to reasonably evaluate two fouling mechanisms occurring sequentially or simultaneously, which are frequently observed in actual membrane filtration processes (Iritani and Katagiri 2016). These combined models can approximate highly complicated membrane fouling behaviors often encountered in membrane filtration, with particular emphasis placed on the combination of membrane pore blockage and cake formation on the membrane surface.

The development of combined models has also extended to different operational modes. While initial work focused on constant pressure conditions, researchers have developed combined fouling models for constant flux operations, which are more commonly used in membrane bioreactor (MBR) processes (Yin et al. 2021). Specialized applications have included modifications of dead-end filtration models that incorporate three main fouling mechanisms for sidestream configuration membrane bioreactor situations (Paul 2013).

However, combined models still face certain limitations. Some approaches simply assume that filtration can be separated into different successive stages with only one type of fouling occurring at a time, potentially neglecting effects such as small particle deposition on membrane pore walls that occur throughout the entire filtration process (Liu, Chen, and Sanaei 2020). Additionally, some combined models do not consider factors such as particle diffusion, which may limit their comprehensive representation of complex fouling phenomena.

I.3. Conclusion

Membrane filtration clogging is a complex phenomenon caused by the gradual accumulation of particles, macromolecules, or other solutes within or on the membrane. This leads to a steady decline in permeability and filtration efficiency. Despite its significance in engineering, clogging is challenging to comprehend and predict due to its reliance on numerous mechanisms influenced by operating conditions.

Several researchers have proposed combined models to overcome the limitations of classical clogging models in identifying the underlying fouling mechanisms. These shortcomings highlight the need for new modeling approaches that provide mechanistic insight and reliable predictions across different scales and operating conditions. Consequently, there is a growing demand to develop hybrid or more advanced models capable of realistically representing membrane clogging. This research follows that direction, and in the following chapters, we present further work on modeling membrane clogging with the goal of proposing a more universal and robust framework.

Chapiter II:

Empirical fractional approaches for modeling membrane filtration clogging

This chapter is an article published in

Membranes journal

Reader's guide

Membrane filtration is a widely applied separation technology in fields such as water treatment, biotechnology, and pharmaceuticals. Despite its advantages, its performance is often limited by clogging, a phenomenon caused by the progressive accumulation of particles on or within the membrane structure, leading to a reduction in permeability and efficiency. Understanding and predicting this phenomenon is therefore essential for improving filtration performance and extending membrane lifespan (G. R. Bolton, Boesch, and Lazzara 2006; Hentabli et al. 2021; Iritani 2013; McLoughlin, McMinn, and Magee 2003; Tien, Ramarao, and Yasarla 2014).

This chapter aims to improve the modeling and understanding of membrane clogging mechanisms and volume accumulation in filtration by introducing empirical fractional estimations evaluated through statistical error criteria. The work is divided into two main parts. The first part proposes eight empirical fractional equations to model clogging in membrane filtration, optimized using the Dragonfly Algorithm. These equations describe the accumulated volume as a function of time. The second part focuses on identifying clogging mechanisms for the given datasets using Hermia's general equation in combination with the proposed models.

The chapter is structured as follows: the methodology introduces the proposed models, the database, and the optimization procedure used for parameter identification. This is followed by the presentation and discussion of results, including an analysis of clogging mechanisms through Hermia's framework and a comparison with existing models. The chapter concludes by summarizing the main contributions and highlighting the advantages of the most efficient model.

II.1. Materials and methods

II.1.1. Clogging of membrane filtration

biotechnological products, yet its efficiency is often limited by protein fouling. The accumulation of material on the membrane surface progressively reduces permeate flux, particularly under constant transmembrane pressure, and results in shorter membrane lifespan, higher maintenance, and increased operational costs (Ciobanu et al. 2006).

This fouling is commonly described by Hermia's classical blocking models (Hermia 1982), where new definitions have been introduced for the old physical mechanisms, and these

mechanisms have been given more descriptive names: pore blocking (formerly complete blocking) and direct adsorption (formerly standard blocking), which are related to changes in the number of open pores. Long-term adsorption (formerly intermediate blocking) is related to changes in pore radius, and finally, boundary layer resistance (formerly cake filtration) refers to the development of additional resistance to flow in series with that provided by the membrane(Bowen, Calvo, and Hernández 1995; Iritani and Katagiri 2016; Zydney 2022). The filtration behaviour associated with these mechanisms can be expressed in a unified mathematical framework relating cumulative filtrate volume to time Equation (I.2. 3).

II.1.2. The proposed empirical fractional estimation models

Mathematical models describing membrane clogging are generally classified as empirical, phenomenological, or semi-empirical. Empirical models, derived from experimental data correlations, are particularly useful when the physical mechanisms are not fully understood, while phenomenological models rely on fundamental transport principles grounded in physical. Semi-empirical approaches combine both aspects, correlating observed data with physical insight (Sandoval-García et al. 2025; de Souza Matias et al. 2019). A cornerstone in this field is the unified framework introduced by (Hermia 1982), from which four classical clogging mechanisms, were derived. These models have been widely applied to describe flux decline under various operating conditions (C. C. Ho and Zydney 2000; Iritani et al. 1995; Tien, Ramarao, and Yasarla 2014; Zydney 2022). However, they also present limitations, particularly their inability to explain certain experimental observations such as the increase in membrane capacity with higher flow rates (Bolton et al. 2006). To overcome such limitations, several combined and modified models have been developed to account for simultaneous or sequential fouling mechanisms (G. Bolton, Lacasse, and Kuriyel 2006; C.-C. Ho and Zydney 2000; Hou, Wang, and Song 2017b; Kim, Yoo, and Yoo 2011). For example (G. Bolton, Lacasse, and Kuriyel 2006) showed that a cake-adsorption model provided a better fit to protein filtration data, while (Affandy, Keshavarz-Moore, and Versteeg 2013) demonstrated a mechanistic transition from intermediate to standard clogging during plasmid DNA filtration.

Building upon these insights, this chapter proposes a different approach through the development of empirical fractional estimation models. These models are directly inspired by the analysis of experimental data collected on retentate accumulation in membrane filtration

systems over time. The accumulation volume was measured at successive intervals, revealing distinct clogging patterns that served as the basis for the mathematical formulation. Unlike phenomenological models derived from physical laws, the proposed equations are not primarily intended to explain the fouling mechanisms themselves, but rather to provide an accurate and predictive description of clogging dynamics as reflected in experimental observations. The strength of this approach lies in its direct link to empirical data, ensuring that the models capture real-world behavior. Consequently, these equations offer a robust framework for analyzing past filtration experiments and for forecasting the performance of membrane systems under new operating conditions. The empirical fractional estimation models proposed for the clogging of membrane filtration are presented below.

$$v = \frac{a.t^N}{1 + b.t^N} \tag{II. 1}$$

Where v is accumulative volume (m^3), t is time of filtration (min), a ($m^3.min^{-N}$) and b (min^{-N}) are constants, the boundary conditions are given by $v(t = 0) = 0$, and $v(t \to \infty) = \frac{a}{b} \to v_\infty$. In the limiting case where $t \to \infty$, the ratio $\frac{a}{b}$ may represent the asymptotic cumulative volume v_∞ (m^3) . This value corresponds to the maximum permeate volume that can be achieved if filtration reaches completion, meaning no further permeate is produced. In this situation, the cumulative volume reflects the total amount of material accumulated at the membrane surface.

$$v = v_\infty \left(\frac{a.t^N}{1 + a.t^N} \right) \tag{II. 2}$$

Where a (s^{-N}) is constant parameter, and the boundary conditions are given by $v(t = 0) = 0$, and $v(t \to \infty) = v_\infty$,

$$v = v_\infty \left(\frac{t^N}{a + t^N} \right) \tag{II. 3}$$

Where a is constant parameter (min^{-N}), the boundary conditions are $v(t = 0) = 0$, $v(t \to \infty) = v_\infty$

$$v = a.v_{\infty}\left(\frac{t^{N}}{1+t^{N}}\right)^{m} \quad \text{(II. 4)}$$

Where a is constant parameter, and v_{∞} (m^3), accumulative volume maximum, the boundary conditions are $v(t=0)=0$, and $v(t\to\infty)=a.v_{\infty}\to v_{\infty}$.

$$v = d\left(\frac{a.t^{N}}{c+b.t^{N}}\right)^{m} \quad \text{(II. 5)}$$

Where a(min^{-N}) , b (min^{-N}), c, and d (m^3), are contents parameters, the boundary conditions are $v(t=0)=0$, and $v(t\to\infty)\to v_{\infty}$, this possible case.

$$v = \frac{a.t^{N}}{1+b.t^{N}} \quad \text{(II. 6)}$$

Where a $(m^3.min^{-N})$ and b (min^{-N}), are constants parameters, the boundary conditions are $v(t=0)=0$, and $v(t\to\infty)=\frac{a}{b}\to v_{\infty}$, this is case possible, In the limiting case where $t\to\infty$, the ratio $\frac{a}{b}$ may represent the asymptotic cumulative volume v_{∞}.

$$v = v_{\infty}\left(\frac{1-e^{-a.t}}{1+c\,(1-e^{-b.t})}\right) \quad \text{(II. 7)}$$

Where a (min^{-1}), b (min^{-1}), and c, are constants parameters, the boundary conditions are $v(t=0)=0$, and $v(t\to\infty)=v_{\infty}.K\to v_{\infty}$, , in the limiting case where $t\to\infty$, the ratio $v_{\infty}.K$ may represent the asymptotic cumulative volume v_{∞}.

$$v = v_{\infty}\left(\frac{1-e^{-a.t^{N}}}{1+c\left(1-e^{-b.t^{N}}\right)}\right) \quad \text{(II. 8)}$$

Where a (min^{-N}), b (min^{-N}), and c, are constants parameters, the boundary conditions are $v(t=0)=0$, and $v(t\to\infty)=v_{\infty}K\to v_{\infty}$, in the limiting case where $t\to\infty$, the ratio $v_{\infty}K$ may represent the asymptotic cumulative volume v_{∞}.

II.1.3. Building a database

In this chapter, we utilized data available in the literature from two references (Affandy, Keshavarz-Moore, and Versteeg 2013; G. R. Bolton, Boesch, and Lazzara 2006). The database

employed for validating the proposed empirical fractional estimation models of membrane clogging was extracted from these papers using GetData Graph Digitizer 2.24. The entire database collected from the literature was divided into four parts according to the different experimental conditions encountered.

The first database, (DB II. 1), comes from the study by (G. R. Bolton, Boesch, and Lazzara 2006), in which experimental data were generated using a Viresolve 180 composite PVDF membrane, designed to retain viruses larger than 20 nm while allowing proteins up to 160 kDa to pass. Two protein solutions were employed: bovine serum albumin (BSA) at a concentration of 1.0 g/L, and human plasma IgG prepared at 0.1 g/L in buffer solution. The BSA experiments were conducted under constant pressure conditions at 2, 5, 10, and 20 psi, with the filtrate volume recorded as a function of time until the permeate flux had decreased by about 90%. In contrast, the IgG experiments were performed under both constant pressure and constant flow modes, providing complementary database. For constant pressure tests, pressures of 5, 25, and 50 psi were applied, and data were collected until the flux declined to approximately one-quarter of its initial value. For constant flow tests, the feed was pumped at different flow rates (0.087, 0.19, 0.27, and 0.37 mL/s), corresponding to initial pressures between 4.5 and 20 psi, and the pressure evolution was monitored until it had increased roughly fourfold compared to the initial value. These databases, obtained under well-controlled operating conditions, have been widely used to evaluate fouling models since they combine both constant pressure and constant flow measurements for different proteins and operating ranges. For this chapiter we use the data for constant pressure.

The second database, (DB II. 2), consists of experimental data reported by (Affandy, Keshavarz-Moore, and Versteeg 2013) from sterile filtration studies of plasmid DNA using 0.22 μm PVDF membranes operated under constant transmembrane pressure. Two plasmids were employed (pQR150, ~20 kb, and pGEc47, ~56 kb), representing large and structurally complex DNA molecules. Filtration experiments were carried out at transmembrane pressures of 5 and 8 psi, and the permeate volume was monitored as a function of time to evaluate flux decline. In addition, the concentration of DNA in the permeate was measured to quantify solute transmission during filtration. Analysis of this database revealed that higher operating pressures accelerated fouling and flux decline, but also initially enhanced DNA transmission, likely due to pressure-

induced deformation of the plasmid coils facilitating passage through membrane pores. Mechanistically, the results showed that intermediate blocking dominated in the early stages of filtration, whereas standard blocking became the prevailing fouling mode at longer times. These experiments thus provide a valuable database for evaluating clogging models, as they capture both flux decline and macromolecular transmission under well-defined pressure-driven conditions. The collected data DB II. 1and DB II. 2, presents in Table annex 1.1 and

Table annex 1. 2, in the annex 1, respectively. The Table II. 1, present the statistical analysis of the database variables (DB II. 1and DB II. 2).

Table II. 1: Statical analysis of the database variable (DB II. 1and DB II. 2).

Databases	Solution	Pressures (psi)	Variable	Min	Max	Mean	STD
DB II. 1	BSA	P= 2	$t(min)$	0.3799	86.6097	37.0694	27.1393
			$v(m^3)$	726.6440	10173.0000	7778.2459	2251.0000
		P= 5	$t(min)$	0.3799	85.0902	33.3203	26.5737
			$v(m^3)$	1937.7200	22283.7000	16709.8511	6142.7000
		P= 10	$t(min)$	0.0000	108.6420	43.4582	37.5477
			$v(m^3)$	1211.0700	51833.9000	38064.5412	15885.0000
		P= 20	$t(min)$	0.3788	81.0607	25.6379	25.6661
			$v(m^3)$	4117.6500	63944.6000	43293.8061	18128.0000
DB II. 2	pQR150	P= 5	$t(min)$	0.0000	35.0000	11.5195	9.4282
			$v(10^{-6}m^3)$	0.0000	4.2216	2.3813	1.5266
		P= 8	$t(min)$	0.0000	35.0000	9.1865	7.4096
			$v(10^{-6}m^3)$	0.0000	4.6639	2.9845	1.6623
	pGEc47	P= 5	$t(min)$	0.0000	35.0000	10.0541	8.8337
			$v(10^{-6}m^3)$	0.0000	6.6177	3.8831	2.4134
		P= 8	$t(min)$	0.0000	35.0000	10.0298	8.8963
			$v(10^{-6}m^3)$	0.0000	6.2080	4.0005	2.3466

II.1.4. Dragonfly algorithm coupled with nonlinear regression (DA_nlinfit)

To identify the unknown parameters of the proposed models, the Dragonfly Optimization Algorithm (DA) was employed. DA is a swarm-based metaheuristic optimization method inspired by the static and dynamic swarming behaviors of dragonflies. It is a flexible algorithm

with several advantages: it requires only a few control parameters and has been successfully applied in both research and industrial contexts (Mesli et al. 2022). For model calibration, curve fitting techniques were applied to experimental data. Curve fitting involves constructing a mathematical function to approximate an experimental curve and adjusting its parameters to minimize the discrepancy between predicted and measured data (Hentabli et al. 2021). In this chapter, nonlinear least squares regression (nlinfit in MATLAB) was coupled with DA to improve parameter estimation. The nonlinear regression technique requires initial guesses for the model coefficients. Poorly chosen initial values may lead to slow convergence or trapping in local minima, while carefully selected ones accelerate convergence. To address this, initial parameter values were first estimated using DA. The optimization process was executed 10 times to ensure robustness, and the parameter set yielding the best fit was retained. This optimal set was then used as the initial guess in the nlinfit function, which employs the Levenberg–Marquardt algorithm for nonlinear regression (Hentabli et al. 2021).

The Dragonfly Algorithm (DA) is a nature-inspired optimization method that simulates the static and dynamic swarming behaviors of dragonflies. The optimization process in DA is governed by five key behaviors: separation, alignment, cohesion, attraction to food sources, and distraction from enemies. These behaviors are mathematically modeled as follows: (Mirjalili 2016).

Separation – this ensures that each dragonfly avoids crowding its neighbors

$$\vec{S} = \sum_{j=i}^{N} \left(\vec{X} - \vec{X}_j\right) \tag{II. 9}$$

Alignment – this aligns the velocity of each dragonfly with the average velocity of its neighbors:

$$\vec{A} = \frac{1}{N} \sum_{j=i}^{N} \vec{X}_j \tag{II. 10}$$

Cohesion – this moves the dragonfly towards the center of its neighboring swarm:

$$\vec{c} = \frac{1}{N}\sum_{j=i}^{N} \vec{X}_j - \vec{X} \quad \text{(II. 11)}$$

Attraction to food source – guides the dragonfly towards the best solution (food):

$$\vec{F} = \vec{X}_{food} - \vec{X} \quad \text{(II. 12)}$$

Distraction from enemy – drives the dragonfly away from undesirable positions:

$$\vec{E} = \vec{X}_{enemy} + \vec{X} \quad \text{(II. 13)}$$

Here $\vec{X}$ is the position of the current dragonfly, $\vec{X}_j$ and $\vec{V}_j$ are the position velocity of the j^{th} neighboring dragonfly, $\vec{X}_{food}$ is the position of the food source, and $\vec{X}_{enemy}$ is the position of the enemy.

The step vector $\Delta\vec{X}$, which determines the movement of each dragonfly in the search space, is calculated as weighted sum of these behaviors:

$$\Delta\vec{X}_{i+1} = s.\vec{S} + a.\vec{A} + c.\vec{C} + f.\vec{F} + e.\vec{E} + w.\Delta\vec{X}_t \quad \text{(II. 14)}$$

Where s, a, c, f, e, and w are the weights for separation, alignment, cohesion, food attraction, enemy distraction, and inertia, respectively.

Finally, the position of each dragonfly is updated by adding the step vector:

$$\vec{X}_{t+1} = \vec{X}_t + \Delta\vec{X}_{t+1} \quad \text{(II. 15)}$$

This iterative process continues until convergence criteria are met, allowing the algorithm to explore and exploit the search space effectively.

In both DA and nlinfit, the relative root mean squared error (nRMSE) was used as the objective function to be minimized.

This two-step approach (DA initialization followed by nonlinear regression) ensures accurate parameter identification while reducing the risk of poor convergence and local optima. Figure II. 1, is a summary of the method steps of modeling.

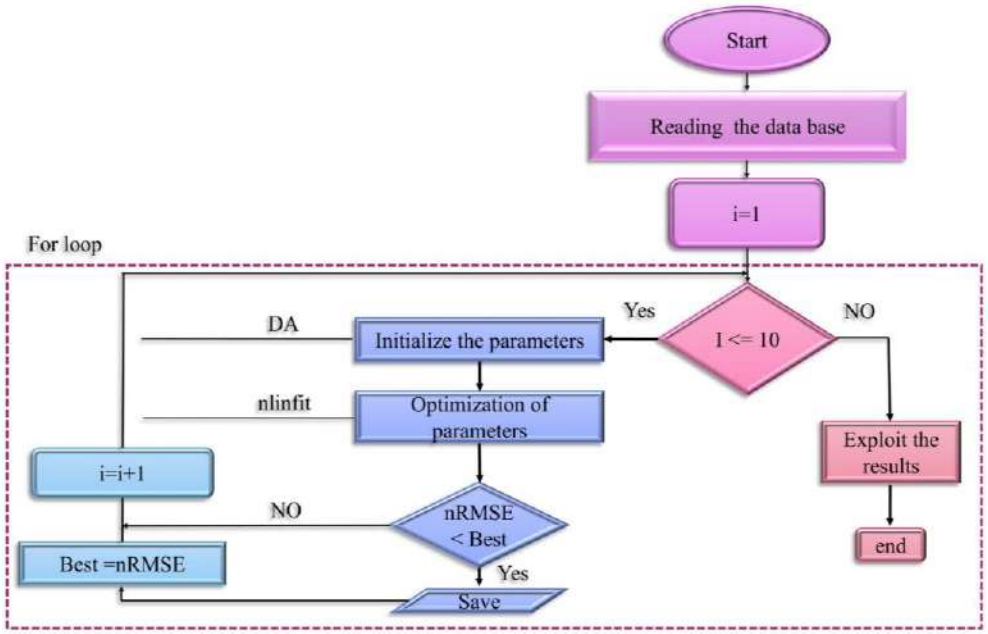


Figure II. 1: Procedure of the optimization algorithm (Dragonfly Algorithm Nonlinear Regression (DA_nlinfit)).

II.1.5. Evaluation of the proposed models' performance

The optimal parameter values were determined by minimizing an objective function that incorporates both experimental and computed data. Each empirical fractional estimation model was tested under pressure-driven filtration conditions using database containing volume–time measurements from the first and second databases (DB II. 1and DB II. 2). The performance of these models was assessed through several statistical error indices, namely the sum of squares of residuals (SSR), normalized root mean squared error (nRMSE), coefficient of determination (R^2), variance accounted for (VAF), normalized mean absolute error (nMAE), normalized Chi-square statistic (nChi), and the standard error of prediction (SEP) (Ammi, Khaouane, and Hanini 2018, 2021; Ammi 2016; Dahmani, Ammi, and Hanini 2023).

The mathematical expressions of these error indices are presented in equations ((II. 16)-(II. 25). As a general guideline, R^2 values above 0.5 indicate satisfactory agreement, while values

exceeding 0.9 denote excellent correlation (Ammi 2016). Model accuracy is classified according to nRMSE values: excellent when nRMSE < 10%, good for 10% < nRMSE < 20%, fair for 20% < nRMSE < 30%, and low when nRMSE > 30% (Dahmani, Ammi, and Hanini 2023). All statistical analyses and computations were carried out using MATLAB software R2021b.

$$SSR = \sum_{i=1}^{M} \left(y_{exp.i} - y_{cal.i}\right)^2 \quad \text{(II. 16)}$$

$$R^2 = 1 - \frac{SSR}{\sum_{i=1}^{M} \left(y_{exp.i} - \overline{y_{exp.i}}\right)^2} \quad \text{(II. 17)}$$

$$VAF = \left[1 - \frac{var(y_{exp.i} - y_{cal.i})}{var(y_{exp.i})}\right].100 \quad \text{(II. 18)}$$

$$RMSE = \sqrt{\frac{SSR}{M}} \quad \text{(II. 19)}$$

$$nRMSE = \left[\frac{RMSE}{\sum_{I=1}^{M} \left(\frac{y_{cal,i}}{M}\right)}\right].100 \quad \text{(II. 20)}$$

$$MAE = \frac{1}{M} \sum_{i=1}^{M} \left(y_{exp.i} - y_{cal.i}\right) \quad \text{(II. 21)}$$

$$nMAE = \left[\frac{MAE}{\sum_{I=1}^{M} \left(\frac{y_{cal,i}}{M}\right)}\right].100 \quad \text{(II. 22)}$$

$$Chi = \frac{SSR}{(M - \dim)} \quad \text{(II. 23)}$$

$$nChi = \left[\frac{chi}{\sum_{I=1}^{M} \left(\frac{y_{cal,i}}{M}\right)}\right].100 \quad \text{(II. 24)}$$

$$SEP(\%) = \left(\frac{RMSE}{y_e}\right).100 \quad \text{(II. 25)}$$

where M is the number of data points, $y_{exp.i}$ and $y_{cal.i}$ refer to the experimental values and calculated values obtained from the proposed model, respectively; y_e is the average value of experimental data, and var is the variance.

II.1.6. Parameter identifiability analysis

Given a model, a criterion, and a database, identifiability refers to the ability to determine a unique set of parameters that minimizes the criterion, regardless of the initial parameter values (D. Janzén et al. 2015; D. L. I. Janzén et al. 2019; Villaverde, Barreiro, and Papachristodoulou 2016). Two main notions of identifiability are distinguished: structural identifiability, which concerns whether the system's structure allows unique parameter estimation, and practical identifiability, which depends on the quantity and quality of the available data.

Certain models, such as Model (II. *5*), are not identifiable because they are over-parameterized: regardless of the initial parameter conditions used during the optimization process, the product $(d \times a^m)$ remains constant. In this work, we did not perform a dedicated identifiability analysis, since the models under consideration are closer to black-box approaches. Their parameters lack direct physical meaning and are instead adjusted (black-box approach) to ensure that the models reproduce the experimental data with sufficient accuracy.

II.2. Results and discussion

II.2.1. Performance of the proposed model by statistical error analysis

The performance validation of the proposed empirical fractional estimation models for membrane filtration clogging, assessed using statistical error metrics under varying transmembrane pressures (2, 5, 8, 10, and 20 psi) with two databases (DB II. 1and DB II. 2), is presented in Table II. 2 and Table II. 3, and their adjustment parameter presented in Table annex 1. 3 and Table annex 1. 4, in annex 1. The findings indicate that the models exhibit consistent performance across different pressures and filtration solutions, thereby confirming their robustness and reliability. Among the proposed models, Model 5 achieved the best overall performance, yielding the lowest error values with nRMSE between 0.8674% and 2.2959%, nMAE between 0.6229% and 1.8938%, SEP between 0.8764% and 2.2954%, and nChi between 0.0315% and 0.1792%. The other models demonstrated higher accuracy under specific pressure conditions.

This good agreement is further supported by strong statistical indicators, with coefficients of determination (R^2) consistently above 0.99 and variance accounted for (VAF) greater than 99%. For instance, Model 6 achieved R^2 values between 0.9936 and 0.9997, and VAF values ranging from 99.3558% to 99.9655%.

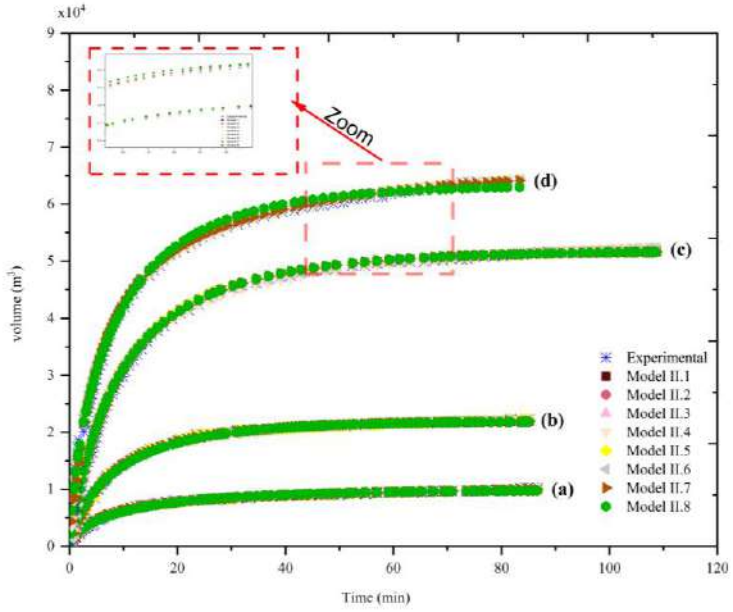
Table II. 2: Validation result of the proposed empirical fractional estimation models for membrane filtration clogging at different pressures for database DB II. 1.

Model	Pressure (psi)	R^2	nRMSE %	nMAE %	nchi %	SEP%	VAF%
(II. 1)	p= 2	0,9945	2,1539	1,7387	0,0372	2,1527	99.4492
	p= 5	0.9981	1,6312	1,2143	0,0456	1,6297	99.8053
	p= 10	0.9993	1,0860	0,8073	0,0473	1,0968	99.9316
	p= 20	0.9978	1,9596	1,2199	0,1746	1,9924	99.7770
(II. 2)	p= 2	0.9936	2,3342	1,9322	0,0431	2,3343	99.3558
	p= 5	0.9975	1,8562	1,2818	0,0586	1,8531	99.7475
	p= 10	0.9989	1,4055	1,0344	0,0763	1,4181	99.8857
	p= 20	0.9978	1,9597	1,2199	0,1723	1,9924	99.7769
(II. 3)	p= 2	0.9936	2,3342	1,9322	0,0431	2,3343	99.3558
	p= 5	0.9975	1,8562	1,2818	0,0586	1,8531	99.7475
	p= 10	0.9989	1,4055	1,0344	0,0763	1,4181	99.8857
	p= 20	0.9978	1,9597	0,1723	0,1723	1,9924	99.7769
(II. 4)	p=2	0.9935	2,3353	1,8942	0,0436	2,3343	99.3540
	p= 5	0.9944	2,7777	1,9910	0,1331	2,7706	99.4377
	p= 10	0.9962	2,5748	2,0319	0,2635	2,5946	99.6179
	p= 20	0.9972	2,2021	1,5700	0,2207	2,2377	99.7186
(II. 5)	p= 2	0.9937	2,2959	1,8938	0,0430	2,2954	99.3744
	p= 5	0.9986	1,3883	1,0382	0,0335	1,3883	99.8591
	p= 10	0.9996	0,8674	0,6229	0,0315	0,8764	99.9565
	p= 20	0.9978	1,9573	1,2129	0,1792	1,9901	99.7771
(II. 6)	p= 2	0.9936	2,3342	1,9322	0,0431	2,3343	99.3558
	p= 5	0.9975	1,8562	1,2818	0,0586	1,8531	99.7475
	p= 10	0.9989	1,4055	1,0344	0,0763	1,4181	99.8857
	p= 20	0.9978	1,9597	1,2199	0,1723	1,9924	99.7769
(II. 7)	p= 2	0.9936	2,3344	1,9323	0,0431	2,3343	99.3558
	p= 5	0.9979	1,6737	1,2447	0,0481	1,6720	99.7943
	p= 10	0.9993	1,1359	0,8730	0,0500	1,1473	99.9253
	p= 20	0.9976	2,0486	1,2692	0,1931	2,0812	99.7562
(II. 8)	p= 2	0.9896	2,9540	2,5005	0,0707	2,9567	98.9606
	p= 5	0.9965	2,1880	1,6395	0,0844	2,1911	99.6473
	p= 10	0.9993	1,1360	0,8704	0,0526	1,1473	99,9253
	p= 20	0.9964	2,5007	1,8950	0,2891	2,5460	99.6358

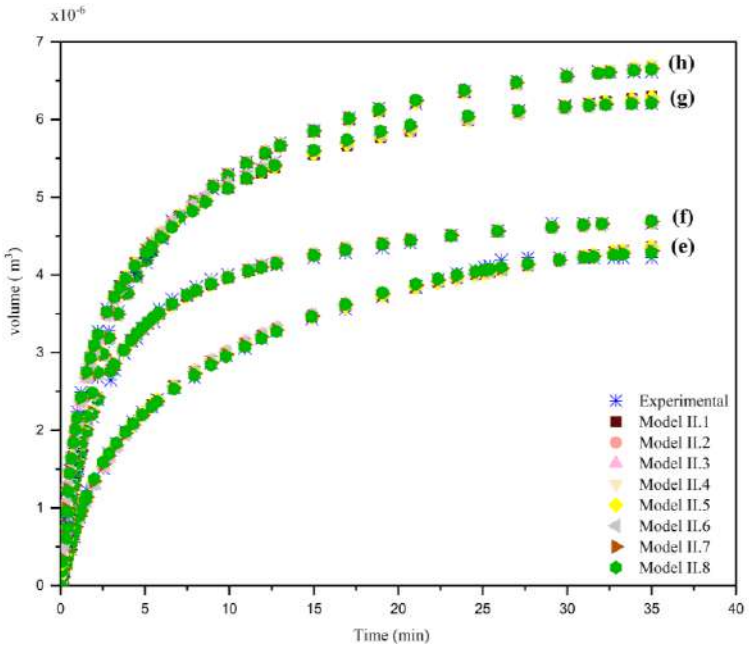
Table II. 3: Validation result of the proposed empirical fractional estimation models for membrane filtration clogging at different pressures for database DB II. 2.

Model	Pressure (psi)	R^2	nRMSE %	nMAE %	nchi %	SEP%	VAF%
(II. 1)	p= 2	0.9988	2,1934	1,7278	2,1963	0,1258	99,8774
	p= 5	0.9987	1,7117	1,2964	1,7122	0,0971	99,8690
	p= 10	0.9997	1,0014	0,8032	1,0018	0,0438	99,9680
	p= 20	0,999	1,4119	1,0921	1,4123	0,0875	99,9035
(II. 2)	p= 2	0.9985	2,3971	2,0241	2,4021	0,1467	99,8533
	p= 5	0.9986	1,7481	1,3161	1,7491	0,0971	99,8635
	p= 10	0,9997	1,0397	0,8081	1,0404	0,0463	99,9655
	p= 20	0,9987	1,6508	1,2562	1,6523	0,1174	99,8679
(II. 3)	p= 2	0,9985	2,3971	2,0241	2,4021	0,1467	99,8533
	p= 5	0.9986	1,7481	1,3161	1,7491	0,0971	99,8635
	p= 10	0,9997	1,0397	0,8081	1,0404	0,0463	99,9655
	p= 20	0,9987	1,6508	1,2562	1,6523	0,1174	99,8679
(II. 4)	p=2	0.9988	2,1495	1,6751	2,1501	0,1217	99,8825
	p= 5	0,9987	1,7058	1,3473	1,7055	0,0972	99,8698
	p= 10	0,9995	1,2139	0,9562	1,2129	0,0644	99,9531
	p= 20	0,9991	1,3594	1,0071	1,3598	0,0825	99,9105
(II. 5)	p= 2	0,9988	2,1497	1,6626	2,1501	0,1260	99,8826
	p= 5	0.9987	1,6887	1,3067	1,6887	0,1005	99,8725
	p= 10	0,9997	0,9682	0,7776	0,9683	0,0438	99,9701
	p= 20	0.9992	1,2824	0,9924	1,2823	0,0775	99,9204
(II. 6)	p= 2	0,9985	2,3971	2,0241	2,4021	0,1467	99,8533
	p= 5	0.9986	1,7481	1,3161	1,7491	0,0971	99,8635
	p= 10	0,9997	1,0397	0,8081	1,0404	0,0463	99,9655
	p= 20	0.9987	1,6508	1,2562	1,6523	0,1174	99,8679
(II. 7)	p= 2	0.9991	1,8282	1,5053	1,8310	0,0881	99,9146
	p= 5	0,9986	1,7424	1,3303	1,7424	0,1005	99,8642
	p= 10	0,9997	0,9523	0,7412	0,9528	0,0386	99,9710
	p= 20	0.9994	1,0870	0,7871	1,0874	0,0525	99,9427
(II. 8)	p= 2	0.9994	1,5879	1,2182	1,5874	0,0672	99,9360
	p= 5	0,9985	1,8481	1,3660	1,8496	0,1172	99,8469
	p= 10	0,9997	0,9269	0,7184	0,9271	0,0386	99,9726
	p= 20	0.9995	1,0274	0,7974	1,0274	0,0475	99,9488

Figure II. 2, provides a graphical comparison of the calculated and experimental filtrate volumes over time for each proposed models under various operating pressures, where (a) P=2psi, (b) P=5psi, (c) P=10 psi and (d) P= 20 psi for DB II. 1and (e) P=5 psi (pQR150), (f) P=8 psi (pQR150), (g) P=5 psi (pGEc47) and (h) P=5 psi (pGEc47) for DB II. 2.



DB II. 1



DB II. 2

Figure II. 2: Comparison between calculated and experimental volumes against time for eight models proposed at different pressures filtration of DB II. 1and DB II. 2.

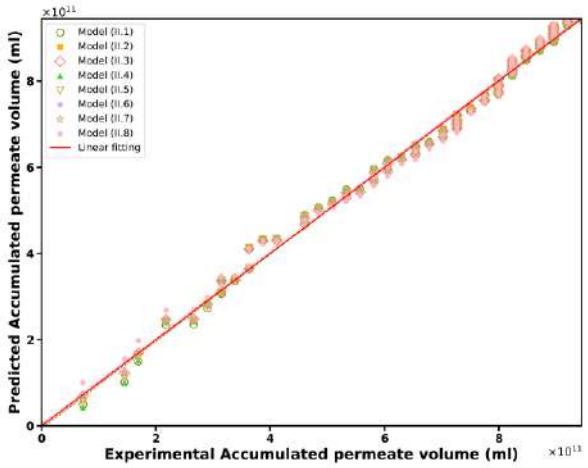
The filtration dynamics also revealed different time scales: in DB II. 1, the maximum filtrate volume was reached in less than 85 minutes, while in DB II. 2 it was achieved in less than 35 minutes. The estimated infinite filtrate volumes (v_∞) where: 1.0173×10^{4}, 2.2283×10^{4}, 5.1833×10^{4}, and 6.3944×10^{4} m^3 at 2, 5, 10, and 20 psi for DB II. 1, respectively. For DB II. 2, the values were 4.2216×10^{-6}, 4.6639×10^{-6}, 6.6177×10^{-6}, and 6.2080×10^{-6} m^3 under 5 psi (pQR150), 8 psi (pQR150), 5 psi (pGEc47), and 8 psi (pGEc47), respectively. These asymptotic volumes reflect pore clogging and indicate the termination of filtration. Importantly, the proposed model enables the estimation of the critical accumulation volume, which can be used to anticipate membrane clogging and to implement corrective measures before complete blockage occurs.

Overall, the strong agreement between experimental and predicted results demonstrates the effectiveness, accuracy, and robustness of the proposed models in capturing clogging dynamics under diverse operating conditions.

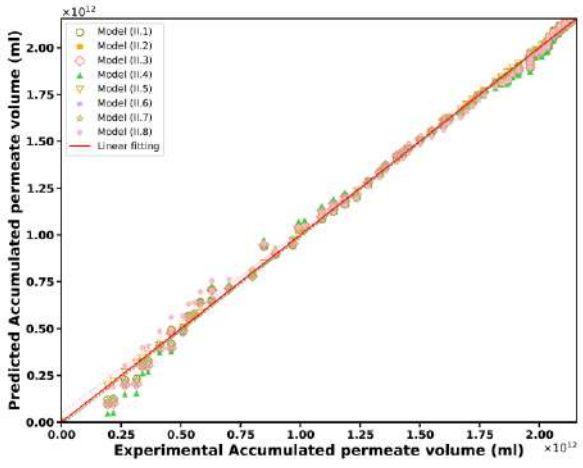
II.2.2. Linear regression analysis of proposed model

Linear regression was applied to evaluate the predictive accuracy of the proposed empirical fractional estimation models. This method provides a direct comparison between predicted and experimental data, allowing assessment of model robustness and reliability.

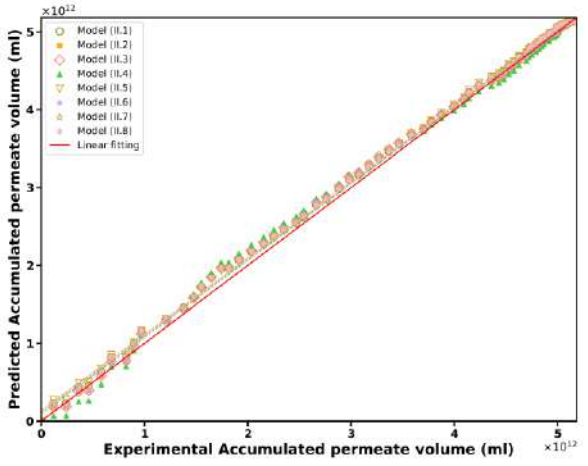
The **Error! Reference source not found.** as shown the regression plot comparison of the predicting data vs. really data, for eight model proposed at different pressures and solutions filtration. Additionally, it provides performance metrics for the eight proposed empirical fractional estimation models. The results highlight the robustness of these models, with regression vectors closely aligning with ideal values ($\alpha=1$ for slope, $\beta=0$ for intercept, and $R=1$ for correlation coefficient). the linear regression vector values present in Table II. 4. Each model was rigorously evaluated across varying pressures and solutions, demonstrating consistent and reliable performance under different filtration conditions.


Model (II.1)
Model (II.2)
Model (II.3)
Model (II.4)
Model (II.5)
Model (II.6)
Model (II.7)
Model (II.8)
Linear fitting
Predicted Accumulated permeate volume (ml)
Experimental Accumulated permeate volume (ml)

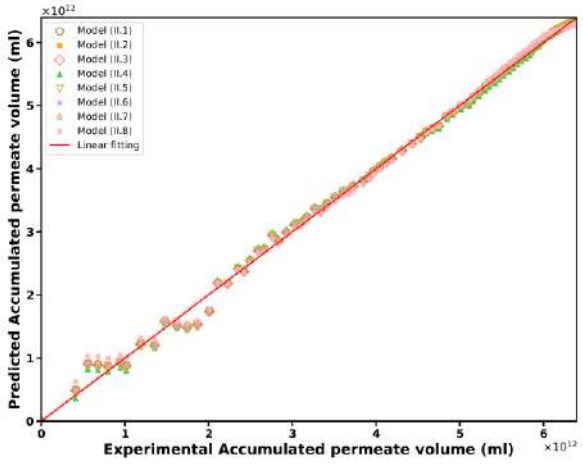
(a)


Model (II.1)
Model (II.2)
Model (II.3)
Model (II.4)
Model (II.5)
Model (II.6)
Model (II.7)
Model (II.8)
Linear fitting
Predicted Accumulated permeate volume (ml)
Experimental Accumulated permeate volume (ml)

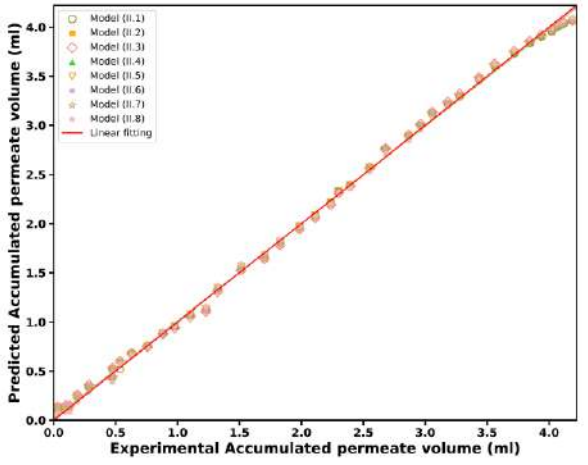
(b)


Model (II.1)
Model (II.2)
Model (II.3)
Model (II.4)
Model (II.5)
Model (II.6)
Model (II.7)
Model (II.8)
Linear fitting
Predicted Accumulated permeate volume (ml)
Experimental Accumulated permeate volume (ml)

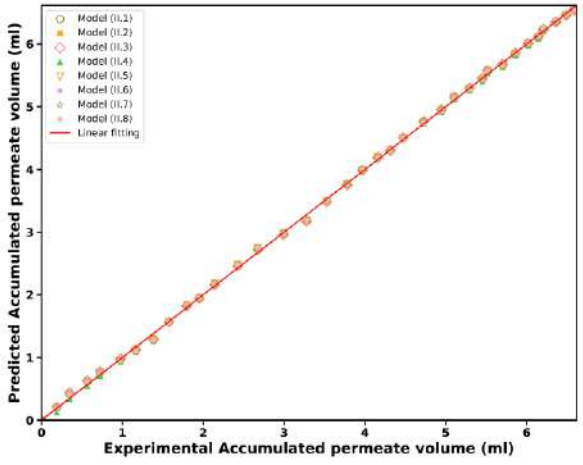
(c)


Model (II.1)
Model (II.2)
Model (II.3)
Model (II.4)
Model (II.5)
Model (II.6)
Model (II.7)
Model (II.8)
Linear fitting
Predicted Accumulated permeate volume (ml)
Experimental Accumulated permeate volume (ml)

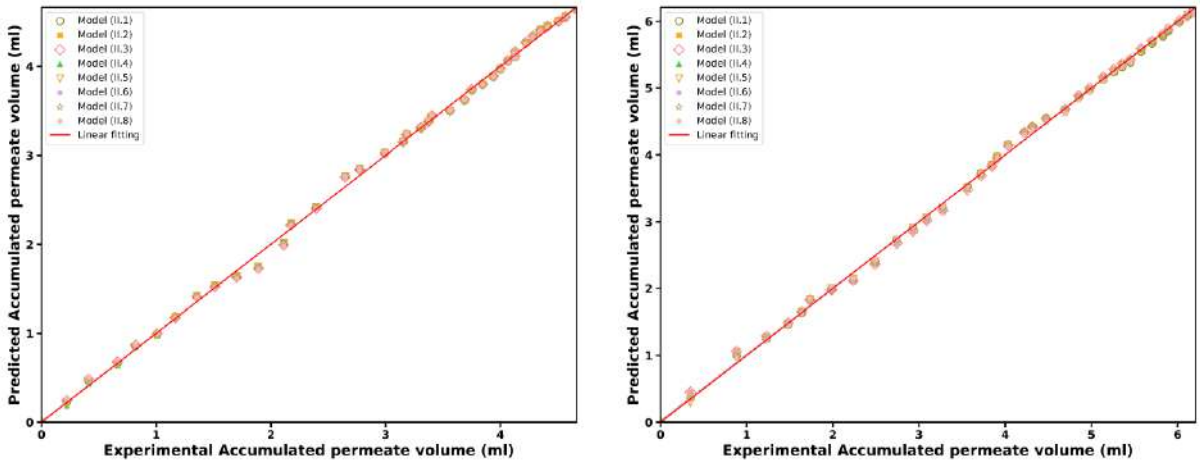
(d)


Model (II.1)
Model (II.2)
Model (II.3)
Model (II.4)
Model (II.5)
Model (II.6)
Model (II.7)
Model (II.8)
Linear fitting
Predicted Accumulated permeate volume (ml)
Experimental Accumulated permeate volume (ml)

(e)


Model (II.1)
Model (II.2)
Model (II.3)
Model (II.4)
Model (II.5)
Model (II.6)
Model (II.7)
Model (II.8)
Linear fitting
Predicted Accumulated permeate volume (ml)
Experimental Accumulated permeate volume (ml)

(f)



(g) (h)

Figure II. 3: Regression plot comparison of the calculated vs. experimental volume values for eight models proposed at different pressures filtration: (a) P=2psi, (b) P=5psi, (c) P=10 psi and (d) P= 20 psi for DB II. 1 and (e) P=5 psi (pQR150), (f) P=8 psi (pQR150), (g) P=5 psi (pGEc47) and (h) P=5 psi (pGEc47) for DB II. 2.

Table II. 4: Linear regression vectors [*Linear Equation*:: $y_{i,cal} = \alpha y_{i,exp} + \beta$] *and the performances of empirical fractional estimation models (R, R², and nRMSE).*

Databases	Solution	Pressures (psi)	α	β	R	R²	nRMSE%
DB II. 1	BSA	P=2	0.9999	10.0000	0.9973	0.9945	2.2748
		P=5	0.9999	-71.0000	0.9988	0.9976	1.8974
		P=10	0.9999	10.0000	0.9993	0.9973	2.3201
		P=20	0.9999	100.0000	0.9987	0.9974	2.2367
DB II. 2	pQR150	P=5	0.9999	$0.0018.10^{-5}$	0.9995	0.9989	2.2384
		P=8	0.9999	$0.0072.10^{-5}$	0.9993	0.9985	1.8578
	pGEc47	P=5	1.0000	$0.0009.10^{-5}$	0.9998	0.9996	1.0907
		P=8	1.0000	$0.0014.10^{-5}$	0.9995	0.9990	1.4092

Figure II. 4, shows another comparison between the proposed models at different pressures and solutions in terms of the relative root mean square error (nRMSE). The proposed models demonstrated a positive outcome with nRMSE values, showcasing the capability and flexibility of empirical fractional estimation models for modeling the clogging of membrane filtration at different pressures and solution conditions. Remarkably, the fifth model stood out by yielding

optimal nRMSE values compared to the other models. All comparisons and results from the previous analyses affirm the effectiveness of the models in predicting the profiles of clogging of membrane filtration.

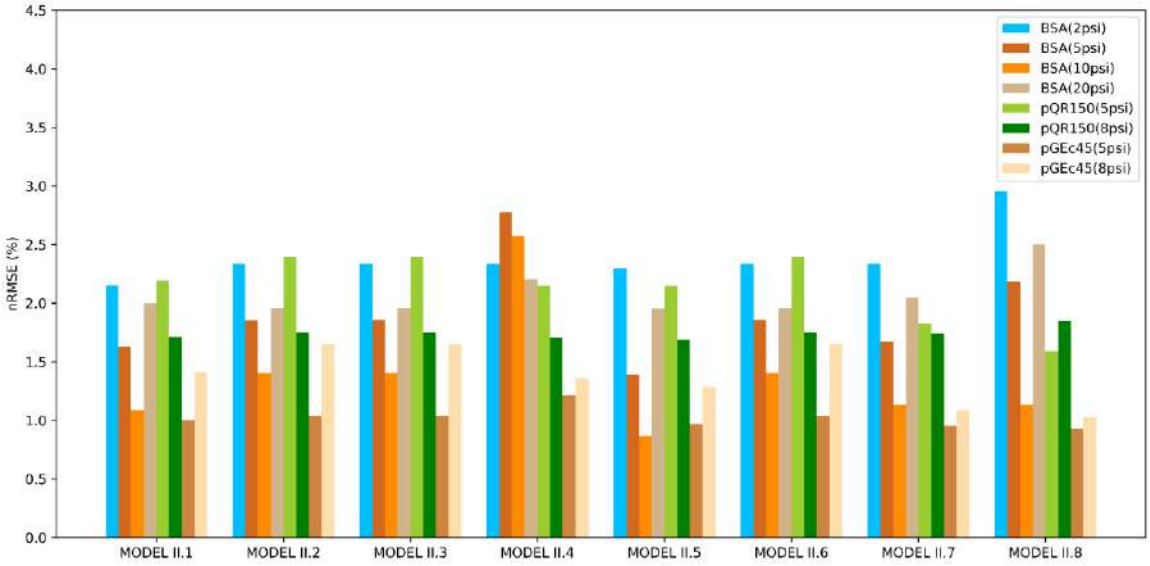


Figure II. 4: nRMSE plot comparison of the proposed models for different pressures and solutions.

II.2.3. Application of Hermia's model to clogging mechanisms

Understanding fouling mechanisms is essential for identifying the optimal filtration conditions, including process parameters, product–membrane interactions, and the optimization of membrane characteristics such as pore structure (Affandy, Keshavarz-Moore, and Versteeg 2013; Zydney and Ho 2002). To analyze membrane clogging, mathematical approaches have been developed to describe the transitions between different clogging mechanisms. In this context, Hermia's model provides a widely used framework.

By applying logarithmic transformation to both sides of Hermia's Equation (I.2. 3) and performing linear regression, the coefficient corresponding to the clogging index n can be determined. This parameter serves as a diagnostic tool to identify the dominant fouling mechanism during filtration.

$$ln\left(\frac{d^2t}{dv^2}\right) = n.ln\left(\frac{dt}{dv}\right) + C \qquad (II.\ 26)$$

Where C is constant ($C = ln(k); k = \exp(C)$) and k present constant of clogging.

It should be emphasized that the reliability of this analysis, namely the statistical accuracy of the estimated values of n, depends strongly on the quality of fit between the mathematical expressions and the original volume–time data. The derivatives of $\left(\frac{dt}{dV}\right)$ and $\left(\frac{d^2t}{dv^2}\right)$ were obtained analytically from Model (II. 6), which provided a good fit while requiring the fewest parameters. Nonetheless, even small deviations between the experimental data and the fitted curve may significantly amplify errors in the calculated derivatives. Since the focus of this study is on the variation of the general law constants, such errors can be partially mitigated by performing best-fit analyses on data subsets. Table II. 5, presents the equations of Model (II. 6), its corresponding derivatives.

Table II. 5: Equations of Model (II. 6), its derivatives.

Model II.6 ($v = f(t)$)	Model II.6 ($t = f(v)$)	First derivate	Second derivate
$v = \frac{a\,t^N}{(1 + b.t^N)}$	$t = \frac{v^m}{(a - b.v)^m}$	$\frac{dt}{dv} = \frac{a.m.v^{m-1}}{(a - b.v)^{m+1}}$	$\frac{d^2t}{dv^2} = \frac{a.m\,(a.m - a + 2.b.v)}{(a - b.v)^{m+2}}$

v: accumulated volume; t: time of filtration. and $m = 1/N$ (m and N constant).

The adjustment parameters (a, b, and m) of Model (II. 6) in Table II. 6, the clogging index (n), the clogging constant (k), and the coefficient of determination (R^2) obtained from Equation (II. 26) are reported. For the BSA solution, the clogging index (n) at different pressures remained close to 1.5, indicating standard clogging (n = 1.5028 at P = 2 psi, n = 1.4976 at P = 5 psi, n = 1.4975 at P = 10 psi, and n = 1.5014 at P = 20 psi). For solution pQR150, the clogging index values were n = 1.3470 at P = 5 psi and n = 1.4237 at P = 8 psi, while for solution pGEc47 they were n = 1.4417 at P = 5 psi and n = 1.3147 at P = 8 psi. These n values fall between 1 and 1.5, corresponding to intermediate and standard clogging. These findings are consistent with results reported in (Affandy, Keshavarz-Moore, and Versteeg 2013; Bowen, Calvo, and Hernández 1995; Tracey and Davis 1994).

Table II. 6: Adjustments parameters (a, b, and m) of model (II. 6), the clogging index (n), clogging constant (k), and coefficient of determination (R).

Databases	Solution	Pressures (psi)	a	b	m	n	k	R^2
DB II. 1	BSA	P=2	0.1774	0.1627	1.0981	1.5028	16.3987	0,9858
		P=5	0.2943	0.1254	0.9016	1.4976	8.1043	0,9981
		P=10	0.5603	0.1022	0.8903	1.4975	1.3152	0,9931
		P=20	1.2838	0.1836	1.0798	1.5014	0.0611	0,9991
DB II. 2	pQR150	P=5	0.9624	0.1708	1.1989	1.3470	0.3508	0.9989
		P=8	2.1956	0.4334	1.0760	1.4273	0.1283	0.9982
	pGEc47	P=5	2.0020	0.2680	1.0387	1.4417	0.1002	0.9981
		P=8	3.0403	0.4291	1.2492	1.3147	0.0629	0.9926

To further assess the predictive performance, the proposed models were compared with Hermia's standard and combined clogging models. In this comparative analysis, both approaches were applied to the same clogging mechanisms for DB II. 1and DB II. 2, and their performance was evaluated using the relative model fitting error (R^2 and SSR). Hermia's standard model characterizes clogging as gradual pore constriction due to internal fouling, where particles progressively obstruct the membrane pores (Affandy, Keshavarz-Moore, and Versteeg 2013; Laska et al. 2005). The combined model describes a transition from intermediate clogging, caused by particle deposition on the membrane surface, to standard clogging through pore constriction. This dual-mechanism framework provides a more comprehensive description of complex fouling dynamics (Affandy, Keshavarz-Moore, and Versteeg 2013; Bolton, Glen, LaCasse and , Kuriyel 2006). The equations for these models are provided in Table I.2. 2 Equation (Eq. I.2. ***15***) and Equation (Eq. I.2. ***18***) in Table I.2. 3.

When benchmarked against these reference models, the proposed empirical model demonstrated superior predictive capability. As summarized in Table II. 7, it provided more accurate estimations of filtrate volume accumulation under the tested clogging conditions, capturing the dynamics of material buildup with higher precision than the reference models.

Table II. 7: Results of the comparative analysis of model accuracy.

solution	Pressure (psi)	Relative model fitting error	Reference Model		Proposed Model							
			Equation (Eq. I.2. ***15***)	Equation (Eq. I.2. ***18***)	model (II. 1)	model (II. 2)	model (II. 3)	model (II. 4)	model (II. 5)	model (II. 6)	model (II. 7)	model (II. 8)
SBA	2	R^2	0.9927	0.9934	0.9945	0.9936	0.9936	0.9935	0.9937	0.9936	0.9631	0.9897
		SSR	4.23E+06	3.80E+06	0.0318	0.0372	0.0372	0.0372	0.0361	0.0372	0.1846	0.0600
	5	R^2	0.9964	0.9964	0.9981	0.9975	0.9975	0.9944	0.9986	0.9975	0.9920	0.9978
		SSR	1.55E+07	1.55E+07	0.0845	0.1096	0.1096	0.2221	0.0611	0.1096	0.2440	0.0892
	10	R^2	0.9977	0.9977	0.9993	0.9989	0.9989	0.9962	0.9996	0.9989	0.9942	0.9989
		SSR	5.29E+07	5.29E+07	0.1571	0.2624	0.2624	0.8774	0.1000	0.2624	0.1000	0.2624
	20	R^2	0.9971	0.9978	0.9978	0.9978	0.9978	0.9972	0.9978	0.9977	0.9978	0.9964
		SSR	8.47E+07	6.60E+07	0.6542	0.6546	0.6546	0.8255	0.6538	0.7152	0.7152	1.0685
pGEc45(56 kb)	5	R^2	0.9963	0.9989	0.9988	0.9985	0.9985	0.9988	0.9988	0.9985	0.9991	0.9994
		SSR	0.3914	0.1211	0.0605	0.0652	0.0565	0.0518	0.0924	0.0652	0.0719	0.0887
	8	R^2	0.9960	0.9968	0.9987	0.9986	0.9986	0.9987	0.9987	0.9986	0.9986	0.9985
		SSR	0.3270	0.2606	0.1275	0.1745	0.1052	0.1190	0.1745	0.0654	0.0757	0.0677
pGEc45(56 kb)	5	R^2	0.9989	0.9993	0.9997	0.9997	0.9997	0.9995	0.9997	0.9997	0.9997	0.9997
		SSR	0.2119	0.1402	0.1313	0.1415	0.1258	0.1323	0.1571	0.0748	0.0914	0.0685
	8	R^2	0.9920	0.9981	0.999	0.9987	0.9987	0.9991	0.9992	0.9987	0.9994	0.9995
		SSR	1.0634	0.2575	0.1070	0.1115	0.1041	0.1204	0.1115	0.1211	0.1109	0.1064

II.3. Conclusion

This chapter presents eight empirical fractional estimation models developed to characterize the clogging dynamics in membrane filtration. These models aim to capture the progression of filtrate volume under various operating conditions. Statistical analyses demonstrated that all models exhibited a strong correlation with the experimental data, highlighting their robustness and reliability across different pressures and filtration solutions. Among these models.

The investigation of clogging mechanisms using Hermia's model provided additional insights. For the first database, the clogging index values were close to 1.5, pointing toward a standard clogging mechanism. For the second database, the values lay between 1 and 1.5, suggesting a transition between intermediate and standard clogging. These results are in line with previously published findings and confirm the soundness of the proposed methodology (Bowen, Calvo, and Hernández 1995; Tracey and Davis 1994) and (Affandy, Keshavarz-Moore, and Versteeg 2013).

To contextualize our models, they were evaluated against Hermia's classical formulations. While Hermia's models retain significance for their mechanistic insights, the empirical fractional models presented here demonstrated superior accuracy in predicting filtrate volume over time. This underscores a critical distinction: the proposed models exhibit robust predictive performance but offer limited insight into the underlying physical processes.

In summary, the empirical fractional models introduced in this chapter make a meaningful contribution to the mathematical modeling of membrane clogging. They offer practical and reliable tools for simulating filtration performance, with potential applications in process optimization, design, and monitoring. However, the lack of direct mechanistic interpretation remains a limitation that future research should address. In the next chapter, a new generalized fractional model is proposed, aiming to identify clogging mechanisms in a single step.

Chapiter III:

A new general fractional model for one-step calculation to identify membrane clogging mechanisms

This chapter is an article published in

scientific reports

Reader's guide

This chapter addresses the fractional approach to membrane clogging by presenting its theoretical basis, methodological framework, and validation results. It introduces the fractional formulation of the general clogging equation and its solutions, which constitute the foundation of the proposed models. The datasets used for validation are then described, followed by the optimization algorithm applied for parameter estimation and the criteria adopted for evaluating model performance. The results and discussion section covers both the theoretical validation of the fractional model, highlighting its reduction to classical models when $\alpha = 1$, and the experimental validation through the optimization of the parameters n, k, and α. A comparative analysis is also provided between the general EDF model and models reported in the literature. The chapter closes with a general conclusion that synthesizes the main outcomes and underlines the contribution of the fractional modeling approach to the study of membrane clogging.

III.1. Background

Fractional calculus is a generalization of classical differentiation and integration, extending these operations to arbitrary, non-integer orders (Alanzi et al. 2025; M. R. S. Ammi, El Kinani, and Torres 2012). It concerns integral and derivative operators of real or complex order and their applications, lying at the intersection of probability, differential equations, and mathematical physics (Sayevand and Moradi 2021).

The concept dates back to 1695, when Leibniz, in correspondence with L'Hôpital, introduced the idea of a half-order derivative (Atangana and Owolabi 2017; Bourdin 2017). He proposed extending his formula for the k^{th} derivative of a product (with k a positive integer) to any real order $k > 0$, and later referred to derivatives of arbitrary order in letters to Bernoulli (Bourdin 2017). What began as a speculative idea gradually evolved into a rich mathematical theory (Benkerrouche et al. 2022).

For nearly three centuries, fractional calculus developed as a largely theoretical discipline, pursued mainly by mathematicians (M. R. S. Ammi, El Kinani, and Torres 2012). Its practical value became evident only in recent decades, as fractional derivatives and differential equations found applications in a wide range of scientific and engineering problems (Atangana and Owolabi 2017).

The central notion is the substitution of natural numbers with rational (or real) numbers in the order of differentiation. Despite its apparent simplicity, this extension introduces powerful features, notably the ability to describe memory and non-local effects (Redhwan et al. 2024). Such properties allow fractional models to capture hereditary characteristics and long-term dependencies that cannot be represented by classical integer-order approaches (Debnath 2003; Seemab et al. 2021). The non-locality and memory effects are the main reasons behind the growing interest in fractional methods across scientific disciplines (Sayevand and Moradi 2021)

Today, fractional calculus is widely applied in diverse areas. Its mathematical framework supports models in physics, chemistry, biology, economics, signal and image processing, calculus of variations, control theory, electrochemistry, viscoelasticity, and electrical circuits (M. R. S. Ammi, El Kinani, and Torres 2012). Fractional partial differential equations, in particular, have become central tools for developing nonlinear models and analyzing dynamical systems, with applications in chaos theory, finance, disordered media, and optics (Alkan 2024). Beyond these, fractional models are increasingly used in bioengineering, system dynamics, control, and medicine (Redhwan et al. 2024).

The phenomenological understanding, control, and limitation of clogging mechanisms are currently a major focus of applied research in membrane technology (Alborzi et al. 2022). Numerous models in the literature describe and identify different clogging mechanisms, ranging from initial pore blockage to deposit formation and cake filtration (Hermia 1985; Iritani and Katagiri 2016). Most of these models are based primarily on empirical models established by Herman and Bredéé (Hermans and Bredée 1935) and modified by Hermia (Hermia 1985). A limitation of these models is their consideration of clogging as related to a single, unique mechanism (C.-C. Ho and Zydney 2000). Given these limitations, various authors continuously propose improvements to Hermia's models (Dahdouh and Wisniewski 2018; Zydney and Ho 2002). They developed a combined model that describes clogging as a transition between pore clogging and cake filtration mechanisms, to describe clogging behavior during protein microfiltration at constant pressure (Mondal and De 2010; Slimane et al. 2018).

To identify different types of clogging phenomena with a single mechanism, Hermia (Hermia 1985) developed a general model for constant pressure filtration , linking the evolution of the cumulative filtrate volume as a function of time $t(v)$, considering that the second derivative of

$t(v)$ is directly proportional to the power of order n $(0 < n < 2)$ of the first derivative of $t(v)$; this model assumes that all membrane pores are of the same size, forming a network of cylindrical pores. These simplifying assumptions fail to account for the more complex reality, as multiple parameters and mechanisms may coexist (Affandy, Keshavarz-Moore, and Versteeg 2013; Xu et al. 2020).

III.2. Fractional approach to membrane clogging

The phenomenon of membrane clogging can be modeled by focusing on the dissipation of a liquid's kinetic energy through the membrane's porous matrix. This modeling involves a complex situation considering various interactions and the coexistence of multiple phenomena across the solution, the membrane, the solution membrane interface, and the operational conditions. The general ordinary partial differential equation (EDPO) for clogging is governed by two parameters (*k* and *n*) Equation (I.2. 3).

$$\frac{d^2t}{dv^2} = k\left(\frac{dt}{dv}\right)^n \qquad \text{(I.2. 3)}$$

With *n* and *k* being constants related to each clogging mechanism, *t* representing the filtration time, and *v* the cumulative filtrate volume. The constant *n* serves as a criterion to identify different mechanisms of membrane pore clogging. Each value of n corresponds to a specific state: $n = 0$ for cake filtration, $n = 1$ for intermediate clogging, $n = 1.5$ for standard clogging, and $n = 2$ for complete clogging. *n* can take intermediate values up to 2.5 for special cases (Hermia 1982; Mokarizadeh and Raisi 2021; Xiao et al. 2019; Xu et al. 2020).

Since the early development of numerical mathematical models, researchers have implemented numerous computational applications to model and predict membrane clogging processes. Progress has been limited, partly because membrane engineering lags behind other branches of engineering in adopting new mathematical theories. Although computational power has increased exponentially and mathematical models have become much more complex than early work, the fundamental issue of dealing with strict constraints and unreliable assumptions persists. As discussed in this chapiter, classical clogging theory is still commonly used, though its applicability to adsorption or biological clogging is recognized as limited and questionable. Classical clogging, according to Hermia (Hermia 1985), continues to be accepted with some

reservations and is taught as a foundation for clogging applications in membrane engineering processes.

Furthermore, membrane engineering lags behind other branches of engineering in terms of innovation and the implementation of new methods and mathematical theories.

The clogging model is based on Hermia (Hermia 1985) requires additional parameters related to the membrane structure to achieve an adequate fit according to the new criterion for identifying different membrane clogging mechanisms. Therefore, if one aims to quantify the clogging phenomenon in a single computational step realistically, fractional calculus could be a powerful mathematical tool capable of providing a breakthrough and significant advancement in the mathematical modeling of membrane clogging. Consequently, the general clogging equation should be modified to include the three parameters (n, k, and α) to incorporate a fractional calculus formulation**:**

$$[\mathcal{D}_v^{2\alpha} t(v)] = \frac{d^{2\alpha} t}{dv^{2\alpha}} = k_n [\mathcal{D}_v^{\alpha} t(v)]^n \qquad \text{(III. 1)}$$

Where $(\mathcal{D}^{\alpha} t)$ is the fractional operator, α is the arbitrary fractional order given by Equation (III. *1*), $(\boldsymbol{\alpha > 0})$. When $\alpha = 1$, the classical clogging equation is obtained (I.2. *3*).

The clogging phenomenon is highly nonlinear, as evidenced by the non-reproducibility of experimental results. This is because different clogging mechanisms can coincide in both space and time, particularly in situations involving significant variations in particle/membrane interactions.

Fractional calculus is a new mathematical tool with applications across various engineering and industrial disciplines. It can be used to describe the dynamic response of a system and/or a transport phenomenon, such as mass transfer (Agutter, Malone, and Wheatley 2000) , heat transfer (Jaques et al. 2017; de Souza Matias et al. 2022), momentum transfer (Khan and Rasheed 2022), charge transfer in nanostructured materials (Šuvakov and Tadić 2010), and diffusion in disordered media with memory effects (Jaques et al. 2017; Simpson et al. 2013). Many researchers have since explored the utility of fractional calculus in solving complex phenomena through ordinary partial differential equations (EDPO) (Almeida 2017).

The main advantages of fractional differential equations over their integer-order counterparts lies in their ability to capture memory effects and non-local behavior, making them particularly suitable for describing physical phenomena with hereditary characteristics and long-term dependencies (Debnath 2003; Seemab et al. 2021). The non-local property and memory effect of fractional derivatives and integrals constitute the main reason for their widespread adoption across various scientific disciplines (Sayevand and Moradi 2021). However, to our knowledge, no one has applied fractional calculus to quantify membrane clogging using Hermia's equation (1982) (I.2. *3*).

Fractional calculus allows the clogging phenomenon to be subdivided into two phenomena based on the fractional number α: $\alpha = 1$ for ordinary clogging and $\alpha > 0$ for fractional clogging.

In ordinary clogging, particles take longer to travel a specific distance compared to a normal distribution. Conversely, in fractional clogging, the time required to cover a given distance is shorter than in ordinary clogging. In other words, the residence time of a particle in ordinary clogging is longer than that in fractional clogging.

Indeed, fractional calculus involves using a non-integer order derivative, which represents a generalization of traditional calculus. In this approach, the natural derivative order $m \epsilon N$, in the differential equation is replaced by the fractional order α defined by Caputo [1967]. Commonly known as the Caputo derivative. This derivative has proven particularly useful operators for modeling non-local behaviors by fractional differential equations (Sayevand and Moradi 2021). The fractional order α given by Equation (III. 1) can be represented using Caputo's approach (Caputo 1967), (Equation (III. 2)). It is significant because, once determined, it allows for the use of initial conditions in problems involving fractional order Equations (Podlubny 1999):

$$\mathcal{D}_t^{\alpha} f(t) = \frac{d^{\alpha} f}{dt^{\alpha}} = \frac{1}{\Gamma(\alpha - m)} \cdot \int_0^t \frac{f^m(\xi)}{(t-\xi)^{\alpha - m + 1}} d\xi \quad \text{, for } m - 1 < \alpha < m + q \qquad \text{(III. 2)}$$

In which $(\mathcal{D}^{\alpha} t)$ is the fractional operator, f is the function differentiable m times $\left(f^{(0)} = f, f^{(1)} = \frac{df}{dt}, \ldots\right)$, α is the fractional number $(m - 1 < \alpha < m + q)$, and Γ is the Gamma function defined by:

$$\Gamma(x) = \int_0^{\infty} e^{-t}.t^{x-1}dt\,, \qquad x\epsilon\mathcal{R}^{+} \tag{III. 3}$$

The Laplace and Fourier integral transforms are among the most commonly used tools for solving ordinary differential equations (EDOs) (de Souza Matias et al. 2019). Although the fractional order α equation is not well-known, it has a well-defined Laplace transform. This is due to the inverse Laplace transform of the Laplace transform. The Laplace transform of a function *f*(*t*), where t ϵ $\Re^{+}$, is defined by Equation (III. 4):

$$\mathcal{L}[f^{\alpha}(t)] = F(s) = \int_0^{\infty} e^{-st}f(t)dt \tag{III. 4}$$

As demonstrated, one can determine the fractional order equation (Liang, Wu, and Chen 2015; de Souza Matias et al. 2022). Equation (III. 5) shows the general relationship for obtaining the Laplace transform of a fractional order equation (α) as a non-integer number with $(m-1 < \alpha < m+q)$; $\left(f^{(0)} = f, f^{(1)} = \frac{df}{dt}, \ldots\right)$:

$$\mathcal{L}[f^{\alpha}(s)] = s^{\alpha}.\mathcal{L}[f(t)](s) - \sum_{k=0}^{m-1}\left[s^{\alpha-1-k}.f^{(k)}(t=0)\right] \tag{III. 5}$$

Therefore, if $\alpha > 0$, Equation (III. *5*) can be simplified to Equation (III. 6) by considering only the first term $k = 0$, which is:

$$\mathcal{L}[f^{\alpha}(s)] = s^{\alpha}.\mathcal{L}[f(t)](s) - s^{\alpha-1}f(t=0) \tag{III. 6}$$

Moreover, if $0 < \alpha < 2$ Equation (III. *5*) can be simplified to Equation (III. 7) by considering only the first two terms for $k = 0$ and $k = 1$, which is:

$$\mathcal{L}[f^{\alpha}(s)] = s^{\alpha}.\mathcal{L}[f(t)](s) - s^{\alpha-1}f(t=0) - s^{\alpha-2}f'(t=0) \tag{III. 7}$$

The systematic development of fractional differential equations began in earnest during the 20th century, marking a crucial transition from theoretical mathematics to practical applications (Gholami 2020). A pivotal moment occurred in 1954 when J.H. Barrett employed the Mittag-Leffler function to express solutions of linear differential equations of non-integer order, identifying the fundamental role of this function in fractional calculus (Giusti et al. 2020). This mathematical breakthrough was paralleled by early applications in physics, particularly through K.S. Cole's work on electrical conductance of biological systems in 1933 and B. Gross's fundamental contributions to dielectric and mechanical relaxation (Giusti et al. 2020).

The field gained significant momentum in the latter half of the 20th century with the contributions of M. Caputo and F. Mainardi to fractional viscoelasticity, demonstrating that the Mittag-Leffler function consistently appears in material functions of systems described by fractional-order constitutive equations (Giusti et al. 2020). By 2007, the Mittag-Leffler function had earned recognition as the "Queen function of fractional calculus" due to its striking relevance for mathematical modeling of numerous phenomena (Giusti et al. 2020; Haubold, Mathai, and Saxena 2009). The Mittag–Leffler function, introduced in 1903, is defined by an infinite series and represents a generalization of the exponential function. It plays an important role in solving fractional differential equations (FDEs).

Table III. 1, summarizes some useful Laplace transforms for fractional resolution, with a bidirectional mapping ($F(s) \leftrightarrow f(t)$).

Table III. 1: Some useful Laplace transforms.

$F(s)$	$f(t)$	$F(s)$	$f(t)$	$F(s)$	$f(t)$
$\frac{1}{s}$	1	$\frac{1}{s^{\alpha}}$	$\frac{t^{\alpha-1}}{\Gamma(\alpha)}$	$\frac{1}{[(s-q)(s-p)]}$	$\left[\frac{1}{(q-p)}\right][e^{qt} - e^{pt}]$
$\frac{1}{s^2}$	t	$\frac{1}{(s-q)}$	e^{qt}	$\frac{s^{\alpha-\beta}}{(s^{\alpha} \pm m)}$	$t^{\beta-1}\mathrm{E}_{\alpha,\beta}(\mp mt^{\alpha})$

where q and p are real constants with $q \neq p$, and α are arbitrary.

III.3. Materials and methods

III.3.1. Fractional solution of the general clogging equation fractional order α with power n (where $n = n$)

The fractional solution of the general clogging equation (Equation (I.2. *3*)(II. *3*)) at constant pressure during the filtration of a Newtonian fluid or a fluid-solid mixture involves the expression $\left({}^{dt}/_{dv}\right)$ of the EDO for $n = n$:

$$\frac{dt}{dv} = [(1-n)k_n v + C_n]^{\frac{1}{1-n}} \ , \ n \neq 1 \qquad \text{(III. 8)}$$

Introducing the following variable change:

$$V = [(1-n)k_n v + C_n]^{\frac{1}{1-n}} , \ n \neq 1 \qquad \text{(III. 9)}$$

Equation (III. 9) becomes:

$$\frac{dt}{dV} = \frac{1}{k_n} V^{1-n} \quad \text{(III. 10)}$$

The fractional differential equation of Equation (III. 10), can be written as:

$$\mathfrak{D}_V^{\propto} t(V) = \frac{1}{k_n} V^{1-n} \quad \text{(III. 11)}$$

The Laplace transform of Equation (III. 11), using Equation (III. 6) and Table III. 1, is:

$$t(s) = \frac{\Gamma(2-n)}{k_n} . \frac{1}{s^{(2-n+\alpha)}} \quad \text{(III. 12)}$$

The inverse Laplace transform (L^{-1}) of Equation (III. 12), using V and Table 1, yields:

$$t(V) = \frac{\Gamma(2-n)}{k_n \Gamma(2-n+\alpha)} V^{1-n+\alpha} \quad \text{(III. 13)}$$

The combination of Equations (III. 9) and (III. 13) yields:

$$t(v) = \frac{\Gamma(2-n)}{k_n \Gamma(2-n+\alpha)} [(1-n)k_n v + C_n]^{\frac{1-n+\alpha}{1-n}} \quad , n \neq 1 \quad \text{(III. 14)}$$

To satisfy the initial condition $t\ (v\ =\ 0)\ =\ 0$, Equation (III. 14) takes the form:

$$t(v) = \frac{\Gamma(3-n)}{(2-n)k_n \Gamma(2+\alpha-n)} . \left\{ [(1-n)k_n v + C_n]^{\frac{1-n+\alpha}{1-n}} - [C_n]^{\frac{1-n+\alpha}{1-n}} \right\} \quad , n \neq 1 \text{ and } n \neq 2 \quad \text{(III. 15)}$$

Where $k_n = [m^{-3}]$ is constant of clogging.

Calculation of $v(t)$ from Equation (III. 15), which is:

$$v(t) = \frac{1}{(1-n)k_n} . \left\{ \left[\frac{(2-n)k_n \Gamma(2+\alpha-n)}{\Gamma(3-n)} t + C_n^{\frac{1+\alpha-n}{1-n}} \right]^{\frac{1-n}{1+\alpha-n}} - C_n \right\} \quad , n \neq 1 \text{ and } n \neq 1+\alpha \quad \text{(III. 16)}$$

Where $k_n = [s]$.

Calculation of the permeate flux $J(t)$ from Equation (III. 16).

$$J(t) = \frac{dv}{dt} = \frac{(2-n)\Gamma(2+\alpha-n)}{(1+\alpha-n)\Gamma(3-n)} . \left\{ \frac{(2-n)k_n \Gamma(2+\alpha-n)}{\Gamma(3-n)} t + [C_n]^{\frac{1+\alpha-n}{1-n}} \right\}^{\frac{\alpha}{n-1-\alpha}} , n \neq 1 ;\ n \neq 1+\alpha \quad \text{(III. 17)}$$

Where $k_n = [s]$.

Calculation of the integration constant C_n

Starting from $J(t=0)$ J_0 Equation (III. 17) gives

$$C_n = \left[\frac{(1+\alpha-n)\Gamma(3-n)}{(2-n)\Gamma(2+\alpha-n)} J_0\right]^{\frac{n-1}{\alpha}} \quad , n \neq 2 \text{ et } \alpha \neq 0 \qquad \text{(III. 18)}$$

Calculation of $J(v)$

By substituting the expression for *t* (from Equation (III. 15)) into Equation (III. 17), we obtain:

$$J(v) = \frac{(2-n)\Gamma(2+\alpha-n)}{(1+\alpha-n)\Gamma(3-n)} . \{(1-n)k_n v + C_n\}^{\frac{\alpha}{n-1}} \quad , n \neq 1 \text{ et } n \neq 1+\alpha \qquad \text{(III. 19)}$$

Where $k_n = [m^{-3}]$.

Starting from $J(v=0) = J_0$, we obtain Equation (III. *18*).

The results of the fractional solutions for specific values of *n* (*n* = 1 and *n* = 2), as well as for intermediate values (*n* = 0, 0.5, 1.5, and 2.5), proposed in Equation (I.2. *3*) under constant pressure, are provided in Table.

Table III. 2: Proposed new fractional models EDF (n, k, α) for different values of n from Equation (I.2. 13) at constant pressure (cases of $v = f(t)$ and $t = f(v)$).

Function	$\frac{d^{2\alpha}t}{dv^{2\alpha}} = k_n\left[\frac{d^{\alpha}t}{dv^{\alpha}}\right]^n$	$v = f(t)$		$t = f(v)$	
Cake Filtration	*n = 0*	$v(t) = \frac{1}{k_0}.\left\{\left[\frac{2k_0\Gamma(2+\alpha)}{\Gamma(3)}t + C_0^{(1+\alpha)}\right]^{\frac{1}{1+\alpha}} - C_0\right\}$	(III. 20)	$t(v) = \frac{\Gamma(3)}{2k_0\Gamma(2+\alpha)}.\{[k_0v + C_0]^{1+\alpha} - [C_0]^{1+\alpha}\}$	(III. 21)
Near-Intermediate clogging	*n = 0.5*	$v(t) = \frac{1}{0.5k_{0.5}}.\left\{\left[\frac{1.5k_{0.5}\Gamma(1.5+\alpha)}{\Gamma(2.5)}t + C_{0.5}^{\frac{0.5+\alpha}{0.5}}\right]^{\frac{0.5}{0.5+\alpha}} - C_{0.5}\right\}$	(III. 22)	$t(v) = \frac{\Gamma(2.5)}{1.5k_{0.5}\Gamma(1.5+\alpha)}.\left\{[0.5k_{0.5}v + C_{0.5}]^{\frac{0.5+\alpha}{0.5}} - [C_{0.5}]^{\frac{0.5+\alpha}{0.5}}\right\}$	(III. 23)
Intermediate Clogging	*n = 1*	$v(t) = (\alpha-1)J_0t + \frac{1}{k_1}\left[\ln\left\{1 + \frac{k_1J_0\Gamma(\alpha+1)}{\Gamma(2)}t\right\}\right]^{\frac{1}{\alpha}}$	(III. 24)	$t(v,t) = \frac{\Gamma(2)}{k_1J_0\Gamma(\alpha+1)}.\{-1 + exp[k_1v - k_1(\alpha-1)J_0t]^{\alpha}\}$	(III. 25)
Standard Clogging	*n = 1.5*	$v(t) = \frac{1}{-0.5k_{1.5}}.\left\{\left[\frac{0.5k_{1.5}\Gamma(0.5+\alpha)}{\Gamma(1.5)}t + C_n^{\frac{-0.5+\alpha}{-0.5}}\right]^{\frac{-0.5}{-0.5+\alpha}} - C_{1.5}\right\}$	(III. 26)	$t(v) = \frac{\Gamma(1.5)}{0.5k_{1.5}\Gamma(0.5+\alpha)}.\left\{[-0.5k_{1.5}v + C_{1.5}]^{\frac{-0.5+\alpha}{-0.5}} - [C_{1.5}]^{\frac{-0.5+\alpha}{-0.5}}\right\}$	(III. 27)
Complete Clogging	*n = 2*	$v(t) = \frac{J_0}{k_2}\left\{1 - \left[\exp\left(\frac{(-1)^{\alpha}k_2\Gamma(\alpha+1)}{\Gamma(2)}t\right)\right]^{\frac{1}{\alpha}}\right\}$	(III. 28)	$t(v) = \frac{(-1)^{\alpha}\Gamma(2)}{k_2\Gamma(\alpha+1)}.ln\left[1 - \frac{k_2}{J_0}v\right]^{\alpha}$	(III. 29)
Standard Clogging (2nd type)	*n = 2.5*	$v(t) = \frac{1}{-1.5k_{2.5}}.\left\{\left[\frac{-0.5k_{2.5}\Gamma(-0.5+\alpha)}{\Gamma(0.5)}t + C_{2.5}^{\frac{-1.5+\alpha}{-1.5}}\right]^{\frac{-1.5}{-1.5+\alpha}} - C_{2.5}\right\}$	(III. 30)	$t(v) = \frac{\Gamma(0.5)}{-0.5k_{2.5}\Gamma(-0.5+\alpha)}.\left\{[-1.5k_{2.5}v + C_{2.5}]^{\frac{1-n+\alpha}{1-n}} - [C_n]^{\frac{-1.5+\alpha}{-1.5}}\right\}$	(III. 31)
Initial Condition		*v (t=0) =0*		*t (v=0) =0*	

Table III. 3: Proposed new fractional models EDF (n, k, α) for different values of n from Equation (I.2. 13) *at constant pressure (cases of $J = f(t)$ and $J = f(v)$).*

Function	$\frac{d^{2\alpha}t}{dv^{2\alpha}} = k_n\left[\frac{d^{\alpha}t}{dv^{\alpha}}\right]^n$	$J = f(t)$		$J = f(v)$	
Cake Filtration	*n = 0*	$J(t) = \frac{2\Gamma(2+\alpha)}{(1+\alpha)\Gamma(3)}.\left\{\frac{2k_0\Gamma(2+\alpha)}{\Gamma(3)}t + [C_0]^{\frac{1+\alpha}{1}}\right\}^{\frac{-\alpha}{1+\alpha}}$	(III. 32)	$J(v) = \frac{\Gamma(2+\alpha)}{(1+\alpha)}.\{k_0 v + C_0\}^{-\alpha}$	(III. 33)
Near-Intermediate clogging	*n = 0.5*	$J(t) = \frac{1.5\Gamma(1.5+\alpha)}{(0.5+\alpha)\Gamma(2.5)}.\left\{\frac{1.5k_{0.5}\Gamma(0.5+\alpha)}{\Gamma(2.5)}t + [C_{0.5}]^{\frac{0.5+\alpha}{0.5}}\right\}^{\frac{-\alpha}{0.5+\alpha}}$	(III. 34)	$J(v) = \frac{1.5\Gamma(1.5+\alpha)}{(0.5+\alpha)\Gamma(2.5)}.\{0.5k_{0.5}v + C_{0.5}\}^{\frac{\alpha}{-0.5}}$	(III. 35)
Intermediate Clogging	*n = 1*	$J(t) = (\alpha-1)J_0 + \frac{J_0\Gamma(\alpha+1)}{\alpha\Gamma(2)\left\{1+\frac{k_1J_0\Gamma(\alpha+1)}{\Gamma(2)}t\right\}}\left[\ln\left\{1 + \frac{k_1J_0\Gamma(\alpha+1)}{\Gamma(2)}t\right\}\right]^{\frac{1}{\alpha}-1}$	(III. 36)	$J(t,v) = (\alpha-1)J_0 + \frac{J_0\Gamma(\alpha+1)[k_1v - k_1(\alpha-1)J_0t\,]^{1-\alpha}}{\alpha\Gamma(2)exp[k_1v - k_1(\alpha-1)J_0t\,]^{\alpha}}$	(III. 37)
Standard Clogging	*n = 1.5*	$J(t) = \frac{0.5\Gamma(0.5+\alpha)}{(-0.5+\alpha)\Gamma(1.5)}.\left\{\frac{0.5k_{1.5}\Gamma(0.5+\alpha)}{\Gamma(1.5)}t + [C_{1.5}]^{\frac{-0.5+\alpha}{-0.5}}\right\}^{\frac{\alpha}{0.5-\alpha}}$	(III. 38)	$J(v) = \frac{0.5\Gamma(0.5+\alpha)}{(-0.5+\alpha)\Gamma(1.5)}.\{-0.5k_{1.5}v + C_{1.5}\}^{\frac{\alpha}{0.5}}$	(III. 39)
Complete Clogging	*n = 2*	$J(t) = \frac{(-1)^{\alpha+1}J_0\Gamma(\alpha+1)}{\alpha\Gamma(2)}\left[\exp\left(\frac{(-1)^{\alpha}k_2\Gamma(\alpha+1)}{\Gamma(2)}t\right)\right]^{\frac{1}{\alpha}}$	(III. 40)	$J(v) = \frac{(-1)^{\alpha+1}J_0\Gamma(\alpha+1)}{\alpha\Gamma(2)}\left(1-\frac{k_2}{J_0}v\right)$	(III. 41)
Standard Clogging (2nd type)	*n = 2.5*	$J(t) = \frac{-0.5\Gamma(-0.5+\alpha)}{(-1.5+\alpha)\Gamma(0.5)}.\left\{\frac{-0.5k_{2.5}\Gamma(-0.5+\alpha)}{\Gamma(0.5)}t + [C_{2.5}]^{\frac{-1.5+\alpha}{-1.5}}\right\}^{\frac{\alpha}{1.5-\alpha}}$	(III. 42)	$J(v) = \frac{-0.5\Gamma(-0.5+\alpha)}{(-1.5+\alpha)\Gamma(0.5)}.\{-1.5k_{2.5}v + C_{2.5}\}^{\frac{\alpha}{1.5}}$	(III. 43)
Initial Condition		$J(t=0) = f(J_0)$		$J(v=0) = f(J_0)$	

Where: C_n is a constant, defined by the following equation for each value of n:

$$C_n = \left[\frac{(1+\alpha-n)\Gamma(3-n)}{(2-n)\Gamma(2+\alpha-n)}J_0\right]^{\frac{n-1}{\alpha}} \quad \text{(III. 44)}$$

$$C_0 = \left[\frac{(1+\alpha)\Gamma(3)}{(2)\Gamma(2+\alpha)}J_0\right]^{\frac{-1}{\alpha}} \quad \text{(III. 45)}$$

$$C_{0.5} = \left[\frac{(0.5+\alpha)\Gamma(2.5)}{1.5\Gamma(1.5+\alpha)}J_0\right]^{\frac{-0.5}{\alpha}} \quad \text{(III. 46)}$$

$$C_{1.5} = \left[\frac{(-0.5+\alpha)\Gamma(1.5)}{0.5\Gamma(0.5+\alpha)}J_0\right]^{\frac{0.5}{\alpha}} \quad \text{(III. 47)}$$

$$C_{2.5} = \left[\frac{(-1.5+\alpha)\Gamma(0.5)}{-0.5\Gamma(-0.5+\alpha)}J_0\right]^{\frac{1.5}{\alpha}} \quad \text{(III. 48)}$$

III.3.2. Collection of the databases

For this chapter, data were sourced from three available datasets in the literature to provide a comprehensive basis for validating and refining the proposed models, each representing different mechanisms of membrane clogging. These datasets were selected for their reliability and relevance to the investigated mechanisms. Specifically, the data encompasses three distinct clogging mechanisms: cake filtration, intermediate blocking, and standard blocking.

First database (DB III. 1), obtained from Salahi et al. (Salahi, Abbasi, and Mohammadi 2010), investigated the decline of permeate flux during the ultrafiltration (UF) of oily wastewater using a polyacrylonitrile (PAN) membrane with a molecular weight cut-off of 20 kDa. The feed solution was collected from the API separator of the Tehran refinery. To study the influence of operating conditions, the authors performed nine experiments designed through an orthogonal array (L9), varying four parameters at three levels: feed temperature (25, 37.5, and 50 °C), transmembrane pressure (1.5, 3, and 4.5 bar), cross-flow velocity (0.25, 0.75, and 1.25 m/s), and pH (4, 7, and 10). This systematic approach allowed the assessment of permeate flux and fouling resistance under different operating conditions, thereby identifying the most significant factors affecting UF performance. In the present chapter, we specifically use the experimental data obtained from three conditions: Experiment 1 (TMP = 1.5 bar, T = 25 °C, CFV = 0.25 m/s, pH = 4), Experiment 5 (TMP = 3.0 bar, T = 37.5 °C, CFV = 1.25 m/s, pH = 4), and Experiment 6 (TMP = 4.5 bar, T = 37.5 °C, CFV = 0.25 m/s, pH = 7) DB III. 1.

For the second database (DB III. 2), obtained from Aslam et al. (Aslam, Lee, and Kim 2015), the study investigated the combined effects of particle size and membrane pore size on membrane fouling by examining the permeate flux decline of mixed liquor suspension from an autotrophic nitrogen removal sequencing batch reactor (SBR) at a constant pressure of 2.76×10^4 Pa. Initially, the flux decline was rapid but became more gradual over time. The supernatant solution, prepared by settling the mixed liquor suspension for 30 minutes, exhibited a more pronounced flux decline compared to the mixed liquor suspension, despite containing smaller particle sizes and fewer foulant materials. Particle size distributions revealed that most particles in both feed suspensions were larger than 0.1 µm, with the supernatant having a higher proportion of smaller particles compared to the mixed liquor suspension. The particle size distribution ranged from 1 to 50 µm for the mixed liquor suspension and from 0.3 to 10 µm for

the supernatant. This difference was attributed to the removal of settleable particles during the settling process. The experiments utilized porous microfiltration membranes with a 0.1 µm pore size, indicating that most particles in the feed suspensions were deposited on the membrane. In the present chapter, we use the dataset corresponding to the supernatant solution. The third dataset corresponds to the same data presented in Chapter II (DB II. 2), for the study by (Affandy, Keshavarz-Moore, and Versteeg 2013). The data collect presented in Table annex 2. 1 and Table annex 2. 2, in annex 2. Table III. 4, summarizes the conditions of the three datasets used in this chapter. The statistical analysis of the database variables shows in Table III. 5.

Table III. 4: Summary of experimental data for different clogging mechanisms in membrane filtration.

Database	Pressure (TMP)	Temperature (T)	Membrane Type	Solution Type	Clogging mechanisms	References
DB III. 1	1.5 bar	25 °C	Polyacrylonitrile (PAN)	Oily wastewater	cake filtration (n=0)	(Salahi, Abbasi, and Mohammadi 2010)
	3 bar	37.5 °C				
	4.5 bar	37.5 °C				
DB III. 2	2.76×10^4 Pa	35 °C	Glass-Fiber Filter, Pore Size: 1.2 µm	Microbial suspensions from a sequencing batch reactor (SBR) (Supernatant solution)	intermediate clogging (n=1)	(Aslam, Lee, and Kim 2015)
DB III. 2	5 Psi	25°C	Polyvinylidene fluoride (PVDF) membrane	pQR150 (kanamycin resistance, 20 kb)	standard clogging (n=1.5)	(Affandy, Keshavarz-Moore, and Versteeg 2013; Cherifi et al. 2025)
	8 Psi	25°C				
	5 Psi	25°C		pGEc47 (tetracycline resistance, 56 kb)		
	8 Psi	25°C				

Table III. 5: Statistical analysis of experimental data.

Databases	Solution	Pressures	Variable	Min	Max	Mean	STD
DB III. 1	Oily wastewater	1.5 bar	t(h)	0.0106	2.5181	1.0779	0.8043
			J(L/m^2.h)	80.8989	537.0790	185.8502	122.4404
		3bar	t(h)	0.0032	2.5179	1.0817	0.8113
			J(L/m^2.h)	146.0670	943.8200	320.9238	204.6456
		4.5 bar	t(h)	0.0031	2.5184	1.0889	0.8020
			J(L/m^2.h)	116.8540	838.2020	263.9201	179.5795
DB III. 2	Microbial suspensions from a sequencing batch reactor (SBR) (Supernatant solution)	2.76.104 Pa	t(min)	0.0859	796.6690	394.2782	232.9630
			J(normalized)	0.0859	0.8912	0.2455	0.2038
			t(min)	0.0748	19.7201	9.7166	5.8355
			Q(m^3/min)	3.24E-06	1.10E-04	1.19E-05	1.66E-05
DB II. 2	pQR150 (kanamycin resistance, 20 kb)	5 Psi	t(min)	0.0000	35.0000	11.5195	9.4282
			v(ml)	0.0000	4.2216	2.3813	1.5266
		8 Psi	t(min)	0.0000	35.0000	9.1865	7.4096
			v(ml)	0.0000	4.6639	2.9845	1.6623
	pGEc47 (tetracycline resistance, 56 kb)	5 Psi	t(min)	0.0000	35.0000	10.0541	8.8337
			v(ml)	0.0000	6.6177	3.8831	2.4134
		8 Psi	t(min)	0.0000	35.0000	10.0298	8.8963
			v(ml)	0.0000	6.2080	4.0005	2.3466

III.3.3. Optimization algorithm

We utilized the Dragonfly Algorithm to compute suitable initial parameters by minimizing the root mean square error (RMSE). The parameter set that yielded the best fit was then used as the initial input of the nlinfit function in MATLAB, which employs the Levenberg–Marquardt algorithm for nonlinear regression. The hybrid approach improved the convergence behavior and provided more accurate parameter estimation in a curve-fitting problem. To confirm the robustness and reliability of the model, the entire optimization process was independently repeated three times (i.e., three separate full runs of optimization), each involving internal iterations. Figure III. 1. presents a diagram outlining the main steps of the modeling process.

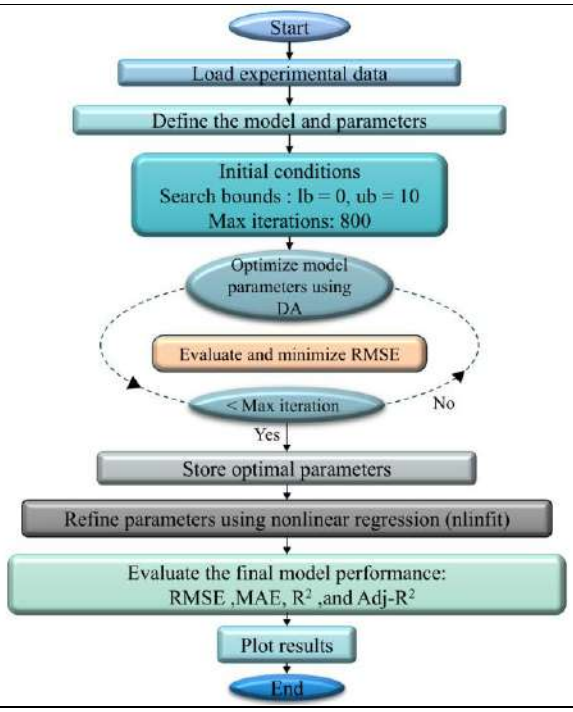


Figure III. 1: Structure of the DA coupled with nlinfit optimization Algorithm.

III.3.4. Evaluating the performance of proposed models

In this chapiter, we begin by evaluating the proposed models using experimental data and standard statistical performance metrics, including the correlation coefficient (R), Equation (III. 49), indicates the strength and direction of the linear relationship between the calculated and experimental values. It ranges from -1 to +1, with +1 signifying a perfect positive correlation, -1 a perfect negative correlation, and 0 denoting no correlation at all. Typically, values between ±0.8 and ±1 are interpreted as very strong correlations, values from ±0.6 to ±0.8 are considered strong correlations, while values below ±0.5 suggest weaker relationships (Jierula et al. 2021). The coefficient of determination (R^2), Equation (III. 50), reflects the proportion of variance in the observed data explained by the model. An R^2 value close to 1 implies that the model provides an excellent fit to the data, whereas a value near 0 indicates that the model fails to explain the observed variability and the adjusted, R^2 (Adj_R^2), Equation (III. 51), is a corrected version of the R^2 that accounts for the number of parameters included in the model. It increases only when a new predictor enhances the model's performance beyond what would be expected by random chance. To measure the accuracy of predictions in terms of error magnitude, several metrics are used, including the root mean squared error (RMSE) Equation (II. 19) , and the mean absolute

error (MAE) Equation (II. 21), are present in chapter II. These are known as scale-dependent metrics because their values depend on the units of the data. They range from 0 to positive infinity, with lower values indicating more accurate predictions (Ammi, Khaouane, and Hanini 2021; Cherifi et al. 2025).

$$R = \frac{\frac{1}{M}\sum_{i=1}^{M}\left(y_{exp.i} - \overline{y_{exp}}\right)\left(y_{cal.i} - \overline{y_{cal.i}}\right)}{\sqrt{\frac{1}{M}\sum_{i=1}^{M}\left(y_{exp.i} - \overline{y_{exp.i}}\right)^2}\sqrt{\frac{1}{M}\sum_{i=1}^{M}\left(y_{cal.i} - \overline{y_{cal.i}}\right)^2}} \quad \text{(III. 49)}$$

$$R^2 = 1 - \frac{\sum_{i=1}^{M}\left(y_{exp.i} - y_{cal.i}\right)^2}{\sum_{i=1}^{M}\left(y_{exp.i} - \overline{y_{exp.i}}\right)^2} \quad \text{(III. 50)}$$

$$Adj{-}R^2 = 1 - (1 - R^2)\left(\frac{M-1}{M-(F+1)}\right) \quad \text{(III. 51)}$$

As an additional evaluation method in this chapter, we compare our proposed models with those reported in the literature. Since these models may use different units or data scales, normalized and percentage-based metrics are employed to ensure a fair comparison. Specifically, the relative root mean squared error (nRMSE), defined in chapiter II Equation (II. 20), and the mean absolute percentage error (MAPE), given in Equation (III. 52), are used to quantify prediction accuracy on a relative scale. A 0% value for both MAPE and nRMSE indicates perfect prediction accuracy, while values exceeding 100% reflect poor model performance.(Dahmani, Ammi, and Hanini 2023; Jierula et al. 2021).

$$MAPE = \frac{1}{M}\sum_{i=1}^{M}\left|\frac{y_{cal.i} - y_{exp.i}}{y_{exp.i}}\right| \cdot 100 \quad \text{(III. 52)}$$

Where M is the number of data points, F is number of parameters in the model, $y_{exp.i}$ and $y_{cal.i}$ refer to the experimental value and calculated values obtained from the proposed model, respectively. $\overline{y_{exp.i}}$ is the mean value of the experimental value and $\overline{y_{cal.i}}$ is the mean value of the calculated value obtained by proposed model. The unit of RMSE and MAE are the same as those of y_{exp}.

III.4. Results and discussion

III.4.1. Theoretical validation of the fractional model

III.4.1.1. Reduction to classical models (α = 1 Case)

The first validation of the proposed general fractional model of order *n* ($n = n$) is verified by replacing $\alpha = 1$, in the general expression defined by parameters (*n, k, α*). This substitution, applied to the equations for ($t(v)$, $v(t)$, $J(t)$, and $J(v)$), leads to the classical general solution of Equation 1 at constant pressure.

For $\alpha = 1$ Equation (III. 15), gives:

$$t(v) = \frac{1}{(2-n)k_n}\left\{[(1-n)k_n v + C_n]^{\frac{2-n}{1-n}} + [C_n]^{\frac{2-n}{1-n}}\right\},\ n \neq 1 \text{ and } n \neq 2; \quad k_n = [m^{-3}] \qquad \text{(III. 53)}$$

he Equation for $v(t)$ obtained from Equation (III. 16), for $\alpha = 1$, is given by

$$v(t) = \frac{1}{(1-n)k_n}\left\{\left[(2-n)k_n t + [C_n]^{\frac{n-2}{n-1}}\right]^{\frac{n-2}{n-1}} + C_n\right\},\ n \neq 1 \text{ and } n \neq 2; \quad k_n = [s^{-}] \qquad \text{(III. 54)}$$

The permeate flux $J(t)$ from Equation (III. 17), and for $\alpha = 1$

$$J(t) = \left[(2-n)k_n t + [C_n]^{\frac{n-2}{n-1}}\right]^{\frac{1}{n-2}},\ n \neq 1 \text{ and } n \neq 2; \quad k_n = [s^{-}] \qquad \text{(III. 55)}$$

The integration constant C_n, given that $J(t=0) = J_0$ Equation (III. *55*), gives

$$C_n = {J_0}^{n-1} \qquad \text{(III. 56)}$$

Equation of $J(v)$ giving from Equation (III. 19), for $\alpha = 1$

$$J(v) = [(1-n)k_n v + C_n]^{\frac{1}{n-1}}; \quad k_n = [m^{-3}] \qquad \text{(III. 57)}$$

We also verified the model for the six values of *n* (0; 0.5; 1; 1.5; 2; and 2.5). The validation results for ($v = f(t)$; $t = f(v)$; $J = f(t)$ and $J = f(v)$) are summarized in Table III. 6 and Table III. 7. On the one hand, it is observed that the fractional equations $[t(v), v(t), J(t), J(v)]$ for $\alpha = 1$, are identical to the corresponding classical equations $\{t(v), v(t), J(t), J(v)\}$, on the other hand, the expressions of ($v = f(t)$; $t = f(v)$; $J =$

$f(t)$ and $J = f(v)$) for the four values of *n* commonly used in the literature (0; 1; 1.5; 2), are the same as those provided by (Iritani and Katagiri 2016).

Table III. 6:Results of the first validation of the proposed new fractional sub-models (n, k, α) for $\alpha = 1, (v = f(t);\ v = f(v))$, at different values of n via classical ordinary sub-models.

Function $\frac{d^{2\alpha}t}{dv^{2\alpha}} = k_n\left[\frac{d^{\alpha}t}{dv^{\alpha}}\right]^n$ **for α=1**	$\frac{d^2t}{dv^2} = k_n\left(\frac{dt}{dv}\right)^n$	$v = f(t)$		$t = f(v)$	
Cake Filtration	***n = 0* (*)**	$v = \frac{1}{kJ_0}\left[-1 + (1 + 2kJ_0^2t)^{\frac{1}{2}}\right]$	(III. 58)	$t = \frac{k}{2}v^2 + \frac{1}{J_0}v$	(III. 59)
Near-Intermediate clogging	*n = 0.5*	$v = \frac{2}{k}\left[\left(1.5kt + J_0^{-1.5}\right)^{\frac{1}{3}} - J_0^{-0.5}\right]$	(III. 60)	$t = \frac{2}{3k}\left[\left(J_0^{-0.5} + 0.5kv\right)^3 - J_0^{-1.5}\right]$	(III. 61)
Intermediate Clogging	***n = 1* (*)**	$v = \frac{1}{k}ln[1 + kJ_0t]$	(III. 62)	$t = \frac{1}{kJ_0}[-1 + \exp(kv)]$	(III. 63)
Standard Clogging	***n = 1.5* (*)**	$v = \frac{2J_0t}{\left(2 + kJ_0^{0.5}t\right)}$	(III. 64)	$t = \frac{2v}{\left(2J_0 - kJ_0^{0.5}v\right)}$	(III. 65)
Complete Clogging	***n = 2* (*)**	$v = \frac{J_0}{k}[1 - \exp(-kt)]$	(III. 66)	$t = -\frac{1}{k}ln[-kJ_0^{-1}v + 1]$	(III. 67)
Standard Clogging (2nd type)	*n = 2.5*	$v = \frac{-2}{3k}\left[\left(-0.5kt + J_0^{0.5}\right)^3 - J_0^{1.5}\right]$	(III. 68)	$t = \frac{-2}{k}\left[\left(-1.5kv + J_0^{1.5}\right)^{1/3} - J_0^{0.5}\right]$	(III. 69)
Initial condition		*v (t=0) =0*		*t (v=0) =0*	

Table III. 7: Results of the first validation of the proposed new fractional sub-models (n, k, α) for $\alpha = 1, (J = f(t);\ J = f(v))$, at different values of n via classical ordinary sub-models.

Function $\frac{d^{2\alpha}t}{dv^{2\alpha}} = k_n\left[\frac{d^{\alpha}t}{dv^{\alpha}}\right]^n$ **for α=1**	$\frac{d^2t}{dv^2} = k_n\left(\frac{dt}{dv}\right)^n$	$J = f(t)$		$J = f(v)$	
Cake Filtration	***n = 0* (*)**	$J = \frac{J_0}{(1 + 2kJ_0^2t)^{\frac{1}{2}}}$	(III. 70)	$J = \frac{J_0}{(1 + kJ_0v)}$	(III. 71)
Near-Intermediate clogging	*n = 0.5*	$J = \left[1.5kt + J_0^{-1.5}\right]^{-\frac{2}{3}}$	(III. 72)	$J = \left[0.5kv + J_0^{-0.5}\right]^{-2}$	(III. 73)
Intermediate Clogging	***n = 1* (*)**	$J = \frac{J_0}{(1 + kJ_0t)}$	(III. 74)	$J = J_0\exp(-kv)$	(III. 75)
Standard Clogging	***n = 1.5* (*)**	$J = \frac{J_0}{\left(1 + 0.5kJ_0^{0.5}t\right)^2}$	(III. 76)	$J = J_0\left(1 - 0.5kJ_0^{-0.5}v\right)^2$	(III. 77)
Complete Clogging	***n = 2* (*)**	$J = J_0\exp(-kt)$	(III. 78)	$J = J_0 - \mathrm{kv}$	(III. 79)
Standard Clogging (2nd type)	*n = 2.5*	$J = \left[-0.5kt + J_0^{0.5}\right]^2$	(III. 80)	$J = \left[-1.5kv + J_0^{1.5}\right]^{\frac{2}{3}}$	(III. 81)
Initial condition		$J(v = 0) = J_0$		*t (v=0) =0*	

Note: For $\alpha = 1$ at different values of *n*, we have:

$$C_n = \left[\frac{(2-n)\Gamma(3-n)}{(2-n)\Gamma(3-n)}J_0\right]^{\frac{n-1}{1}} = J_0^{n-1}\ ;\ \text{Where: } C_0 = J_0^{-1};\ C_{0.5} = J_0^{-0.5}\ ;\ C_{1.5} = J_0^{0.5}\ ;\ C_{2.5} = J_0^{1.5}$$

III.4.2. Validation of the model using experimental data

III.4.2.1. Optimization of parameters (n, k, and α) for the general proposed clogging model (EDPO and EDF)

The second validation is performed on three (3) experimental databases collected from literature under different conditions (Table III. 4), corresponding to varying mechanisms of clogging commonly described in the literature (cake filtration n=0; intermediate blocking n=1; and standard blocking n=1.5). To determine the type of clogging according to the value of n, we work with the general expressions $J(t)$ or $v(t)$ for a single calculation step using experimental data. The general normal model (EDPO) is expressed by Equation (III. 54) or Equation (III. 55), with parameters (n, k, and α = 1), and the general fractional model (EDF) by Equation (III. 16) or Equation (III. 17) with parameters (n, k, and α). Depending on whether J_0 is known or unknown, the functions are numerically implemented in MATLAB using the parameters (n, k, and α) by employing the Dragonfly Algorithm (DA) coupled with the nlinfit optimization algorithm, along with the corresponding statistical performance criteria (R^2, Adj_R^2, RMSE, and MAE). Depending on the case, equations (III. 64), (III. 70), and (III. 74) are used for the normal model (n, k, and α = 1), and equations (III. 26), (III. 32), and (III. 36) for the fractional model (n, k, and α). These equations represent the specific sub-models corresponding to different clogging mechanisms. The results are summarized in Table annex 2. 3, and the plots comparing experimental values to those obtained from the EDPO and EDF models, including their respective sub-models for the same mechanisms, are presented as a function of time (Figure annex 2. 1), in annex 2. Each proposed model was applied across all pressure conditions, providing a good fit and reliable overall performance.

Figure III. 2 shows the linear regression plots of the EDF and EDPO models, while Table III. 8 summarizes the optimization results with the corresponding regression parameters. It can be observed from Figure III. 2 that the regression plots of the two proposed general models (EDPO and EDF) were approximately the same, making it difficult to clearly distinguish their performance. Thus, it is essential to compare the models using accuracy metrics. The evaluation results using scale-dependent metrics are shown in Table III. 8. These results demonstrate the ability of both the EDPO and EDF models to accurately represent the clogging behavior observed under various operating conditions. The EDF model consistently provided slightly

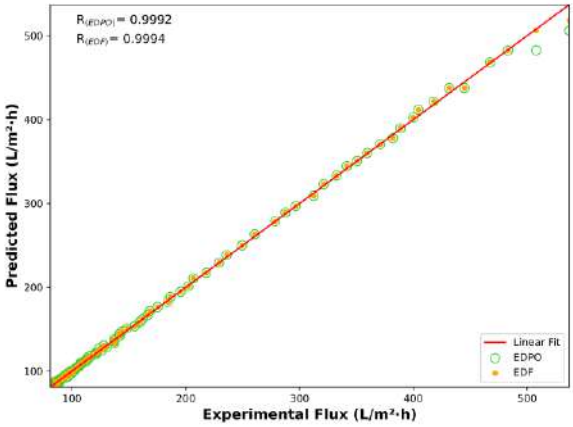
better fits than the EDPO model across all tested pressures and solutions. For R^2, Adj_R^2, and R, the values obtained using the EDF model ranged from 0.9954 to 0.9994, 0.9952 to 0.9992, and 0.9980 to 0.9997, respectively, which were the highest values among the two models. In comparison, the values obtained from the EDPO model ranged from 0.9951 to 0.9992 for R^2, 0.9950 to 0.9990 for Adj_R^2, and from 0.9976 to 0.9996 for R.

The evaluation results for RMSE, and MAE, further support the superior performance of the EDF model. The minimum values obtained for EDF were 0.015, and 0.0116, respectively. In contrast, the corresponding maximum values for the EDPO model were 13.8312, and 7.739. Based on both correlation and scale-dependent metrics, it can be inferred that the EDF model demonstrates the best performance in determining the mechanism of membrane filtration clogging.

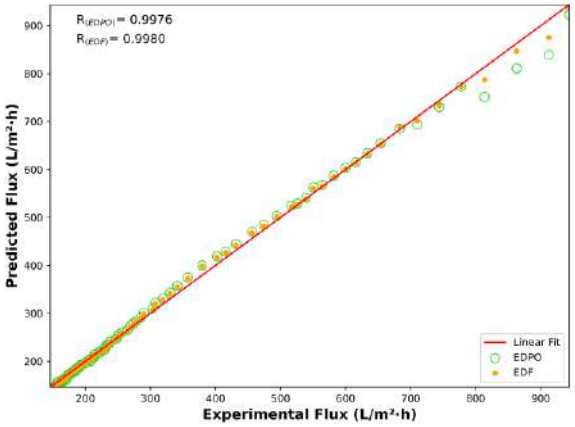
The value of n obtained using the general fractional model is the same as that given by the empirical fractional model in the study (Cherifi et al. 2025) for DB II. *2*. This finding confirms the validity of the previously proposed empirical fractional model, while clearly demonstrating the practical advantages of the new general fractional model (EDF).

Furthermore, the use of the first proposed general fractional model of order *n* (n, k, α) for abnormal clogging, based on fractional calculus under different operating conditions (pressures and solutions), provided a better fit to the filtration data than the second proposed normal general model of power *n* (n, k, $\alpha = 1$). This was observed across different clogging mechanisms: cake filtration ($0.3 \leq n \leq 0.5$), intermediate blocking ($n \leq 1.01$), and standard blocking ($1.39 < n \leq 1.66$).

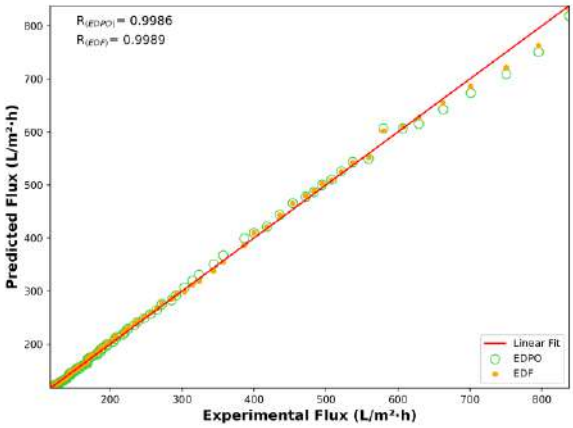
It is important to recall that this validation approach allows us to deduce the type of clogging from the general fractional model in a single optimization step.


$R_{(EDPO)}$= 0.9992
$R_{(EDF)}$= 0.9994
Predicted Flux (L/m²·h)
Experimental Flux (L/m²·h)
Linear Fit
EDPO
EDF

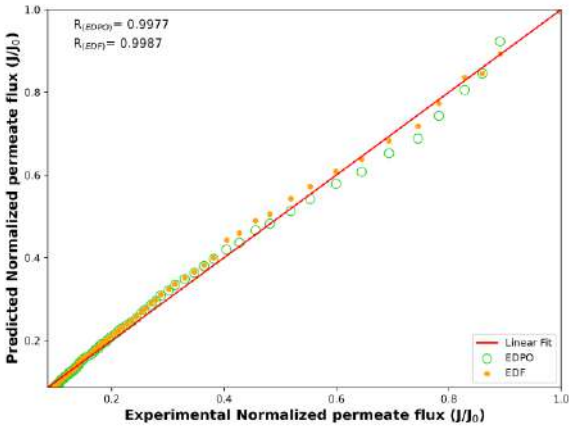
(a)


$R_{(EDPO)}$= 0.9976
$R_{(EDF)}$= 0.9980
Predicted Flux (L/m²·h)
Experimental Flux (L/m²·h)
Linear Fit
EDPO
EDF

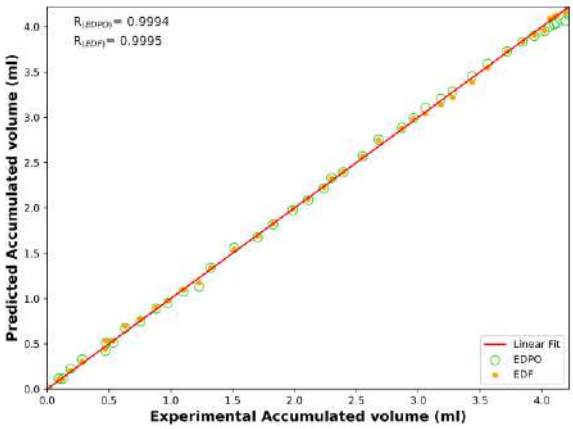
(b)


$R_{(EDPO)}$= 0.9986
$R_{(EDF)}$= 0.9989
Predicted Flux (L/m²·h)
Experimental Flux (L/m²·h)
Linear Fit
EDPO
EDF

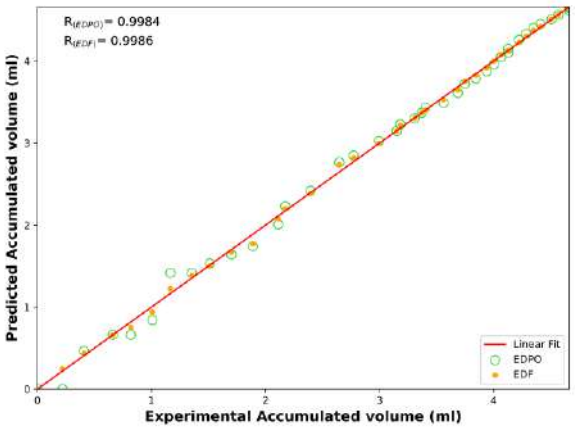
(c)


$R_{(EDPO)}$= 0.9977
$R_{(EDF)}$= 0.9987
Predicted Normalized permeate flux (J/J0)
Experimental Normalized permeate flux (J/J0)
Linear Fit
EDPO
EDF

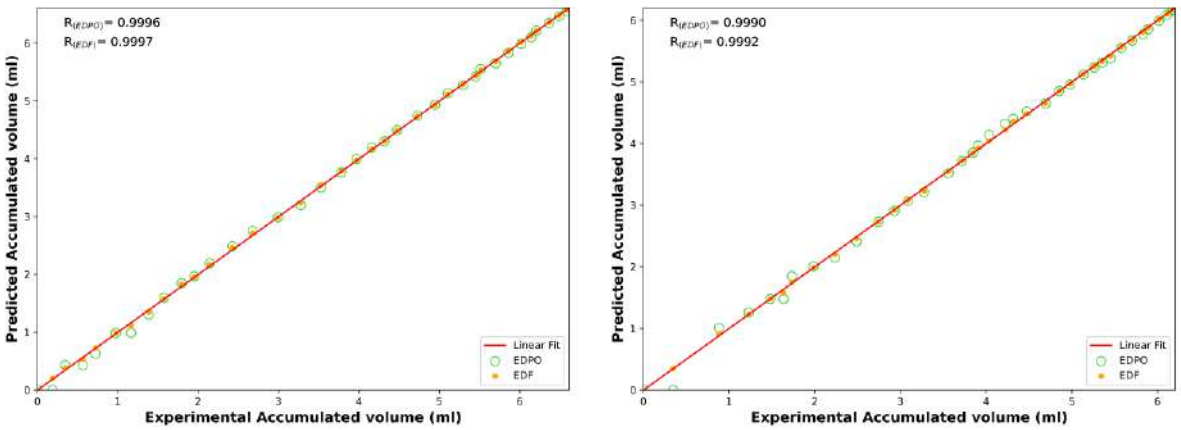
(d)


$R_{(EDPO)}$= 0.9994
$R_{(EDF)}$= 0.9995
Predicted Accumulated volume (ml)
Experimental Accumulated volume (ml)
Linear Fit
EDPO
EDF

(e)


$R_{(EDPO)}$= 0.9984
$R_{(EDF)}$= 0.9986
Predicted Accumulated volume (ml)
Experimental Accumulated volume (ml)
Linear Fit
EDPO
EDF

(f)



(g) (h)

Figure III. 2: Regression plots comparing the calculated and experimental values using the proposed EDF and EDPO models under different clogging mechanisms, pressures, and solutions: for DB III. 1 (a–c), three tests with n = 0 at 1.5 × 10⁵, 3.0 × 10⁵, and 4.5 × 10⁵ Pa; for DB III. 2 (d), test with n = 1 at P = 2.76 × 10⁴ Pa; and for DB II. 2 with n = 1.5: (e) P = 3.447 × 10⁴ Pa (pQR150), (f) P = 5.516 × 10⁴ Pa (pQR150), (g) P = 3.447 × 10⁴ Pa (pGEc47), and (h) P = 5.516 × 10⁴ Pa (pGEc47).

Table III. 8: optimized values of n, k, and α for different clogging types tested with the normal (EDPO) and fractional (EDF) models whit linear fitting parameters.

Condition			**$J = f(t)$ and/ or $v = f(t)$**							**Linear Fitting Parameters**		
solution	Pressure (Pa)	Equation	*n*	*k*	α (*1)	RMSE	R^2	MAE	Adj-R^2	a	b	R
Oily wastewater	1.5×10^5	EDPO	0.3054	1.3948×10^{-4}	1.0000	4.7482	0.9983	2.4355	0.9984	0.9894	1.4883	0.9992
		EDF	0.6918	3.9006×10^{-4}	0.4437	4.7433	0.9986	2.2983	0.9985	0.9897	1.4883	0.9994
	3.0×10^5	EDPO	0.1289	1.9130×10^{-5}	1.0000	13.8312	0.9955	7.7391	0.9953	0.9777	5.2581	0.9976
		EDF	0.5390	4.0388×10^{-5}	0.5292	13.7102	0.9958	7.7380	0.9954	0.9777	5.2591	0.9980
	4.5×10^5	EDPO	0.1935	4.1619×10^{-5}	1.0000	9.5149	0.9973	5.1336	0.9972	0.9724	6.7546	0.9986
		EDF	0.3964	5.5454×10^{-5}	0.7485	9.1982	0.9975	5.1136	0.9973	0.9829	3.3285	0.9989
Microbial suspensions from a sequencing batch reactor (SBR) (Supernatant solution)	2.76×10^4	EDPO	1.3601	0.0043	1.0000	0.0163	0.9951	0.0117	0.9950	0.9894	0.0009	0.9977
		EDF	1.1810	0.0063	0.4772	0.0150	0.9954	0.0116	0.9952	0.9900	0.0006	0.9987
pQR150 (kanamycin resistance, 20 kb)	3.447×10^4	EDPO	1.1421	0.6577	1.0000	0.0518	0.9988	0.0398	0.9986	0.9981	0.0050	0.9994
		EDF	1.4423	0.2130	3.1124	0.0518	0.9989	0.0399	0.9988	0.9981	0.0024	0.9995
	5.516×10^4	EDPO	1.4057	0.6595	1.0000	0.0809	0.9965	0.0567	0.9963	1.0079	-0.0312	0.9984
		EDF	1.6600	0.5947	1.6268	0.0809	0.9967	0.0547	0.9964	1.0079	-0.0312	0.9986
pGEc47 (tetracycline resistance, 56 kb)	3.447×10^4	EDPO	1.4139	0.4173	1.0000	0.0613	0.9992	0.0440	0.9990	1.0066	-0.0348	0.9996
		EDF	1.4912	0.3963	1.1868	0.0613	0.9994	0.0349	0.9992	1.0066	-0.0348	0.9997
	5.516×10^4	EDPO	1.2516	0.6499	1.0000	0.0807	0.9980	0.0526	0.9977	1.0077	-0.0390	0.9990
		EDF	1.3969	0.4640	1.5775	0.0807	0.9982	0.0506	0.9978	1.0077	-0.0390	0.9992

Note 1: (*1) For the EDPO model, α is fixed at 1, while for the EDF model, α is calculated through optimization.

Note 2: For DB III. 1and DB III. 2 we use Equation (III. 55) and (III. 17) for EDPO and EDF respectively.

For DB II. 2 we use Equation (III. 54) and (III. 16) for EDPO and EDF respectively

III.4.3. Comparison between the general EDF model and literature models

In this section, we compare the effectiveness of the proposed fractional EDF model with the Hermia models from the literature (listed in Table III. 9). For each mechanism, we provide a model either from the same reference used in the database or, in some cases, from another reference.

Table III. 9: Reference model equations.

Model name	Mechanisms	Equation		Fouling parameter	Reference
Ref 1	Cake filtration (n=0)	$\frac{1}{J^2} = \frac{1}{J_0^2} + k_c t$	(III. 82)	k_c [s/m^6]	(Salahi, Abbasi, and Mohammadi 2010)
Ref 2	Intermediate clogging (n=1)	$\frac{1}{J} = \frac{1}{J_0} k_i A t$	(III. 83)	k_i [L/m^3]	(Salahi, Abbasi, and Mohammadi 2010)
Ref 3	Intermediate clogging (n=1)	$\frac{1}{Q} = \frac{1}{Q_0} k_i t$	(III. 84)	k_i [m^{-1}]	(Aslam, Lee, and Kim 2015)
Ref 4	Standard clogging (n=1.5)	$V = (V_0.t).\left(1 + t\frac{K_s.V_0}{A_0}\right)^{-1}$	(Eq. I.2. ***15***)	K_s [m^{-1}]	(Affandy, Keshavarz-Moore, and Versteeg 2013)
Ref 5	Intermediate–standard clogging (n=1-1.5)	$V = \frac{A_0}{K_{ic}}.ln\left(1 + \frac{2K_{ic}.(V_0/A_0).t}{2+K_s(V_0/A_0).t}\right)$	(Eq. I.2. ***18***)	K_{ic} [m^{-1}] and K_s [m^{-1}]	(Affandy, Keshavarz-Moore, and Versteeg 2013)

The first model, referred to as Ref 1, is based on the Hermia model for the cake filtration mechanism ($n = 0$). It is expressed as a function of filtration flux and represents a situation where the particles or oil droplets in the feed are significantly larger than the membrane pores. These particles cannot enter the membrane and instead accumulate on the surface, forming a cake (or gel) layer. This layer increases resistance to the flow and causes a gradual decline in filtration flow over time (Salahi, Abbasi, and Mohammadi 2010).

For the intermediate clogging mechanism ($n = 1$), we compare two models from the literature. The first model, Ref 3 comes from the same database reference. In that study, based on the permeate flow rate (Q), the authors found that for glass-fiber filters with a pore size of 1.2 μm, intermediate pore blocking was identified as the primary fouling mechanism. This conclusion was drawn based on the best fit of experimental data to different pore-blocking models (Aslam, Lee, and Kim 2015). To provide a better basis for comparison, we also consider another model, Ref 2, from (Salahi, Abbasi, and Mohammadi 2010), which is expressed as a function of filtration flux. This mechanism occurs when the particles are approximately the same

size as the pores: they can particles partially enter and block some of the pores, reducing the flow without fully clogging them.

For the case of standard clogging, we compare two models from (Affandy, Keshavarz-Moore, and Versteeg 2013). The first model, Ref 4, represents standard clogging mechanisms ($n = 1.5$) as a function of cumulative volume, where the pore diameter of the membrane decreases over time due to the accumulation of particles or materials. This leads to an increase in filtration resistance, and this constriction makes it difficult for the filtrate to pass through, thereby reducing filtration efficiency. The second model, Ref 5, combines standard clogging and intermediate clogging, indicating that the overall clogging mechanism may involve multiple clogging types occurring simultaneously rather than a single, isolated process.

The objective is to assess how well the EDF model captures the dynamics of membrane clogging and how its predictions and parameters in one step compare with those of more traditional and combined models. To carry out this comparison, we utilized the following evaluation criteria: R^2, R, nRMSE (%), and MAPE (%). Since the original data is not always available on the same scale or may vary significantly across experiments, it is more appropriate to use percentage-based error metrics. These indicators facilitate consistent comparisons among different datasets, regardless of the units or magnitudes involved.

Table III. 10, summarizes the results of compression between the EDF model and the other models of litterateur, showing that the EDF model consistently delivers very good performance, with nRMSE values ranging from 0.93% to 1.73% and R^2 values above 0.995. One of the advantages of the EDF model is its general formulation, which is based on a fractional exponent (n, α, and k). Figure annex 2. 1 shows the compression plot as a function of time, while the linear regression of the EDF model and the literature model are presented in in Figure annex 2. 2 in annex 2. In Figure III. 3, R and R^2 are shown with columns to measure the goodness of the linear fit of the regression model. The nRMSE and MAPE are shown with a variation curve to evaluate the prediction errors.

This makes it adaptable to different clogging behaviors, unlike classical models that are tied to a specific mechanism.

The equation Ref 1, which describes cake clogging shows decent results, but its errors are slightly higher than those of the EDF model (nRMSE ranging from 1.4927% to 2.0193%, maximum MAPE of 7.5279%, and R^2 and R values between 0.9962–0.9982 and 0.9814–0.9991, respectively).

- The equation Ref 2 describes intermediate clogging, offers only a single result for a specific mechanism, which limits its flexibility (nRMSE, MAPE, R^2, and R values are 1.9958%, 5.5236%, 0.9953, 0.9988, respectively).

- The equation Ref 3 is slightly different, as it expresses the clogging in terms of flow rate (Q) instead of flux. This makes a direct comparison tricky, but the model still performs well in its context (nRMSE, MAPE, R^2, and R values are 0.9195%, 3.9570%, 0.9990, 0.9995, respectively).

- Ref 4, which describes the standard clogging mechanism, shows a wider variation in error values, with nRMSE reaching up to 2.63%, MAPE reaching 7.8023%, and the best R^2 and R values being 0.9989 and 0.9994, respectively.

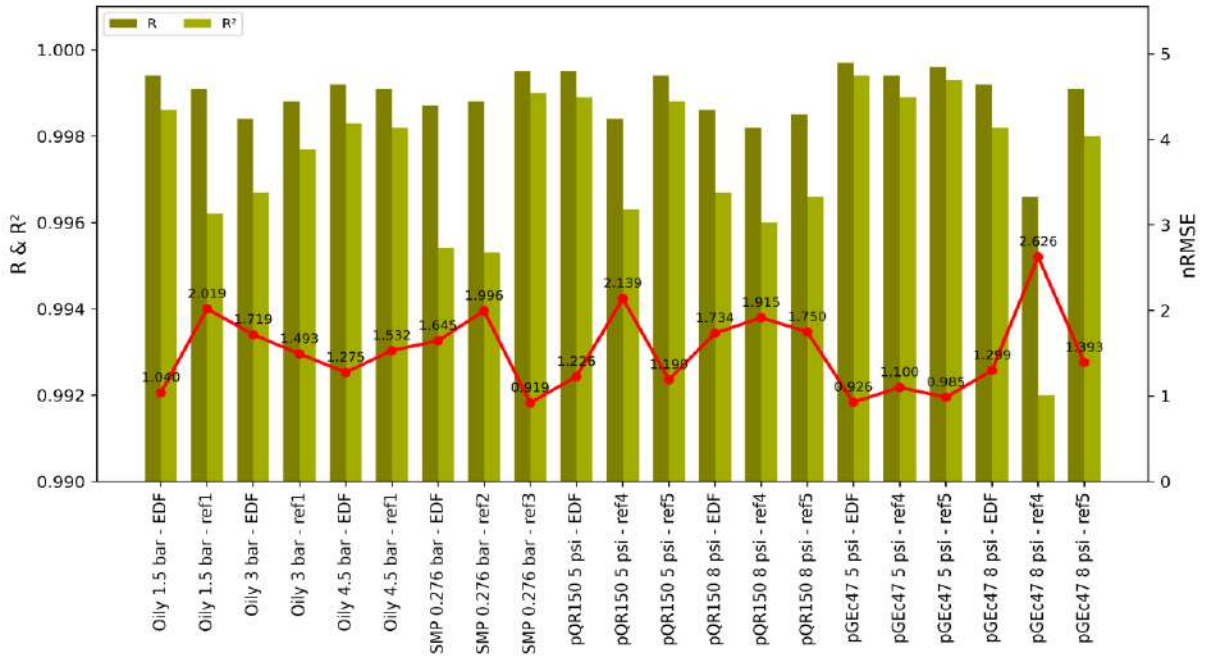
- Ref 5 combines two clogging mechanisms (intermediate and standard). It gives good results, but the EDF model remains competitive while being more general and less complex to implement. The best value given by this model for nRMSE, MAPE, R^2, and R, are 1.7495%, 5.6812%, 0.9993, and 0.9996 in that order.

***Important note**: When using percentage-based errors like MAPE, it's necessary to remove any zero values from the actual data. Otherwise, division by zero can lead to incorrect results.*

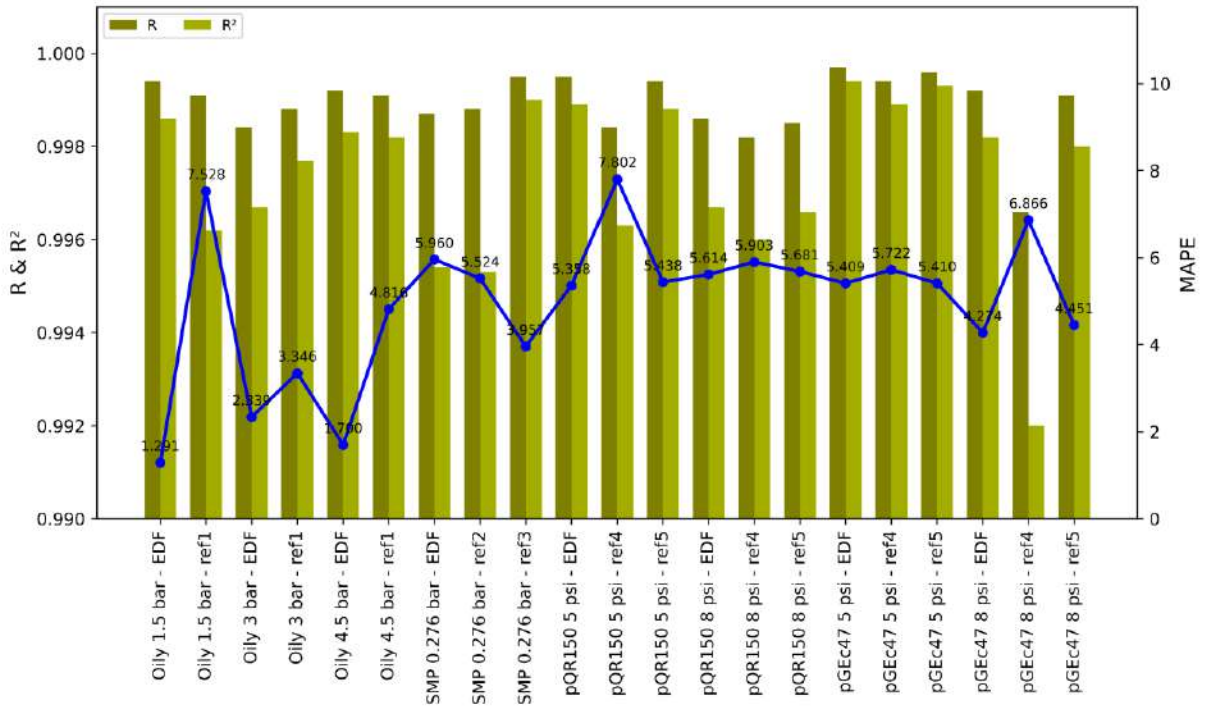
Overall, the EDF model stands out due to its accuracy, simplicity, and ability to generalize across different clogging mechanisms, which makes it a strong and practical alternative to classical models.

Table III. 10: Comparative evaluation of the proposed fractional EDF model and literature-based clogging models.

Condition		v=f(t) and/ or J = f(t)							Linear Fitting Parameters			
Solution	Pressure (Pa)	Equation	n	K_{ic}	K	α (*1)	nRMSE (%)	MAPE (%)	R^2	a	b	R
Oily wastewater	1.5×10^5	EDF	0.6918	\	3.90×10^{-4}	0.4437	1.0398	1.2912	0.9986	0.9687	1.00×10^{-6}	0.9994
		Ref 1	0.0000	\	6.07×10^{-5}	1.0000	2.0193	7.5279	0.9962	0.9871	1.00×10^{-6}	0.9991
	3.0×10^5	EDF	0.5390	\	4.04×10^{-5}	0.5292	1.7186	2.3392	0.9967	1.0783	8.00×10^{-7}	0.9984
		Ref 1	0.0000	\	1.77×10^{-5}	1.0000	1.4927	3.3459	0.9977	1.0035	1.00×10^{-7}	0.9988
	4.5×10^5	EDF	0.3964	\	5.55×10^{-5}	0.7485	1.2751	1.6997	0.9983	1.0436	6.00×10^{-7}	0.9992
		Ref 1	0.0000	\	2.85×10^{-5}	1.0000	1.5319	4.8162	0.9982	0.9814	9.00×10^{-7}	0.9991
Microbial suspensions from a sequencing batch reactor (SBR) (Supernatant solution)	2.76×10^4	EDF	1.0106	\	1.0659	0.2028	1.6450	5.9600	0.9954	1.1768	0.7297	0.9987
		Ref 2	1.0000	\	8.2886	1.0000	1.9958	5.5236	0.9953	0.9500	0.3800	0.9986
		Ref 3	1.0000	\	1.51×10^{-4}	1.0000	0.9195	3.9570	0.9990	0.9990	161.7100	0.9995
pQR150 (kanamycin resistance, 20 kb)	3.447×10^4	EDF	1.4423	\	0.2130	3.1124	1.2265	5.3582	0.9989	0.9981	-0.0024	0.9995
		Ref 4	1.5000	\	1.3706	1.0000	2.1390	7.8023	0.9963	1.0154	-0.0547	0.9984
		Ref 5	1-1.5	8.6945	0.2032	1.0000	1.1896	5.4382	0.9988	0.9977	0.0065	0.9994
	5.516×10^4	EDF	1.6600	\	0.5947	1.6268	1.7341	5.6140	0.9967	1.0079	-0.0312	0.9986
		Ref 4	1.5000	\	1.2690	1.0000	1.9148	5.9028	0.9960	1.0166	-0.0615	0.9982
		Ref 5	1-1.5	4.2523	1.0703	1.0000	1.7495	5.6812	0.9966	1.0063	-0.0250	0.9985
pGEc47 (tetracycline resistance, 56 kb)	3.447×10^4	EDF	1.4912	\	0.3963	1.1868	0.9264	5.4091	0.9994	1.0066	-0.0348	0.9997
		Ref 4	1.5000	\	0.7732	1.0000	1.0997	5.7222	0.9989	1.0123	-0.0641	0.9994
		Ref 5	1-1.5	2.2718	0.7703	1.0000	0.9845	5.4096	0.9993	1.0053	-0.0280	0.9996
	5.516×10^4	EDF	1.3969	\	0.4640	1.5775	1.2993	4.2737	0.9982	1.0077	-0.0390	0.9992
		Ref 4	1.5000	\	0.9772	1.0000	2.6264	6.8658	0.9920	1.0263	-0.1338	0.9966
		Ref 5	1-1.5	12.4813	0.2960	1.0000	1.3925	4.4506	0.9980	1.0066	-0.0336	0.9991



(A)



(B)

Figure III. 3: Evaluation results of EDF and model of reference using scale-dependent metrics. (A) Evaluation results using nRMSE. (B) Evaluation results using MAPE. Abbreviations: (1) Oily: Oily wastewater, (2) SMP: Microbial suspensions from a sequencing batch reactor (SBR), supernatant, (3) pQR150: Plasmid pQR150 (kanamycin resistance, 20 kb), and (4) pGEc47: Plasmid pGEc47 (tetracycline resistance, 56 kb).

III.4.4. Summary of result

The second proposed general ordinary model of order n $(n, k, \alpha = 1)$ provided, in a single calculation step, n coefficients that fall within the typical clogging range reported in the literature (Affandy, Keshavarz-Moore, and Versteeg 2013; Aslam, Lee, and Kim 2015; Salahi, Abbasi, and Mohammadi 2010).

The particular general sub-models of order n $(n, k, \alpha = 1)$, derived from the fractional solution at α=1, contributed to validating and confirming the quality of the fractional sub-models (n, k, α), by producing predictive results consistent with those reported in the literature.

Based on the optimized results, the fractional calculation approach improved the fitting of the kinetic curves $\{v = f(t)$ and $J = f(t)\}$ and led to more accurate clogging predictions compared to the classical approach, which tends to underestimate both the clogging and the fractional parameter α. Furthermore, it is confirmed that the clogging sub-models using fractional calculus better describe the clogging process than the normal particular sub-models.

The differences in the n power, which characterize the type of clogging, can be attributed to the optimization calculation using the Dragonfly Algorithm (DA_nlinfit) in a single calculation step. They can also be attributed to the various established experimental conditions and to the fact that the membrane structure characteristics cause certain assumptions of Hermia's model to not be satisfied.

The optimized results indicated that the particular normal sub-models generally overestimated the clogging identification criterion (n) in most cases. This overestimation can be explained by the presence of internal fouling within the membranes, which induces changes in the membrane structural topology, including porosity, tortuosity, swelling and/or compression (due to fouling), and surface charge density (distribution of surface electric charges), thereby rendering the assumptions established by Hermia's model inadequate.

The arbitrary fractional orders (α) for the abnormal clogging model were always different from unity and varied depending on the type of clogging. There was an overlap of the confidence intervals for the parameter α, showing that the average of α (average $\alpha = 0.5 \pm \Delta\alpha$). However, the fractional values of α in the general model suggest that clogging is abnormal since the non-

integer fractional order differs from unity ($\alpha \neq 1$). This indicates that the clogging did not follow Hermia's classical behavior.

It is noted that the power n and the coefficient k of the general fractional model (n, k, α) showed an increase compared to the classical clogging model $(n, k, \alpha = 1)$.

The use of fractional calculus to quantify abnormal clogging processes provides an additional quality in modeling. Moreover, this quantification offers insight into the nature of the clogging process, considering the non-phenomenological meaning of α. This point should be noted, as the time exponents n and α are descriptive parameters of the filtration process, while the constant (k) should remain almost constant under different process conditions due to its relation to the membrane structure. The parameter α indicates whether the process is normal ($\alpha = 1$), over-clogging ($\alpha > 1$), or under-clogging ($\alpha < 1$), leaving only the terms related to n and k as variables dependent on the process conditions.

III.5. Conclusion

Membrane clogging is a complex phenomenon influenced by multiple parameters. In this chapter, two general models were proposed and evaluated: the fractional-order model (n, k, α) and the classical model $(n, k, \alpha = 1)$, both relying on a single optimization step. The results demonstrated that these models can successfully describe the clogging process with high accuracy, as reflected by determination coefficients ($0.9951 < R^2 < 0.9994$), mean absolute errors ($0.0116 < MAE < 7.7391$), and root mean square errors ($0.015 < RMSE < 13.7105$).

The fractional-order model (n, k, α) consistently outperformed the classical model by providing a more flexible and robust description of clogging mechanisms, validated through four test cases corresponding to different equations of clogging (cake filtration, intermediate blocking, and standard blocking). Importantly, the optimized values of n obtained from both models always belonged to the real domain $n\epsilon[0\,;\mathcal{R}^+]$, converging toward the particular values ($n = 0; n = 1; n = 1.5$) widely reported in the literature, and thus confirming their reliability in characterizing real processes.

The optimization quality was strongly affected by the Gamma function, yet the DA–nlinfit hybrid algorithm ensured stable parameter estimation and reliable convergence. Overall, the findings confirm that both the fractional general model and its classical counterpart can be applied to effectively predict the type of membrane clogging in a single-step optimization process.

Despite the strong performance of these models, it should be noted that the available data do not fully capture the complexity of clogging in real systems. Nevertheless, the datasets used here, also employed in previous studies with excellent results, remain the most reliable references available in the literature. The consistency of outcomes across different works reinforces the robustness and relevance of the present approach.

Finally, this work opens perspectives for extending the proposed methodology to abnormal clogging models using fractional calculus, with a particular focus on non-Newtonian fluids and the biological aspects of membrane fouling in future experimental investigations.

General conclusion and perspective

General conclusion

Membrane clogging remains one of the main challenges limiting the efficiency and reliability of filtration processes. The accumulation of particles, organic, inorganic, or biological matter on or within the membrane leads to a decline in flux, increased operating costs, and reduced membrane lifespan. Understanding and predicting this phenomenon has therefore been a central concern in membrane research. However, classical models remain constrained by simplifying assumptions and their inability to fully capture the complexity of clogging mechanisms.

In this context, the present thesis addressed the issue of membrane clogging through the development of two complementary approaches based on fractional calculus.

The first contribution focused on the development and evaluation of eight new empirical fractional models to describe membrane filtration clogging. Using experimental datasets from the literature and a hybrid optimization approach combining the dragonfly algorithm with nonlinear regression, these models demonstrated strong predictive performance for permeate volume under various operating conditions, with determination coefficients between $0.9896 \leq R^2 \leq 0.9997$ and relative root mean square errors between 0.8674% and 2.9548%. They provide accurate and flexible tools for simulating filtration dynamics. However, while they allow indirect inference of clogging mechanisms through additional analytical methods, they do not directly determine these mechanisms. This limitation was addressed by analyzing the clogging index n using Hermia's equation, which revealed standard clogging for the first dataset ($n \approx 1.5$) and a combination of intermediate and standard clogging for the second ($1 \leq n \leq 1.5$).

The second contribution introduced a general fractional differential model (EDF) as a new alternative to classical clogging models. Defined by the parameters n, k, and α, this model was validated through theoretical derivation and experimental testing on three datasets representing different clogging mechanisms. Comparative analysis with Hermia-based models showed that EDF achieves higher accuracy (nRMSE between 0.93% and $1.73\%, R^2 > 0.995$) and offers greater adaptability. Unlike traditional models that require testing multiple formulations to identify the mechanism, the EDF determines the clogging index n directly in a single step, enabling straightforward mechanism identification. The fractional parameter α increases

flexibility, allowing the model to reduce to classical formulations when $\alpha = 1$ or extend to capture more complex dynamics when $\alpha \neq 1$. This unified formulation overcomes the main limitations of classical models and eliminates the need for combined approaches proposed in previous studies.

Overall, this thesis contributes to bridging the gap between fractional calculus and membrane filtration science by offering new models that enhance predictive capacity and improve the understanding of clogging behavior. Future perspectives include extending the EDF framework to abnormal clogging phenomena, non-Newtonian fluids, and biological fouling, as well as exploring hybrid strategies that integrate mechanistic and empirical approaches for more comprehensive modeling.

By combining mathematical innovation with experimental validation, this work establishes a robust foundation for future studies aimed at improving the sustainability, efficiency, and reliability of membrane-based separation processes.

Perspective:

Future perspectives concern both contributions developed in this thesis. For the empirical fractional models, future work could aim at extending their application to a wider variety of operating conditions and membrane types, as well as enriching the database with new experiments designed specifically to validate and compare these models across different pore-size regimes and feed compositions. Their structure could also be refined to improve the physical interpretability of the parameters and to better link them with specific clogging mechanisms. Regarding the general EDF model, future research may focus on its extension to abnormal clogging behaviors, highly concentrated suspensions, and non-Newtonian fluids using fractional-calculus tools. In the future, we also plan to extend this analysis to include other models of abnormal clogging and to conduct clogging experiments that incorporate biological aspects during filtration. Additional perspectives include coupling both modeling approaches with pore-scale imaging for deeper mechanistic insight, exploring real-time integration in monitoring systems, and developing hybrid frameworks that combine fractional modeling with machine-learning algorithms to enhance prediction accuracy and adaptability.

References

References

Abdelrasoul, A., H. Doan, and A. Lohi. 2013. “Fouling in Membrane Filtration and Remediation Methods.” In *Mass Transfer - Advances in Sustainable Energy and Environment Oriented Numerical Modeling*, InTech. doi:10.5772/52370.

Affandy, Affaro, Eli Keshavarz-Moore, and Henk K. Versteeg. 2013. “Application of Filtration Blocking Models to Describe Fouling and Transmission of Large Plasmids DNA in Sterile Filtration.” *Journal of Membrane Science* 437: 150–59. doi:10.1016/j.memsci.2013.02.055.

Agutter, Paul S., P. Colm Malone, and Denys N. Wheatley. 2000. “Diffusion Theory in Biology: A Relic of Mechanistic Materialism.” *Journal of the History of Biology* 33(1): 71–111. doi:10.1023/A:1004745516972.

Al-Juboori, Raed A., and Talal Yusaf. 2012. “Biofouling in RO System: Mechanisms, Monitoring and Controlling.” *Desalination* 302: 1–23. doi:10.1016/j.desal.2012.06.016.

Alanzi, Ayed. R. A., Shokrya S. Alshqaq, Raouf Fakhfakh, and Abdellatif Ben Makhlouf. 2025. “Existence and Uniqueness Results for a Class of Fractional Integro-Stochastic Differential Equations.” *Fractal and Fractional* 9(1): 42. doi:10.3390/fractalfract9010042.

Alborzi, Ashkan, I. Min Hsieh, Danny Reible, and Mahdi Malmali. 2022. “Analysis of Fouling Mechanism in Ultrafiltration of Produced Water.” *Journal of Water Process Engineering* 49. doi:10.1016/j.jwpe.2022.102978.

Alkan, Aslı. 2024. “Analysis of Fractional Advection Equation with Improved Homotopy Analysis Method.” *Osmaniye Korkut Ata Üniversitesi Fen Bilimleri Enstitüsü Dergisi* 7(3): 1215–29. doi:10.47495/okufbed.1387630.

Almeida, Ricardo. 2017. “A Caputo Fractional Derivative of a Function with Respect to Another Function.” *Communications in Nonlinear Science and Numerical Simulation* 44: 460–81. doi:10.1016/j.cnsns.2016.09.006.

Alsawaftah, Nour, Waad Abuwatfa, Naif Darwish, and Ghaleb Husseini. 2021. “A Comprehensive Review on Membrane Fouling : Mathematical.” *Water* 13(1327): 1–37.

Ammi, Moulay Rchid Sidi, El Hassan El Kinani, and Delfim F.M. Torres. 2012. “Existence and Uniqueness of Solutions to Functional Integro-Differential Fractional Equations.” *Electronic Journal of Differential Equations* 2012(103): 1–9.

Ammi, Yamina, Latifa Khaouane, and Salah Hanini. 2018. “A Model Based on Bootstrapped Neural Networks for Modeling the Removal of Organic Compounds by Nanofiltration and Reverse Osmosis Membranes.” *Arabian Journal for Science and Engineering* 43(11): 6271–84. doi:10.1007/s13369-018-3484-8.

Ammi, Yamina, Latifa Khaouane, and Salah Hanini. 2021. “Stacked Neural Networks for Predicting the Membranes Performance by Treating the Pharmaceutical Active Compounds.” *Neural Computing and Applications* 33(19): 12429–44. doi:10.1007/s00521-021-05876-0.

Ammi, Yammina. 2016. “Modelisation Des Phenomenes de Transport Lors d’osmose Inverse/Nanofiltration.”

Aslam, Muhammad, Po Heng Lee, and Jeonghwan Kim. 2015. "Analysis of Membrane Fouling with Porous Membrane Filters by Microbial Suspensions for Autotrophic Nitrogen Transformations." *Separation and Purification Technology* 146: 284–93. doi:10.1016/j.seppur.2015.03.042.

Atangana, Abdon, and Kolade M. Owolabi. 2017. "New Numerical Approach for Fractional Differential Equations" eds. Abdon Atangana, Gisèle Mophou, Jordan Hristov, and Zakia Hammouch. *arXiv: Numerical Analysis* 13(1): 3. doi:10.1051/mmnp/2018010.

Bacchin, Patrice. 2005. "Principes de Bases de La Filtration Membranaire." *Sciences et Technologies à Membranes*: 9. http://patricebacchin.fr/.

Benavente, Lucia. 2016. "Low Fouling Membranes for Water and Bio Tech Applications." Université Paul Sabatier.

Benkerrouche, Amar, Mohammed Said Souid, Gani Stamov, and Ivanka Stamova. 2022. "Multiterm Impulsive Caputo–Hadamard Type Differential Equations of Fractional Variable Order." *Axioms* 11(11): 634. doi:10.3390/axioms11110634.

Benyahia, Boumédiène. 2020. "Modélisation et Observation Des Bioprocédés à Membranes : Application à La Digestion Anaérobie." *Thèse*.

Bessiere, Yolaine. 2005. "Filtration Frontale Sur Membrane : Mise En Evidence Du Volume Filtre Critique Pour l'anticipation et Le Controle Du Colmatage." : 192.

Bolton, Glen, LaCasse, Dan, and Ralf , Kuriyel. 2006. "Combined Models of Membrane Fouling: Development and Application to Microfiltration and Ultrafiltration of Biological Fluids." *Journal of Membrane Science* 277(1–2): 75–84. doi:10.1016/j.memsci.2004.12.053.

Bolton, Glen, Dan Lacasse, and Ralf Kuriyel. 2006. "Combined Models of Membrane Fouling : Development and Application to Microfiltration and Ultrafiltration of Biological Fluids." 277: 75–84. doi:10.1016/j.memsci.2004.12.053.

Bolton, Glen R., Austin W. Boesch, and Matthew J. Lazzara. 2006. "The Effects of Flow Rate on Membrane Capacity: Development and Application of Adsorptive Membrane Fouling Models." *Journal of Membrane Science* 279(1–2): 625–34. doi:10.1016/j.memsci.2005.12.057.

Bourdin, Loïc. 2017. "Cauchy-Lipschitz Theory for Fractional Multi-Order Dynamics: State-Transition Matrices, Duhamel Formulas and Duality Theorems." *Differential and Integral Equations* 31(7–8): 559–94. doi:10.57262/die/1526004031.

Bowen, W. R., J. I. Calvo, and A. Hernández. 1995. "Steps of Membrane Blocking in Flux Decline during Protein Microfiltration." *Journal of Membrane Science* 101(1–2): 153–65. doi:10.1016/0376-7388(94)00295-A.

Broeckmann, A., J. Busch, T. Wintgens, and W. Marquardt. 2006. "Modeling of Pore Blocking and Cake Layer Formation in Membrane Filtration for Wastewater Treatment." *Desalination* 189(1-3 SPEC. ISS.): 97–109. doi:10.1016/j.desal.2005.06.018.

De Bruijn, J.P.F., F.N. Salazar, and R. Bórquez. 2005. "Membrane Blocking In Ultrafiltration." *Food and Bioproducts Processing* 83(3): 211–19. doi:10.1205/fbp.04012.

Caputo, M. 1967. “Linear Models of Dissipation Whose Q Is Almost Frequency Independent--II.” *Geophysical Journal International* 13(5): 529–39. doi:10.1111/j.1365-246X.1967.tb02303.x.

Castro-Muñoz, Roberto, Elsa Díaz-Montes, Emilia Gontarek-Castro, Grzegorz Boczkaj, and Charis M. Galanakis. 2022. “A Comprehensive Review on Current and Emerging Technologies toward the Valorization of Bio-based Wastes and by Products from Foods.” *Comprehensive Reviews in Food Science and Food Safety* 21(1): 46–105. doi:10.1111/1541-4337.12894.

Charfi, Amine. 2014. “Etude d’un Procédé Membranaire de Traitement Des Eaux Usées : Effet Des Paramètres Biotiques et Abiotiques Sur Le Colmatage de La Membrane.” Université de Carthage. https://hal.science/tel-01098726v2.

Cherifi, Leila, Yamina Ammi, Salah Hanini, Mohamed Hentabli, Ouafa Belkacem, and Jérôme Harmand. 2025. “A Novel Empirical Fractional Approach for Modeling the Clogging of Membrane Filtration During Protein Microfiltration.” *Membranes* 15(4): 99. doi:10.3390/membranes15040099.

Cho, Jaeweon, Gary Amy, and John Pellegrino. 1999. “Membrane Filtration of Natural Organic Matter: Initial Comparison of Rejection and Flux Decline Characteristics with Ultrafiltration and Nanofiltration Membranes.” *Water Research* 33(11): 2517–26. doi:10.1016/S0043-1354(98)00498-9.

Ciobanu, Gabriela, Gabriela Carja, Lacramioara Istrati, and Maria Harja. 2006. “Etude Du Colmatage Des Membranes ♦.” VII(2): 397–404.

Cirillo, Andrea Iginio, Giovanna Tomaiuolo, and Stefano Guido. 2021. “Membrane Fouling Phenomena in Microfluidic Systems: From Technical Challenges to Scientific Opportunities.” *Micromachines* 12(7). doi:10.3390/mi12070820.

Collet, Gaëlle. 2013. “Étude et Modélisation Du Colmatage de Membrane d’ultrafiltration Par Des Suspensions de Matières Organiques et de Particules Minérales.”

Dahdouh, Layal, and Christelle Wisniewski. 2018. “Faisabilité et Performances Filtration de Coproduits Des Industries Vinicoles Par Membranes Fibres Creuses Immergées.” (April).

Dahmani, Abdennasser, Yamina Ammi, and Salah Hanini. 2023. “A Novel Non-Linear Model Based on Bootstrapped Aggregated Support Vector Machine for the Prediction of Hourly Global Solar Radiation.” *Smart Grids and Sustainable Energy* 9(1): 3. doi:10.1007/s40866-023-00179-w.

Debnath, Lokenath. 2003. “Recent Applications of Fractional Calculus to Science and Engineering.” *International Journal of Mathematics and Mathematical Sciences* 2003(54): 3413–42. doi:10.1155/S0161171203301486.

Duclos-Orsello, Chase, Weiyi Li, and Chia-Chi Ho. 2006. “A Three Mechanism Model to Describe Fouling of Microfiltration Membranes.” *Journal of Membrane Science* 280(1–2): 856–66. doi:10.1016/j.memsci.2006.03.005.

Emmanuel, Hemen, Sara Kazemi, Yousif Abdalla, and Emma Etim. 2024. “Case Studies in Chemical and Environmental Engineering Evaluation of Membrane Bioreactor (MBR) Technology for Industrial Wastewater Treatment and Its Application in Developing Countries : A Review.” *Case Studies in Chemical and Environmental Engineering* 10(August): 100886. doi:10.1016/j.cscee.2024.100886.

Espinasse, Benjamin. 2003. “Approche Theorique Et Experimentale De La Filtration Tangentielle De Colloïdes : Flux Critique Et Colmatage.” : 214.

Fortunato, Luca, Frank Lipnizki, and Ludovic F. Dumée. 2021. “Editorial: Fouling in Membrane Filtration Systems.” *Frontiers in Chemical Engineering* 3(December): 10–12. doi:10.3389/fceng.2021.812625.

Ghalami Choobar, Behnam, Mohammad Amin Alaei Shahmirzadi, Ali Kargari, and Massoumeh Manouchehri. 2019. “Fouling Mechanism Identification and Analysis in Microfiltration of Laundry Wastewater.” *Journal of Environmental Chemical Engineering* 7(2). doi:10.1016/j.jece.2019.103030.

Gholami, Yousef. 2020. “Existence and Uniqueness Criteria for the Higher-Order Hilfer Fractional Boundary Value Problems at Resonance.” *Advances in Difference Equations* 2020(1): 482. doi:10.1186/s13662-020-02941-1.

Giusti, Andrea, Ivano Colombaro, Roberto Garra, Roberto Garrappa, Federico Polito, Marina Popolizio, and Francesco Mainardi. 2020. “A Practical Guide to Prabhakar Fractional Calculus.” *Fractional Calculus and Applied Analysis* 23(1): 9–54. doi:10.1515/fca-2020-0002.

Gonsalves, V. E. 1950. “A Criťical Investigation on the Viscose Filtration Process.” *Recueil des Travaux Chimiques des Pays-Bas* 69(7): 873–903. doi:10.1002/recl.19500690711.

Grace, H. P. 1956. “Structure and Performance of Filter Media. II. Performance of Filter Media in Liquid Service.” *AIChE Journal* 2(3): 316–36. doi:10.1002/aic.690020308.

Günther, Jan. 2009. “Caractérisation et Optimisation Des Phénomènes de Transfert Dans Un Double Bioréacteur à Membranes.”

Guo, Wenshan, Huu Hao Ngo, and Jianxin Li. 2012. “A Mini-Review on Membrane Fouling.” *Bioresource Technology* 122: 27–34. doi:10.1016/j.biortech.2012.04.089.

Haber, Charbel, Jonathan Skupsky, Ann Lee, and Russ Lander. 2004. “Membrane Chromatography of DNA: Conformation-induced Capacity and Selectivity.” *Biotechnology and Bioengineering* 88(1): 26–34. doi:10.1002/bit.20201.

Habibi, Sepideh. 2014. “An Upscaled Study of a Membrane Filtration Process in Presence of Biofilms.” : 200. https://theses.hal.science/tel-01127571v1.

Haubold, H. J., A. M. Mathai, and R. K. Saxena. 2009. “Mittag-Leffler Functions and Their Applications” ed. Ch Tsitouras. *Journal of Applied Mathematics* 2011(1). doi:10.1155/2011/298628.

Hee-deung, Park, Chang I N-soung, and Lee Kwang-jin. 2015. *Principles of Membrane Bioreactors for Wastewater Treatment Waste Activated Sludge*.

Hentabli, Mohamed, Abd Elmouneïm Belhadj, Hania Benimam, Farid Dahmoune, and Sonia Keskes. 2021. “Vacuum Drying of the Terbinafine HCl Powder: A Kinetics Study and Mathematical Modeling.” *Powder Technology* 383: 220–32. doi:10.1016/J.POWTEC.2021.01.038.

Hermans, P. H., and H. L. Bredée. 1935. “Zur Kenntnis Der Filtrationsgesetze.” *Recueil des Travaux Chimiques des Pays-Bas* 54(9): 680–700. doi:10.1002/recl.19350540902.

Hermia, Jacques. 1966. “Etude Analytique Des Lois de Filtration à Pression Constante.” *Rev. Univ. Mines* 2(5).

Hermia, Jacques. 1982. “Constant Pressure Blocking Filtration Laws - Application To Power-Law Non-Newtonian Fluids.” *Institution of Chemical Engineers. Transactions* 60(3): 183–87. http://hdl.handle.net/2078.1/57489.

Hermia, Jacques. 1985. “Blocking Filtration. Application to Non-Newtonian Fluids.” In *Mathematical Models and Design Methods in Solid-Liquid Separation*, Dordrecht: Springer Netherlands, 83–89. doi:10.1007/978-94-009-5091-7_5.

Ho, Chia-Chi, and Andrew L. Zydney. 2000. “A Combined Pore Blockage and Cake Filtration Model for Protein Fouling during Microfiltration.” *Journal of Colloid and Interface Science* 232(2): 389–99. doi:10.1006/jcis.2000.7231.

Ho, Chia Chi, and Andrew L. Zydney. 2000. “Measurement of Membrane Pore Interconnectivity.” *Journal of Membrane Science* 170(1): 101–12. doi:10.1016/S0376-7388(99)00360-9.

Hou, Lei, Zhan Wang, and Peng Song. 2017a. “A Precise Combined Complete Blocking and Cake Filtration Model for Describing the Flux Variation in Membrane Filtration Process with BSA Solution.” *Journal of Membrane Science* 542: 186–94. doi:10.1016/j.memsci.2017.08.013.

Hou, Lei, Zhan Wang, and Peng Song. 2017b. “A Precise Combined Complete Blocking and Cake Filtration Model for Describing the Flux Variation in Membrane Filtration Process with BSA Solution.” *Journal of Membrane Science* 542: 186–94. doi:10.1016/j.memsci.2017.08.013.

Hu, Ge, Chenyin Zhong, Zhan Wang, and Xi Wang. 2021. “Application of Error Function in Dead-End/Cross-Flow Microfiltration Mode.” *IOP Conference Series: Earth and Environmental Science* 647(1). doi:10.1088/1755-1315/647/1/012007.

Iritani, Eiji. 2013. “A Review on Modeling of Pore-Blocking Behaviors of Membranes During Pressurized Membrane Filtration.” *Drying Technology* 31(2): 146–62. doi:10.1080/07373937.2012.683123.

Iritani, Eiji, and Nobuyuki Katagiri. 2016. “Developments of Blocking Filtration Model in Membrane Filtration.” *KONA Powder and Particle Journal* 2016(33): 179–202. doi:10.14356/kona.2016024.

Iritani, Eiji, Yasuhito Mukai, Yoshiaki Tanaka, and Toshiro Murase. 1995. “Flux Decline Behavior in Dead-End Microfiltration of Protein Solutions.” *Journal of Membrane Science* 103(1–2): 181–91. doi:10.1016/0376-7388(94)00321-O.

Janzén, David, Mats Jirstrand, Neil D. Evans, and Michael Chappell. 2015. “Structural Identifiability in Mixed-Effects Models: Two Different Approaches.” *IFAC-PapersOnLine* 28(20): 563–68. doi:10.1016/j.ifacol.2015.10.201.

Janzén, David L.I., Mats Jirstrand, Michael J. Chappell, and Neil D. Evans. 2019. “Three Novel Approaches to Structural Identifiability Analysis in Mixed-Effects Models.” *Computer Methods and Programs in Biomedicine* 171: 141–52. doi:10.1016/j.cmpb.2016.04.024.

Jaques, A., C. Da Silva, N. Duru, and T. Seal. 2017. “Fractional Calculus Application for Diffusion Controlled Leaching Column Testing.” *International Journal of Mineral Processing* 169: 185–87.

doi:10.1016/j.minpro.2017.09.007.

Jelemenský, Martin, Ayush Sharma, Radoslav Paulen, and Miroslav Fikar. 2016. “Time-Optimal Control of Diafiltration Processes in the Presence of Membrane Fouling.” *Computers and Chemical Engineering* 91: 343–51. doi:10.1016/j.compchemeng.2016.04.018.

Jierula, Alipujiang, Shuhong Wang, Tae-Min OH, and Pengyu Wang. 2021. “Study on Accuracy Metrics for Evaluating the Predictions of Damage Locations in Deep Piles Using Artificial Neural Networks with Acoustic Emission Data.” *Applied Sciences* 11(5): 2314. doi:10.3390/app11052314.

Kalboussi, Nesrine. 2018. “Détection Précoce et Contrôle de Colmatage d’une Membrane de Filtration.”

Khan, Mumtaz, and Amer Rasheed. 2022. “Numerical Study of Diffusion-Thermo Phenomena in Darcy Medium Using Fractional Calculus.” *Waves in Random and Complex Media*: 1–18. doi:10.1080/17455030.2022.2098414.

Kim, M. J., G. Y. Yoo, and C. K. Yoo. 2011. “Development of Combined Fouling Model in a Membrane Bioreactor.” *Asia-Pacific Journal of Chemical Engineering* 6(3): 423–32. doi:10.1002/apj.589.

Lakhdar ABOUDA. 2024. “CONTRIBUTION TO THE FRACTIONAL MODELLING OF FILTRATION.”

Larson, Jonathan W., Gregory R. Yantz, Qun Zhong, Rebecca Charnas, Christina M. D’Antoni, Michael V. Gallo, Kimberly A. Gillis, et al. 2006. “Single DNA Molecule Stretching in Sudden Mixed Shear and Elongational Microflows.” *Lab Chip* 6(9): 1187–99. doi:10.1039/B602845D.

Laska, Michael E., Ralph P. Brooks, Marshall Gayton, and Narahari S. Pujar. 2005. “Robust Scale-up of Dead End Filtration: Impact of Filter Fouling Mechanisms and Flow Distribution.” *Biotechnology and Bioengineering* 92(3): 308–20. doi:10.1002/bit.20587.

Li, Haigang, Huanjin Xia, and Yingxin Mei. 2016. “Modeling Organic Fouling of Reverse Osmosis Membrane: From Adsorption to Fouling Layer Formation.” *Desalination* 386: 25–31. doi:10.1016/j.desal.2016.02.037.

Liang, Song, Ranchao Wu, and Liping Chen. 2015. “Laplace Transform of Fractional Order Differential Equations.” *Electronic Journal of Differential Equations* 2015(139): 1–15.

Liu, Shi Yue, Zhengyi Chen, and Pejman Sanaei. 2020. “Effects of Particles Diffusion on Membrane Filters Performance.” *Fluids* 5(3): 121. doi:10.3390/fluids5030121.

Ludwig, T., D. Gaida, C. Keysers, J. Pinnekamp, M. Bongards, P. Kern, C. Wolf, and A. L. Sousa Brito. 2012. “An Advanced Simulation Model for Membrane Bioreactors: Development, Calibration and Validation.” *Water Science and Technology* 66(7): 1384–91. doi:10.2166/wst.2012.249.

Mafirad, S., M. R. Mehrnia, H. Azami, and M. H. Sarrafzadeh. 2011. “Effects of Biofilm Formation on Membrane Performance in Submerged Membrane Bioreactors.” *Biofouling* 27(5): 477–85. doi:10.1080/08927014.2011.584619.

Malaeb, Lilian, Pierre Le-Clech, Johannes S. Vrouwenvelder, George M. Ayoub, and Pascal E. Saikaly. 2013. “Do Biological-Based Strategies Hold Promise to Biofouling Control in MBRs?” *Water Research* 47(15): 5447–63. doi:10.1016/j.watres.2013.06.033.

McLoughlin, C. M., W. A.M. McMinn, and T. R.A. Magee. 2003. "Microwave-Vacuum Drying of Pharmaceutical Powders." *Drying Technology* 21(9): 1719–33. doi:10.1081/DRT-120025505.

Mehrabi, Mohammad, and Vahid Vatanpour. 2024. "Polyimide-Based Separation Membranes for Liquid Separation: A Review on Fabrication Techniques, Applications, and Future Perspectives." *Materials Today Chemistry* 35: 101895. doi:10.1016/j.mtchem.2024.101895.

Mesli, Chehrazad, Maamar Laidi, Salah Hanini, Asma Adda, Mohammed Moussaoui, and Mohamed Hentabli. 2022. "Fractional Calculus-Based Modelling of Membrane Filtration." *Kemija u industriji* 71(1–2): 1–7. doi:10.15255/KUI.2021.007.

Michel Jaffrin. 2015. *Membrane Filtration Processes*.

Mirjalili, Seyedali. 2016. "Dragonfly Algorithm: A New Meta-Heuristic Optimization Technique for Solving Single-Objective, Discrete, and Multi-Objective Problems." *Neural Computing and Applications* 27(4): 1053–73. doi:10.1007/s00521-015-1920-1.

Mokarizadeh, Hadi, and Ahmadreza Raisi. 2021. "Industrial Wastewater Treatment Using PES UF Membranes Containing Hydrophilic Additives: Experimental and Modeling of Fouling Mechanism." *Environmental Technology & Innovation* 23: 101701. doi:10.1016/j.eti.2021.101701.

Mondal, Sourav, and Sirshendu De. 2010. "A Fouling Model for Steady State Crossflow Membrane Filtration Considering Sequential Intermediate Pore Blocking and Cake Formation." *Separation and Purification Technology* 75(2): 222–28. doi:10.1016/j.seppur.2010.07.016.

Monnot, Mathias. 2015. "Conception d'une Filière Intensifiée Par Membrane Pour Le Dessalement Autonome d'eau de Mer : Étude Du Prétraitement et de Son Effet Sur Le Biocolmatage." INSA de Toulouse.

de Morais Coutinho, Cesar, Ming Chih Chiu, Rodrigo Correa Basso, Ana Paula Badan Ribeiro, Lireny Aparecida Guaraldo Gonçalves, and Luiz Antonio Viotto. 2009. "State of Art of the Application of Membrane Technology to Vegetable Oils: A Review." *Food Research International* 42(5–6): 536–50. doi:10.1016/j.foodres.2009.02.010.

Morgane, LE HIR. 2017. "Caractérisation Du Colmatage Des Membranes d'ultrafiltration de Production d'eau Potable Par Des Nanoparticules Fluorescentes."

Pan, Yanqiu, Wei Wang, Tonghua Wang, and Pinjing Yao. 2007. "Fabrication of Carbon Membrane and Microfiltration of Oil-in-Water Emulsion: An Investigation on Fouling Mechanisms." *Separation and Purification Technology* 57(2): 388–93. doi:10.1016/j.seppur.2007.04.024.

Paul, Parneet. 2013. "Development and Testing of a Fully Adaptable Membrane Bioreactor Fouling Model for a Sidestream Configuration System." *Membranes* 3(2): 24–43. doi:10.3390/membranes3020024.

Piry, A., A. Heino, W. Kühnl, T. Grein, S. Ripperger, and U. Kulozik. 2012. "Effect of Membrane Length, Membrane Resistance, and Filtration Conditions on the Fractionation of Milk Proteins by Microfiltration." *Journal of Dairy Science* 95(4): 1590–1602. doi:10.3168/jds.2011-4292.

Podlubny, I. 1999. "Fractional-Order Systems and PI/Sup /Spl Lambda//D/Sup /Spl Mu//-Controllers." *IEEE Transactions on Automatic Control* 44(1): 208–14. doi:10.1109/9.739144.

Qrenawi, Luay I., and A. A. Abuhabib. 2020. "A Review on Sources, Types, Mechanisms, Characteristics, Impacts and Control Strategies of Fouling in Ro Membrane Systems." *Desalination and Water Treatment* 208: 43–69. doi:10.5004/dwt.2020.26448.

Rayess, Youssef El. 2023. "Microfiltration Tangentielle Appliquée à l ' Oenologie : Compréhension et Maîtrise Des Phénomènes de Colmatage To Cite This Version : HAL Id : Tel-04241263."

Redhwan, Saleh S., Maoan Han, Mohammed A. Almalahi, Maryam Ahmed Alyami, Mona Alsulami, and Najla Alghamdi. 2024. "Piecewise Implicit Coupled System under ABC Fractional Differential Equations with Variable Order." *AIMS Mathematics* 9(6): 15303–24. doi:10.3934/math.2024743.

Romdhane, Ahlem. 2014. "Procédés de Séparation Membranaire Pour La Production En Continu de Nanocristaux de Polysaccharides: Approche Expérimentale et Modélisation." https://tel.archives-ouvertes.fr/tel-01153860/%5Cnhttps://tel.archives-ouvertes.fr/tel-01153860/document.

Rouquié, Camille. 2018. "Microfiltrat Ion de Jus de Fruits et Suspensions à Base de Fruits : Faisabilité et Performances d'une Filtrat Ion Par Membranes Immergées."

Salahi, Abdolhamid, Mohsen Abbasi, and Toraj Mohammadi. 2010. "Permeate Flux Decline during UF of Oily Wastewater: Experimental and Modeling." *Desalination* 251(1–3): 153–60. doi:10.1016/j.desal.2009.08.006.

Sandoval-García, V., M.V. Ruano, M. Alliet, C. Brepols, J. Comas, J. Harmand, M. Heran, et al. 2025. "Modeling MBR Fouling: A Critical Review Analysis towards Establishing a Framework for Good Modeling Practices." *Water Research* 268: 122611. doi:10.1016/j.watres.2024.122611.

Sayevand, Khosro, and Valeyollah Moradi. 2021. "A Robust Computational Framework for Analyzing Fractional Dynamical Systems." *Discrete & Continuous Dynamical Systems - S* 14(10): 3763. doi:10.3934/dcdss.2021022.

Seemab, Arjumand, ur Mujeeb Rehman, Michal Feckan, Jehad Alzabut, and Syed Abbas. 2021. "On the Existence and Ulam-Hyers Stability of a New Class of Partial (Φ,χ)-Fractional Differential Equations with Impulses." *Filomat* 35(6): 1977–91. doi:10.2298/FIL2106977S.

Shirato, Mompei, Tsutomu Aragaki, and Eiji Iritani. 1979. "Blocking Filtration Laws for Filtration of Power-Law Non-Newtonian Fluids." *JOURNAL OF CHEMICAL ENGINEERING OF JAPAN* 12(2): 162–64. doi:10.1252/jcej.12.162.

Sim, Lee Nuang, Tzyy Haur Chong, Amir Hooshang Taheri, S. T.V. Sim, Li Lai, William B. Krantz, and Anthony G. Fane. 2018. "A Review of Fouling Indices and Monitoring Techniques for Reverse Osmosis." *Desalination* 434(December): 169–88. doi:10.1016/j.desal.2017.12.009.

Simpson, R., A. Jaques, H. Nuñez, C. Ramirez, and A. Almonacid. 2013. "Fractional Calculus as a Mathematical Tool to Improve the Modeling of Mass Transfer Phenomena in Food Processing." *Food Engineering Reviews* 5(1): 45–55. doi:10.1007/s12393-012-9059-7.

Slimane, Fatma Zohra, Fatma Ellouze, Ghofrane Ben Miled, and Nihel Ben Amar. 2018. "Physical Backwash Optimization in Membrane Filtration Processes: Seawater Ultrafiltration Case." *Journal of Membrane Science and Research* 4(2): 63–68. doi:10.22079/JMSR.2017.66624.1145.

Sophie, mission. 2024. "Formulation et Étude de Nouveaux Détergents Enzymatiques Pour Le Nettoyage

de Membranes d'ultrafiltration de l'industrie Laitière – Développement et Validation de Méthodologies Associées."

de Souza Matias, Gustavo, Camila Andressa Bissaro, Luiz Mario de Matos Jorge, and Diogo Francisco Rossoni. 2019. "The Fractional Calculus in Studies on Drying: A New Kinetic Semi-Empirical Model for Drying." *Journal of Food Process Engineering* 42(1): 1–7. doi:10.1111/jfpe.12955.

de Souza Matias, Gustavo, Fernando Henrique Lermen, Camila Andressa Bissaro, Douglas Júnior Nicolin, Clovis Fischer, and Luiz Mário de Matos Jorge. 2022. "Fractional Calculus to Control Transport Phenomena in Food Engineering: A Systematic Review of Barriers and Data Agenda." *Journal of Food Process Engineering* 45(8). doi:10.1111/jfpe.14060.

Šuvakov, Milovan, and Bosiljka Tadić. 2010. "Modeling Collective Charge Transport in Nanoparticle Assemblies." *Journal of Physics: Condensed Matter* 22(16): 163201. doi:10.1088/0953-8984/22/16/163201.

Tien, Chi, B. V. Ramarao, and Rakesh Yasarla. 2014. "A Blocking Model of Membrane Filtration." *Chemical Engineering Science* 111: 421–31. doi:10.1016/j.ces.2014.01.022.

Touffet, Arnaud. 2014. "Impact de La Qualité de La Ressource, Des Prétraitements et Des Lavages Chimiques." L'UNIVERSITÉ DE POITIERS. http://theses.univ-poitiers.fr.

Tracey, Eve M., and Robert H. Davis. 1994. "Protein Fouling of Track-Etched Polycarbonate Microfiltration Membranes." *Journal of Colloid and Interface Science* 167(1): 104–16. doi:10.1006/jcis.1994.1338.

Uragami, Tadashi. 2017. "Introduction to Membrane Science and Technology." In *Science and Technology of Separation Membranes*, Wiley, 1–12. doi:10.1002/9781118932551.ch1.

Vela, vincent M Cinta, Silvia Alvarez, Jaime Lora Garc, and Enrique Berganti. 2008. "Analysis of Membrane Pore Blocking Models Applied to the Ultrafiltration of PEG." 62: 489–98. doi:https://doi.org/10.1016/j.seppur.2008.02.028.

Villaverde, Alejandro F., Antonio Barreiro, and Antonis Papachristodoulou. 2016. "Structural Identifiability of Dynamic Systems Biology Models" ed. Satoru Miyano. *PLOS Computational Biology* 12(10): e1005153. doi:10.1371/journal.pcbi.1005153.

Wang, Zhiwei, Jinxing Ma, Chuyang Y. Tang, Katsuki Kimura, Qiaoying Wang, and Xiaomeng Han. 2014. "Membrane Cleaning in Membrane Bioreactors: A Review." *Journal of Membrane Science* 468: 276–307. doi:10.1016/j.memsci.2014.05.060.

Water Treatment Suppliers. 2023. "How Do I Know if My RO Membrane Is Clogged?" Consulted June 2025. https://watertreatmentsuppliers.com/how-do-i-know-if-my-ro-membrane-is-clogged/.

.Xiao, Kang, Yinghui Mo, Jianyu Sun, Mingyu Wang, Shuai Liang, Xiaomao Wang, Xia Huang, and T. David Waite. 2019. "An Extended Standard Blocking Filtration Law for Exploring Membrane Pore Internal Fouling Due to Rate-Determining Adsorption." *Separation and Purification Technology* 212: 974–79. doi:10.1016/j.seppur.2018.12.009.

Xu, Hao, Kang Xiao, Jinlan Yu, Bin Huang, Xiaomao Wang, Shuai Liang, Chunhai Wei, Xianghua Wen, and Xia Huang. 2020. "A Simple Method to Identify the Dominant Fouling Mechanisms during

Membrane Filtration Based on Piecewise Multiple Linear Regression." *Membranes* 10(8): 171. doi:10.3390/membranes10080171.

Yin, Shuang, Peng Song, Yujie Chen, Xinpei Du, Xuguo Liu, Hu Zhang, Zhan Wang, and Xi Wang. 2021. "An Investigation of the Membrane Fouling Behaviors in Constant Flux Mode." *IOP Conference Series: Earth and Environmental Science* 647(1): 012203. doi:10.1088/1755-1315/647/1/012203.

Zydney, Andrew L. 2022. "Development of a New Blocking Model for Membrane Fouling Based on a Composite Media Model." *Journal of Membrane Science Letters* 2(1): 100018. doi:10.1016/j.memlet.2022.100018.

Zydney, Andrew L., and Chia Chi Ho. 2002. "Scale-up of Microfiltration Systems: Fouling Phenomena and Vmax Analysis." *Desalination* 146(1–3): 75–81. doi:10.1016/S0011-9164(02)00492-7.

Annexes

Annex 1

Table annex 1.1: Summary of experimental values (database DB II. 1*)*

P=2psi		P=5psi		P=10psi		P=20psi	
t (s)	v (m^3)	t (s)	v (m^3)	t (s)	v (m^3)	t (s)	v (m^3)
22.792	726.644	22.792	1937.72	0	1211.07	22.7273	4117.65
45.584	1453.29	23.569	2179.93	22.792	2422.15	45.4545	7993.08
68.3761	1695.5	45.584	2664.36	23	3633.22	46	10173
113.96	2179.93	46.7425	3148.79	45.584	4602.08	47	6782.01
115.156	2664.36	68.3761	3391	47	5813.15	48	5570.93
138.092	2906.57	69.7578	3633.22	68.3761	6782.01	49	9446.37
161.028	3148.79	91.1681	4117.65	91.1681	8235.29	68.1818	13564
182.336	3148.79	92.9313	4602.08	92	8961.94	70	11868.5
183.964	3391	113.96	4602.08	113.96	9688.58	90.9091	17439.4
206.901	3633.22	115.947	5086.51	136.752	12110.7	93	16228.4
252.694	3633.22	136.752	5328.72	159.544	13806.2	94.9091	18650.5
273.504	3875.43	138.962	5570.93	182.336	14775.1	98.9091	14775.1
275.63	4117.65	159.544	5813.15	205.128	15501.7	113.636	20103.8
321.503	4602.08	162.056	6297.58	227.92	16470.6	159.091	22283.7
341.88	4602.08	182.336	6297.58	250.712	17439.4	160	21072.7
367.296	4844.29	185.151	7024.22	273.504	18166.1	181.818	24221.5
390.232	5086.51	208.324	7993.08	274	19134.9	188	23494.8
413.169	5328.72	254.355	8961.94	296.296	20346	204.545	24948.1
433.048	5328.72	273.504	8477.51	319.088	21557.1	227.273	25917
436.105	5570.93	277.449	9688.58	341.88	22526	230	26643.6
481.898	5813.15	319.088	9930.8	364.672	23494.8	250	28339.1
524.217	5813.15	323.322	10173	387.464	24705.9	266	27612.5
527.692	6055.36	346.416	10899.7	410.256	25432.5	272.727	29308
573.485	6055.36	364.672	10899.7	433.048	26643.6	295.455	30276.8
592.593	6297.58	369.432	11384.1	478.632	27612.5	300	31003.5
619.278	6539.79	387.464	11384.1	501.425	28823.5	318.182	31730.1
665.072	6539.79	392.447	11868.5	547.009	29792.4	340.909	33425.6
683.761	6782.01	410.256	11868.5	592.593	30761.2	345.909	32699
733.722	7024.22	415.462	12352.9	615.385	31730.1	363.636	34152.2
779.516	7024.22	461.335	12837.4	660.969	32699	386.364	35121.1
797.721	7266.44	501.425	13321.8	706.553	33667.8	409.091	36090
825.23	7266.44	530.143	13564	752.137	34636.7	415.091	36816.6
843.305	7266.44	576.016	14048.4	797.721	35847.8	431.818	37301
870.944	7266.44	592.593	14290.7	866.097	37058.8	454.545	38512.1
916.738	7266.44	621.888	14532.9	911.681	37785.5	477.273	39238.8
957.265	7508.65	667.761	15017.3	980.057	38754.3	500	39723.2
985.309	7508.65	713.633	15501.7	1048.43	39965.4	522.727	40449.8
1071.23	7750.87	759.506	15986.2	1139.6	40934.3	545.455	41176.5

1076.82	7750.87	797.721	16012.8	1230.77	41418.7	568.182	41903.1
1145.39	7750.87	805.299	16228.4	1321.94	42387.5	613.636	43114.2
1162.39	7993.08	851.172	16712.8	1435.9	43598.6	659.091	44325.3
1191.18	7993.08	896.965	16955	1549.86	44325.3	704.545	45294.1
1253.56	7993.08	942.758	17197.2	1618.23	44809.7	750	46020.8
1282.61	7993.08	1011.41	17439.4	1686.61	45294.1	772.727	46747.4
1367.52	7993.08	1057.2	17681.7	1823.36	45778.5	795.455	47474
1374.04	7993.08	1148.79	18166.1	1914.53	46263	886.364	48442.9
1465.47	8235.29	1194.58	18408.3	2074.07	46989.6	931.818	49169.6
1504.27	8235.29	1207.98	18650.5	2210.83	47231.8	1000	50138.4
1534.04	8235.29	1240.38	18750.5	2347.58	47474	1045.45	51107.3
1579.75	8235.29	1309.03	18892.7	2461.54	47958.5	1113.64	51591.7
1618.23	8235.29	1354.82	19134.9	2575.5	48200.7	1181.82	52318.3
1625.55	8235.29	1400.53	19134.9	2712.25	48442.9	1272.73	53045
1694.12	8235.29	1413.11	19619.4	2849	48685.1	1340.91	53529.4
1754.99	8235.29	1492.04	19619.4	2962.96	49169.6	1409.09	54256.1
1762.69	8235.29	1560.61	19619.4	3145.3	49169.6	1477.27	54740.5
1808.4	8477.51	1629.26	19619.4	3282.05	49654	1568.18	55224.9
1854.2	8477.51	1674.98	19619.4	3418.8	49896.2	1659.09	55951.6
1868.95	8477.51	1709.4	19861.6	3555.56	49896.2	1750	56436
1968.48	8477.51	1743.63	20103.8	3669.52	49896.2	1863.64	56920.4
2005.7	8477.51	1857.99	20200	3783.48	49896.2	1954.55	57404.8
2082.77	8719.72	1868.95	20346	3943.02	50138.4	2045.45	57889.3
2165.24	8719.72	1903.71	20346	4056.98	50138.4	2159.09	58373.7
2174.28	8719.72	1960.11	20346	4148.15	50380.6	2272.73	58615.9
2242.85	8719.72	1972.28	20346	4239.32	50380.6	2363.64	58858.1
2334.28	8719.72	2040.85	20400	4353.28	50380.6	2500	59342.6
2370.37	8961.94	2086.64	20400	4421.65	50622.8	2590.91	59584.8
2425.7	8961.94	2178.07	20400	4512.82	50865.1	2704.55	59827
2517.13	8961.94	2246.72	20588.2	4603.99	50865.1	2818.18	60069.2
2552.71	8961.94	2315.29	20588.2	4717.95	50865.1	2931.82	60311.4
2608.56	8961.94	2361.01	20588.2	4809.12	51107.3	3045.45	60795.8
2666.67	8961.94	2406.72	20588.2	4900.28	51107.3	3159.09	61038.1
2677.21	8961.94	2452.44	20588.2	4968.66	51107.3	3250	61280.3
2768.64	8961.94	2498.23	20830.4	5037.04	51349.5	3340.91	61280.3
2826.21	8961.94	2543.94	20830.4	5128.21	51591.7	3477.27	61764.7
2882.93	8961.94	2589.66	20830.4	5219.37	51591.7	3568.18	62006.9
2940.17	8961.94	2635.37	20830.4	5310.54	51591.7	3681.82	62249.1
2997.21	8961.94	2703.94	20830.4	5378.92	51591.7	3772.73	62491.3
3088.64	9204.15	2772.52	20830.4	5470.09	51591.7	3886.36	62975.8
3122.51	9204.15	2818.31	21072.7	5584.05	51591.7	4000	62975.8
3180.15	9204.15	2864.02	21072.7	5698.01	51591.7	4113.64	63218
3282.05	9204.15	2932.6	21072.7	5789.17	51591.7	4181.82	63460.2

3294.43	9204.15	3001.17	21072.7	5880.34	51591.7	4250	63702.4
3408.72	9446.37	3069.74	21072.7	5971.51	51833.9	4363.64	63944.6
3418.8	9446.37	3138.39	21314.9	6017.09	51833.9	4431.82	63944.6
3545.86	9446.37	3184.1	21314.9	6108.26	51833.9	4522.73	63944.6
3578.35	9446.37	3275.53	21314.9	6199.43	51833.9	4636.36	63944.6
3637.29	9446.37	3344.1	21314.9	6267.81	51833.9	4727.27	63944.6
3760.68	9446.37	3389.82	21314.9	6313.39	51833.9	4795.45	63944.6
3728.8	9446.37	3435.53	21314.9	6404.56	51833.9	4863.64	63944.6
3820.23	9446.37	3481.32	21557.1	6450.14	51833.9	/	/
3911.66	9446.37	3549.9	21557.1	6472.93	51833.9	/	/
3920.23	9446.37	3595.61	21557.1	6518.52	51833.9	/	/
4034.19	9688.58	3664.18	21557.1	/	/	/	/
4048.8	9688.58	3732.75	21557.1	/	/	/	/
4163.08	9688.58	3801.32	21557.1	/	/	/	/
4193.73	9688.58	3869.9	21557.1	/	/	/	/
4254.51	9688.58	3915.61	21557.1	/	/	/	/
4414.51	9688.58	3984.18	21557.1	/	/	/	/
4490.03	9688.58	4075.69	21799.3	/	/	/	/
4528.88	9688.58	4144.26	21799.3	/	/	/	/
4603.99	9930.8	4189.98	21799.3	/	/	/	/
4643.16	9930.8	4235.69	21799.3	/	/	/	/
4740.74	9930.8	4281.4	21799.3	/	/	/	/
4757.45	9930.8	4327.12	21799.3	/	/	/	/
4786.32	9930.8	4418.63	22041.5	/	/	/	/
4826.02	9930.8	4464.34	22041.5	/	/	/	/
4854.7	9930.8	4532.91	22041.5	/	/	/	/
4923.08	9930.8	4601.48	22041.5	/	/	/	/
4940.31	9930.8	4692.91	22041.5	/	/	/	/
5008.88	10173	4784.34	22041.5	/	/	/	/
5014.25	10173	4875.77	22041.5	/	/	/	/
5082.62	10173	4898.63	22041.5	/	/	/	/
5100.31	10173	4900.28	22283.7	/	/	/	/
5151	10173	5014.25	22283.7	/	/	/	/
5196.58	10173	5059.83	22283.7	/	/	/	/
		5105.41	22283.7	/	/	/	/

Table annex 1. 2: Summary of experimental values (database DB II. 2*)*

5psi	8psi	5psi	8psi

pQR150(20kb)		pQR150(20kb)		pGEc45(56kb)		pGEc45(56kb)	
t(s)	v(ml)	t(s)	v(ml)	t(s)	v(ml)	t(s)	v(ml)
0	0	0	0.220588	0	0.189076	0	0.346639
6.61014	0.0315126	13.22034	0.409664	13.22034	0.346639	19.83048	0.882353
6.61014	0.095044	19.83048	0.819328	13.22034	0.567227	26.44068	1.22899
13.22034	0.12605	19.83048	0.661765	19.83048	0.72479	33.05082	1.63866
19.83048	0.190088	26.44068	1.0084	33.05082	1.16597	33.05082	1.48109
26.44068	0.283613	52.88136	1.16597	33.05082	0.976891	46.27116	1.73319
33.05082	0.472689	52.88136	1.35504	46.27116	1.38655	52.88136	1.98529
33.05082	0.475113	59.4915	1.51261	59.4915	1.57563	59.4915	2.23739
46.27116	0.535714	66.1014	1.70168	72.7116	1.79622	72.7116	2.4895
52.88136	0.630252	72.7116	1.89076	79.3218	1.95378	92.5422	2.7416
66.1014	0.756303	92.5422	2.11134	92.5422	2.14286	105.7626	2.93067
72.7116	0.882353	112.3728	2.17437	112.3728	2.42647	118.983	3.08824
85.932	0.976891	132.2034	2.39496	132.2034	2.67857	132.2034	3.27731
92.5422	1.10294	178.4748	2.64706	152.034	2.9937	165.2544	3.56092
118.983	1.22899	191.6952	2.77311	171.8646	3.27731	191.6952	3.71849
152.034	1.32353	224.7456	2.9937	204.915	3.52941	211.5252	3.84454
171.8646	1.51261	251.1864	3.15126	237.966	3.78151	231.3558	3.90756
198.3048	1.70168	271.017	3.18277	271.017	3.97059	264.4068	4.03361
231.3558	1.82773	290.8476	3.30882	304.068	4.15966	304.068	4.22269
257.7966	1.98529	310.6782	3.37185	323.8986	4.31723	323.8986	4.31723
290.8476	2.11134	330.5082	3.40336	363.5592	4.47479	356.949	4.47479
323.8986	2.23739	350.3388	3.56092	423.051	4.72689	396.6102	4.69538
343.7286	2.30042	396.6102	3.68697	475.932	4.94748	469.3218	4.85294
403.2204	2.39496	449.4918	3.75	542.034	5.10504	515.5932	4.97899
475.932	2.55252	482.5422	3.84454	594.915	5.29412	594.915	5.13655
535.4238	2.67857	535.4238	3.93908	661.014	5.45168	661.014	5.26261
588.3048	2.86765	594.915	4.0021	727.116	5.51471	713.898	5.35714
654.408	2.96218	667.626	4.06513	780	5.70378	760.17	5.45168
713.898	3.05672	713.898	4.12815	898.986	5.86134	898.986	5.57773
766.782	3.18277	766.782	4.12815	1024.578	6.01891	1017.966	5.70378
892.374	3.27731	898.986	4.22269	1130.34	6.14496	1136.952	5.82983
1011.354	3.43487	1011.354	4.28571	1262.544	6.20798	1242.714	5.89286
1143.558	3.56092	1143.558	4.34874	1434.408	6.36555	1447.626	6.01891
1262.544	3.71849	1242.714	4.41176	1619.49	6.4916	1626.102	6.11345
1341.864	3.84454	1388.136	4.5063	1797.966	6.58613	1791.354	6.17647
1407.966	3.93908	1553.388	4.56933	1910.34	6.61765	1877.286	6.20798
1474.068	4.021	1745.082	4.66387	1950	6.61765	1936.782	6.20798
1507.116	4.06126	1857.456	4.66387	1976.442	6.61765	1969.83	6.20798
1525.932	4.09815	1923.558	4.66387	2100	6.61765	2100	6.20798
1566.612	4.11966	2100	4.66387	/	/	/	/
1659.66	4.19159	/	/	/	/	/	/

1772.544	4.22159	/	/	/	/	/	/
1858.986	4.22159	/	/	/	/	/	/
1894.068	4.22159	/	/	/	/	/	/
1965.252	4.22159						
1998.306	4.22159						
2100	4.22159						

Table annex 1. 3: adjustment parameters values of the proposed empirical fractional estimation models for membrane filtration clogging at different pressures for database DB II. 1

Model	Parameter Pressure (psi)	a	b	c	d	n	m	$v_\infty(10^4.m^3)$
Model 1	p= 2	0,1625	0,2262	-	-	1,1459	1,0644	-
	p= 5	0.3148	0.0897	-	-	0.9553	1.0375	-
	p= 10	0.6137	0.0770	-	-	0.9776	1.0509	-
	p= 20	1.2827	0.1799	-	-	0.9193	0.9232	-
Model 2	p= 2	0.1627	-	-	-	0.9107	-	1,0904
	p= 5	0.1254	-	-	-	1.1091	-	2.3470
	p= 10	0.1022	-	-	-	1.1232	-	5.4805
	p= 20	0,1836	-	-	-	0,9261	-	6.9917
model3	p= 2	6,1474		-	-	0.9107	-	1.0904
	p= 5	7.9741		-	-	1.1091	-	2.3470
	p= 10	9.7815	-	-	-	1.1232	-	5.4805
	p= 20	6.9917	-	-	-	0.9261	-	5.4463
Model 4	p=2	3.0194	-	-	-	0.6540	3.1373	0.3878
	p= 5	6.9427	-	-	-	0.7747	3.5101	0.3607
	p= 10	3.2078	-	-	-	0.7734	3.9047	1.8188
	p= 20	5.0704	-	-	-	0,6521	2,8784	1,4920
Model 5	p= 2	0.2909	0.2626	0.7361	0.9602	0.7798	1.5450	-
	p= 5	1.3370	1.8824	101.3699	2.6672	1.5633	0.4960	-
	p= 10	8.7545	9.6073	499.2764	5.5817	1.4998	0.5452	-
	p= 20	11.7122	5.5020	33,0878	3,3907	0.9468	0.9524	-
Model 6	p= 2	0,1774	0.1627	-	-	0.9107	-	-
	p= 5	0.2943	0.1254	-	-	1.1091		-
	p= 10	0.5603	0.1022	-	-	1.1232		-
	p= 20	1.2838	0.1836	-	-	0.9261		-
Model 7	p= 2	$7.9676.10^{-8}$	0,0003	$8.0392.10^{4}$	-	-	-	6,4527
	p= 5	0.0421	0.0404	2.4367	-	-	-	7.5687
	p= 10	0.0362	0.0348	2.3530	-	-	-	17.3622
	p= 20	0.0340	0.0391	4.5158	-	-	-	36.4044
Model 8	p= 2	0.2040	133.0174	0.8961	-	0.6691		1.8866
	p= 5	0.1818	16.4385	0.0163	-	0.7549		2.2345
	p= 10	0.0356	17.6342	0.0342	-	1.0021		2.4051
	p= 20	0.2094	822.8046	0.0909	-	0.7157		6.9198

Table annex 1. 4:adjustment parameters values of the proposed empirical fractional estimation models for membrane filtration clogging at different pressures for database DB II. 2

Model	Parameter Pressure (psi)	a	b	c	d	n	m	$v_\infty(10^{-6}.m^3)$
Model II.1	p= 5 (150)	1.0998	0.3292	-	-	0.9492	0.8331	-
	p= 8 (150)	2.3280	0.5154	-	-	0.9863	0.9580	-
	p= 5 (47)	2.0627	0.3083	-	-	1.0040	0.9776	-
	p= 8 (47)	3.7735	0.7611	-	-	0,9774	0,8952	-
Model II.2	p= 5 (150)	0.1708	-	-	-	0,8341	-	5.6352
	p= 8 (150)	0.4334	-	-	-	0.9294	-	5.0664
	p= 5 (47)	0.2680	-	-	-	0,9627	-	7.4703
	p= 8 (47)	0.4291	-	-	-	0.8005	-	7.0848
Model II.3	p= 5 (150)	5.8551	-	-	-	0.8341	-	5.6352
	p= 8 (150)	5.0664	-	-	-	0.9294	-	2.3075
	p= 5 (47)	3.7313	-	-	-	0.9627	-	7.4703
	p= 8 (47)	2.3303	-	-	-	0,8005	-	7.0848
Model II.4	P= 5 (150)	1.1757		-	-	0.4962	3.1138	6.0713
	p= 8 (150)	0.7917		-	-	0.7533	1.7688	6.6756
	p= 5 (47)	0,877		-	-	0.6924	2.3537	9,2778
	p= 8 (47)	0.8984		-	-	0.6393	1.8040	8.3261
Model II.5	p= 5 (150)	7.5302	5.5527	4.8721	2.5372	0.4803	3.4534	-
	p= 8 (150)	1.8784	0,8817	1,2103	1,7957	0.8124	1.4061	-
	p= 5 (47)	4.3364	1.2671	3.1346	1,6109	0.8640	1,2676	-
	p= 8 (47)	6.2844	5,1563	2,1070	3,7263	0.5342	3.7756	-
Model II.6	p= 5 (150)	0.9624	0.1708	-	-	0.8341	-	-
	p= 8 (150)	2.1956	0.4334	-	-	0.9294	-	-
	p= 5 (47)	2.0020	0.2680	-	-	0.9627	-	-
	p= 8 (47)	3,0403	0,4291	-	-	0,8005	-	-
Model II7	p= 5 (150)	0.0866	0.1633	1.8471	-	-	-	12.8682
	p= 8 (150)	0.0786	0.0906	5.0377	-	-	-	29.1727
	p= 5 (47)	0.0882	0.1075	2.4076	-	-	-	23.3690
	p= 8 (47)	0.1197	0,1725	3,929	-	-	-	31,1071
Model II.8	p= 5 (150)	0.0559	0.1079	3.8352	-	1.1829	-	21.2195
	p= 8 (150)	0.5990	0.1319	-0.3382	-	0.8341	-	3.2295
	p= 5 (47)	0.0884	0.1149	2.4952	-	1.0400	-	23.7414
	p= 8 (47)	0.1032	0.1527	5,0826	-	1,0757	-	38,1018

Annex 2

Table annex 2. 1: Experimental values of Database (DB III. 1)

P= 1.5 bar		P=3 bar		P= 4.5 bar	
t(h)	J(L/m^2.h)	t(h)	J(L/m^2.h	t(h)	J(L/m^2.h
0.010597	537.079	0.003232	943.82	0.003067	838.202
0.019866	507.865	0.018628	912.36	0.015337	795.506
0.019941	483.146	0.024899	862.921	0.02454	750.562
0.02611	467.416	0.04035	813.483	0.033742	701.124
0.041478	444.944	0.034341	777.528	0.042945	662.921
0.041519	431.461	0.046684	743.82	0.052147	629.213
0.050741	417.978	0.059027	710.112	0.055215	606.742
0.056902	404.494	0.062169	683.146	0.055215	579.775
0.063036	400	0.074498	653.933	0.079755	559.551
0.07225	388.764	0.08374	633.708	0.082822	537.079
0.08145	382.022	0.092975	615.73	0.092025	521.348
0.087605	370.787	0.099143	600	0.101227	507.865
0.096819	359.551	0.108378	582.022	0.107362	494.382
0.106026	350.562	0.120673	564.045	0.116564	483.146
0.112174	341.573	0.123774	550.562	0.122699	471.91
0.124441	332.584	0.139109	539.326	0.131902	453.933
0.136716	321.348	0.14833	525.843	0.150307	435.955
0.155103	312.36	0.151417	516.854	0.171779	417.978
0.173511	296.629	0.169846	494.382	0.184049	400
0.185778	287.64	0.188268	474.157	0.196319	386.517
0.204166	278.652	0.203622	456.18	0.239264	357.303
0.23482	260.674	0.234298	431.461	0.266871	343.82
0.265455	249.438	0.255766	415.73	0.303681	323.596
0.296096	235.955	0.271107	402.247	0.328221	314.607
0.323656	229.213	0.301775	379.775	0.358896	303.371
0.36347	217.978	0.350804	357.303	0.398773	292.135
0.387984	206.742	0.390632	341.573	0.42638	285.393
0.427778	202.247	0.427386	330.337	0.45092	271.91
0.458398	195.506	0.46414	319.101	0.490798	265.169
0.489025	186.517	0.491714	307.865	0.521472	256.18
0.522692	184.27	0.534567	303.371	0.555215	247.191
0.559439	175.281	0.568268	289.888	0.588957	238.202
0.59006	168.539	0.608062	285.393	0.619632	233.708
0.626786	166.292	0.638682	278.652	0.656442	224.719
0.66352	161.798	0.663176	274.157	0.696319	220.225
0.691066	159.551	0.690729	269.663	0.723926	217.978
0.73392	155.056	0.736643	265.169	0.754601	208.989

0.75842	148.315	0.76727	256.18	0.785276	206.742
0.795154	143.82	0.797883	251.685	0.825153	204.494
0.82882	141.573	0.82237	249.438	0.858896	195.506
0.85942	141.573	0.859097	247.191	0.886503	195.506
0.899213	137.079	0.898904	238.202	0.923313	188.764
0.932873	137.079	0.93563	235.955	0.953988	186.517
0.960413	137.079	0.969304	231.461	0.993865	186.517
0.99716	128.09	0.993784	231.461	1.02147	182.022
1.03081	130.337	1.03969	229.213	1.05215	182.022
1.05837	123.596	1.07031	222.472	1.09509	175.281
1.09203	125.843	1.10397	222.472	1.12577	170.787
1.12876	121.348	1.14378	213.483	1.15951	168.539
1.1563	121.348	1.1958	213.483	1.19018	168.539
1.19609	116.854	1.22334	211.236	1.21779	168.539
1.21752	114.607	1.26314	206.742	1.26687	168.539
1.26036	114.607	1.29679	208.989	1.28834	166.292
1.28791	112.36	1.32129	202.247	1.32515	161.798
1.33075	112.36	1.36414	200	1.35583	159.551
1.36748	107.865	1.40088	193.258	1.38957	155.056
1.39502	107.865	1.42536	193.258	1.42331	157.303
1.4195	107.865	1.44984	191.011	1.46012	152.809
1.46235	105.618	1.48962	191.011	1.49387	150.562
1.49294	105.618	1.52636	186.517	1.52761	150.562
1.52967	103.371	1.55696	184.27	1.55215	148.315
1.54803	103.371	1.59368	184.27	1.58896	143.82
1.59088	101.124	1.62734	184.27	1.62577	146.067
1.6276	98.8764	1.66714	179.775	1.65951	143.82
1.65208	101.124	1.69162	177.528	1.69018	143.82
1.69187	96.6292	1.72528	177.528	1.72699	141.573
1.72246	98.8764	1.76508	173.034	1.75767	141.573
1.75614	94.382	1.78956	173.034	1.79141	139.326
1.78674	94.382	1.82628	173.034	1.82515	139.326
1.82345	96.6292	1.85994	170.787	1.85276	137.079
1.85712	92.1348	1.88748	170.787	1.89264	137.079
1.88772	94.382	1.93339	168.539	1.92638	134.831
1.92139	89.8876	1.96094	166.292	1.96319	132.584
1.95811	89.8876	1.9854	170.787	1.99387	130.337
1.98565	89.8876	2.02214	164.045	2.02454	130.337
2.02543	89.8876	2.06192	164.045	2.05828	128.09
2.05604	85.3933	2.09254	157.303	2.08589	128.09
2.0897	85.3933	2.12312	164.045	2.12577	128.09
2.12029	87.6404	2.15679	159.551	2.15951	123.596

2.15396	85.3933	2.18739	159.551	2.19018	125.843
2.19067	87.6404	2.22718	157.303	2.22086	121.348
2.22128	85.3933	2.25473	155.056	2.26074	121.348
2.258	85.3933	2.28838	157.303	2.29448	121.348
2.29166	85.3933	2.34347	155.056	2.32515	119.101
2.32226	85.3933	2.38019	155.056	2.34356	119.101
2.35593	83.1461	2.41691	152.809	2.38037	119.101
2.38041	80.8989	2.45363	152.809	2.41104	116.854
2.40795	83.1461	2.48731	150.562	2.45092	116.854
2.44773	80.8989	2.49037	146.067	2.4816	116.854
2.47833	80.8989	2.5179	146.067	2.5184	116.854
2.51811	80.8989	/	/	/	/

Table annex 2. 2: Experimental values of Database (DB III. 2)

t (s)	$\frac{J}{J_0}$	time (min)	1/Q (min/m^3)
0	1	0.074768	9130.02
9.75465	0.891152	0.295736	18268.9
20.9826	0.859674	0.515593	21324.1
27.4201	0.828178	0.808828	25904.7
38.6709	0.782373	1.24854	32015.1
49.9079	0.745164	1.6146	35079.2
57.9743	0.693617	1.83501	41176.3
69.2296	0.644947	2.12852	47277.8
77.2868	0.599131	2.56796	51867.3
88.5376	0.553326	2.93457	57973.2
98.1733	0.518976	3.15471	62549.3
109.41	0.481767	3.52132	68655.3
115.839	0.456002	3.81483	74756.8
128.659	0.427395	4.10807	79337.4
136.679	0.404501	4.4744	83922.4
147.894	0.381619	4.84129	91549.3
157.502	0.364461	5.20763	96134.3
167.11	0.347303	5.50086	1.01E+05
176.718	0.330146	5.86747	1.07E+05
186.327	0.312988	6.23409	1.13E+05
195.926	0.301561	6.45422	1.18E+05
205.529	0.287269	6.89366	1.22E+05
216.721	0.278713	7.18689	1.27E+05
224.718	0.270146	7.4804	1.33E+05
235.914	0.258725	7.84674	1.37E+05
243.907	0.253023	8.21335	1.43E+05

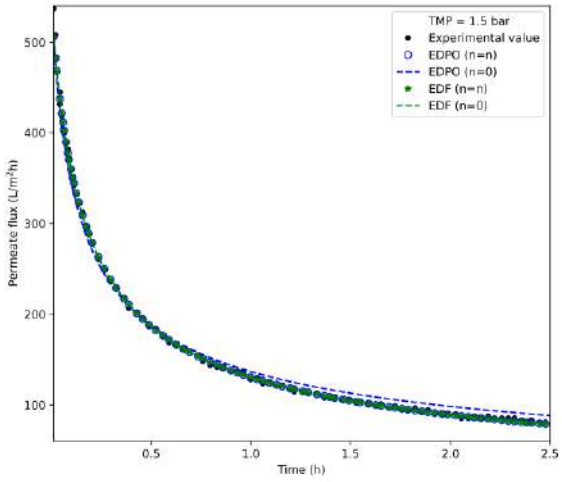
255.099	0.244467	8.57969	1.48E+05
266.29	0.235911	8.87264	1.51E+05
275.884	0.227349	9.23926	1.57E+05
285.479	0.218788	9.53249	1.62E+05
293.472	0.213086	9.82573	1.66E+05
303.062	0.207389	10.2657	1.74E+05
314.253	0.198833	10.559	1.79E+05
325.44	0.193143	10.8519	1.82E+05
333.429	0.190306	11.1454	1.88E+05
343.023	0.181744	11.4387	1.92E+05
351.012	0.178908	11.9515	1.98E+05
363.791	0.176088	12.2444	2.02E+05
370.187	0.17038	12.611	2.08E+05
378.176	0.167544	12.9777	2.14E+05
389.358	0.164718	13.1978	2.18E+05
403.743	0.156174	13.5641	2.23E+05
414.929	0.150483	13.9302	2.26E+05
424.515	0.147652	14.2237	2.32E+05
435.697	0.144827	14.5897	2.35E+05
443.685	0.14199	14.883	2.40E+05
453.266	0.142025	15.2493	2.44E+05
462.852	0.139194	15.5426	2.49E+05
469.243	0.136351	15.9089	2.53E+05
482.018	0.136397	16.2024	2.60E+05
493.204	0.130706	16.569	2.66E+05
504.382	0.130746	16.8622	2.70E+05
510.778	0.125039	17.2283	2.73E+05
523.553	0.125084	17.5946	2.78E+05
533.138	0.122253	17.8151	2.84E+05
542.723	0.119422	18.2545	2.89E+05
552.309	0.116591	18.6208	2.93E+05
563.486	0.116631	18.841	2.98E+05
571.475	0.113795	19.2804	3.02E+05
581.06	0.110964	19.7201	3.08E+05
590.641	0.110998		
601.823	0.108173		
613.001	0.108213		
624.183	0.105387		
633.764	0.105422		
643.349	0.102591		
652.93	0.102625		
662.515	0.099794		

673.693	0.099834
681.677	0.099863
692.859	0.097038
700.843	0.097066
712.021	0.097106
721.606	0.094275
729.595	0.091438
740.772	0.091478
750.353	0.091513
761.535	0.088687
769.519	0.088716
782.298	0.085897
796.669	0.085948

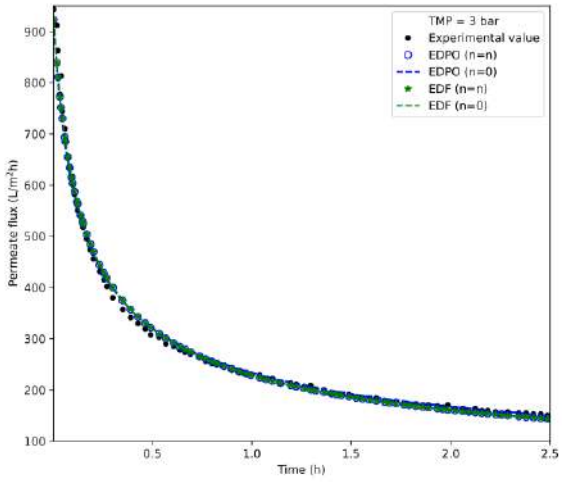
Table annex 2. 3: Evaluation of sub-model performance for different clogging mechanisms EDPO model for (n=0,1, and 1,5) and EDF model for (n=0, 1, and 1.5)

Solution	Pressure (Pa)	Model	n	J_0	k	a	RMSE	R^2
Oily wastewater	1.5×10^5	(EDPO, $n = 0$)	0	537.0790	2.50E-05	1.0000	9.8882	0.9934
		(EDF, $n = 0$)	0	537.0790	1.15E-04	1.4397	4.7433	0.9984
	3.0×10^5	(EDPO, $n = 0$)	0	943.8200	8.61E-06	1.0000	15.1315	0.9945
		EDF, $n = 0$)	0	943.8200	1.77E-05	1.1479	13.7102	0.9955
	4.5×10^5	(EDPO, $n = 0$)	0	838.2020	1.29E-05	1.0000	12.6322	0.9950
		(EDF, $n = 0$)	0	838.2020	3.69E-05	1.2400	9.1982	0.9973
Microbial suspensions from a sequencing batch reactor (SBR) (Supernatant solution)	2.76×10^4	(EDPO, $n = 1$)	1	2.8967	0.0045	1.0000	0.0174	0.9937
		(EDF, $n = 1$)	1	2.8967	0.0042	1.0064	0.0296	0.9819
pQR150 (kanamycin resistance, 20 kb)	3.447×10^4	(EDPO, $n = 1.5$)	1.5	0.8383	0.3688	1.0000	0.0903	0.9963
		(EDF, $n = 1.5$)	1.5	1.1017	0.1833	3.5182	0.0518	0.9988
	5.516×10^4	(EDPO, $n = 1.5$)	1.5	2.1366	0.5931	1.0000	0.0893	0.9960
		(EDF, $n = 1.5$)	1.5	2.3685	0.6167	1.2324	0.0809	0.9967
pGEc47 (tetracycline resistance, 56 kb)	3.447×10^4	(EDPO, $n = 1.5$)	1.5	1.9683	0.3829	1.0000	0.0728	0.9989
		(EDF, $n = 1.5$)	1.5	2.1171	0.3945	1.2080	0.0613	0.9992
	5.516×10^4	(EDPO, $n = 1.5$)	1.5	2.8843	0.5257	1.0000	0.1630	0.9920
		(EDF, $n = 1.5$)	1.5	3.9480	0.3894	1.9872	0.0807	0.9980

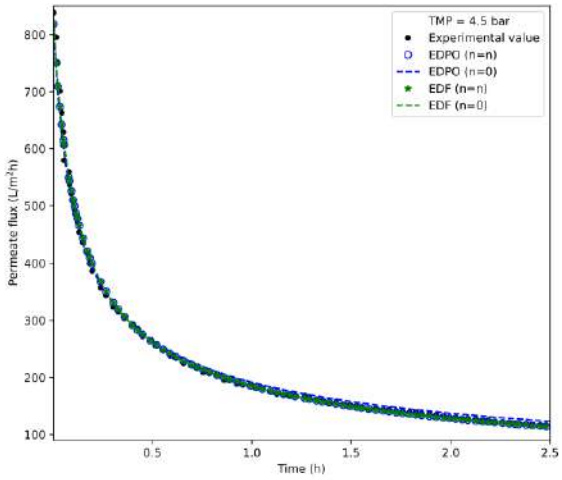
Figure annex 2. 1: shows the plot comparison between experimental values and the value obtained from ordinary partial differential equations and fractionally differential equations models (EDPO and EDF), including their sub-model for the same indicated mechanisms, as a function of time. Each proposed model was applied across all pressure conditions.


TMP = 1.5 bar
Experimental value
EDPO (n=n)
EDPO (n=0)
EDF (n=n)
EDF (n=0)
Permeate flux (L/m²h)
Time (h)

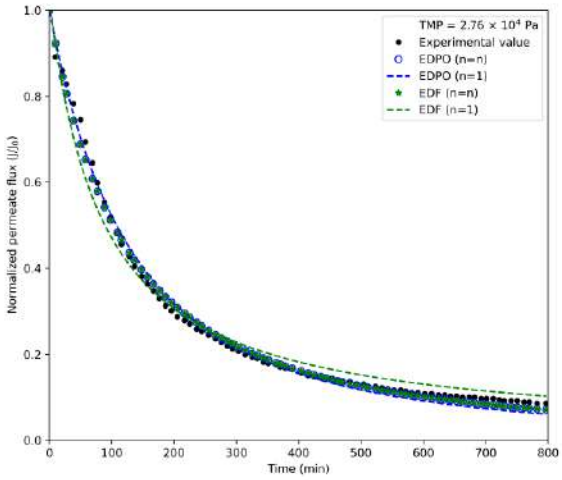
(a)


TMP = 3 bar
Experimental value
EDPO (n=n)
EDPO (n=0)
EDF (n=n)
EDF (n=0)
Permeate flux (L/m²h)
Time (h)

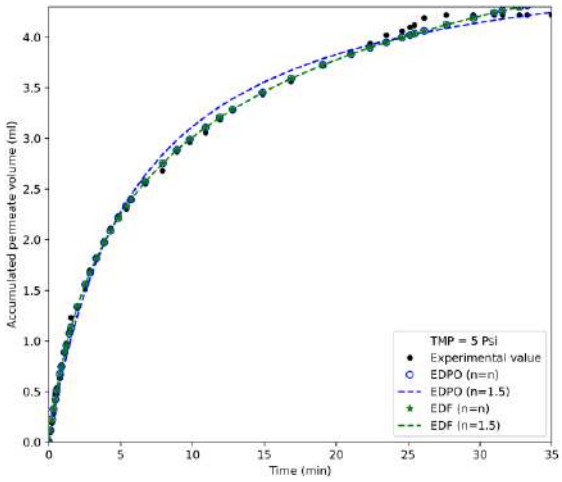
(b)


TMP = 4.5 bar
Experimental value
EDPO (n=n)
EDPO (n=0)
EDF (n=n)
EDF (n=0)
Permeate flux (L/m²h)
Time (h)

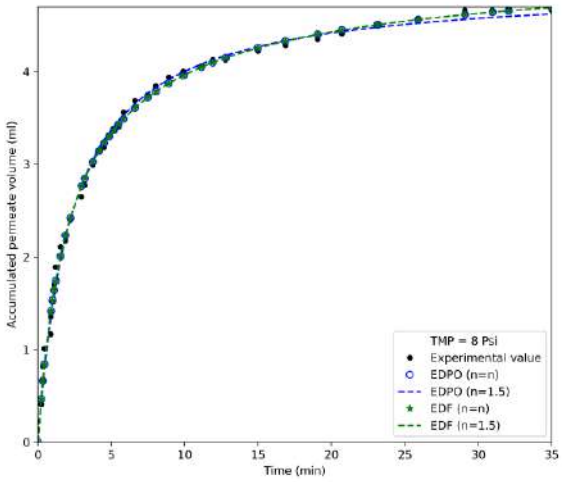
(c)


TMP = 2.76 × 10⁴ Pa
Experimental value
EDPO (n=n)
EDPO (n=1)
EDF (n=n)
EDF (n=1)
Normalized permeate flux (J/J₀)
Time (min)

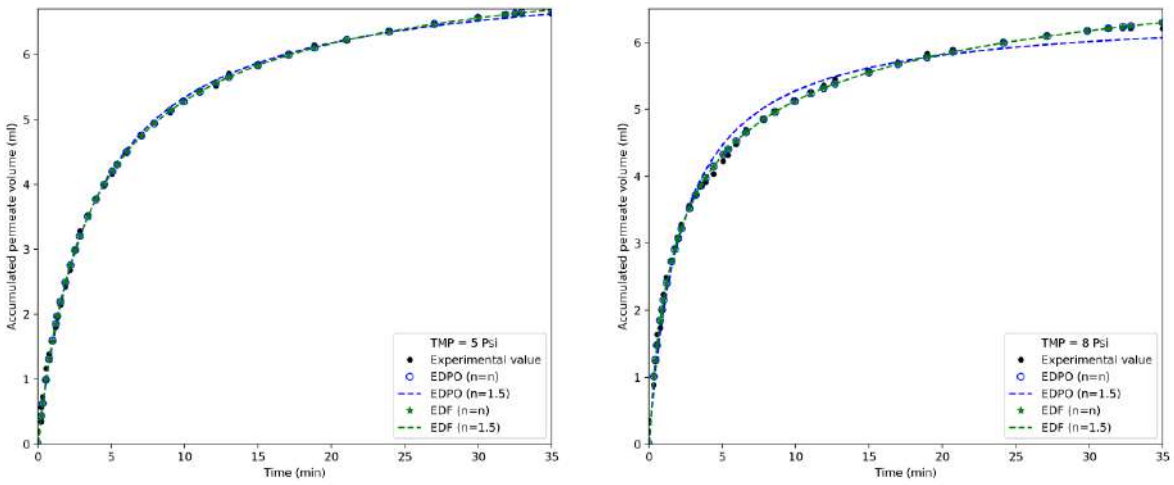
(d)


TMP = 5 Psi
Experimental value
EDPO (n=n)
EDPO (n=1.5)
EDF (n=n)
EDF (n=1.5)
Accumulated permeate volume (ml)
Time (min)

(e)


TMP = 8 Psi
Experimental value
EDPO (n=n)
EDPO (n=1.5)
EDF (n=n)
EDF (n=1.5)
Accumulated permeate volume (ml)
Time (min)

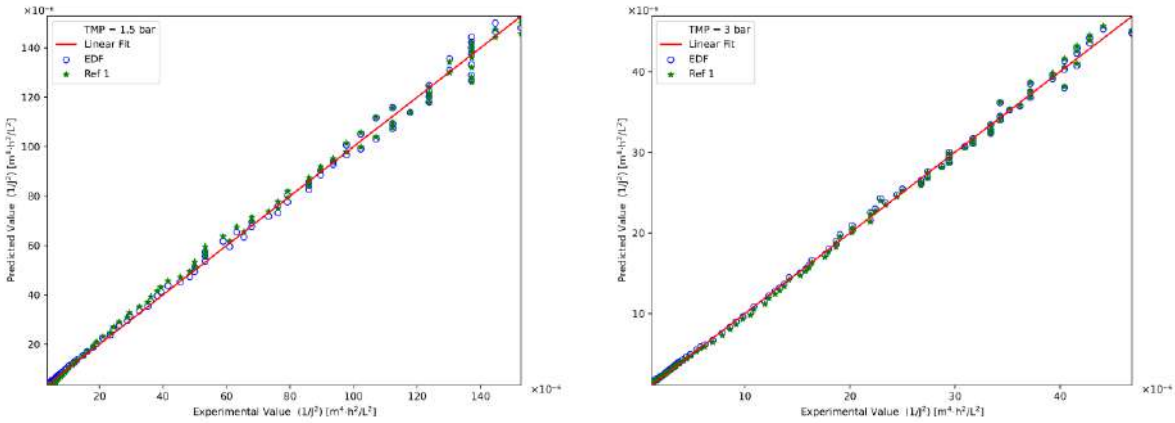
(f)



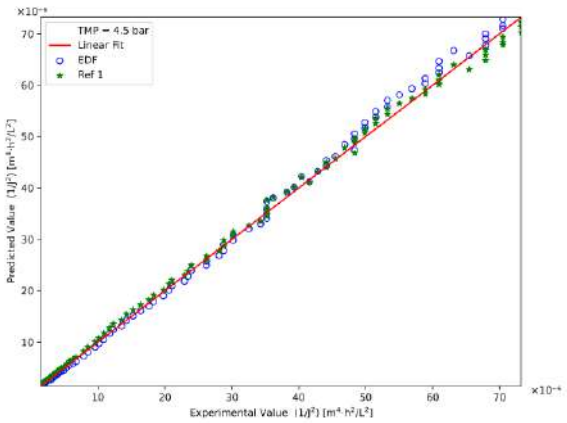
(g) (h)

Figure annex 2. 1: The plot comparison between experimental values and the value obtained from ordinary partial differential equations and fractionally differential equations models (EDPO and EDF), including their sub model for the same indicated mechanisms, as a function of time for DB III. 1: (a-c) for solution of oily wastewater; (d) for DB III. 2: solution of Microbial suspensions from a sequencing batch reactor (SBR) (Supernatant solution); and (e and f) for DB II. 2, for the solution of pQR150 (kanamycin resistance, 20 kb); and (g and h) for the solution of pGEc47(tetracycline resistance, 56 kb

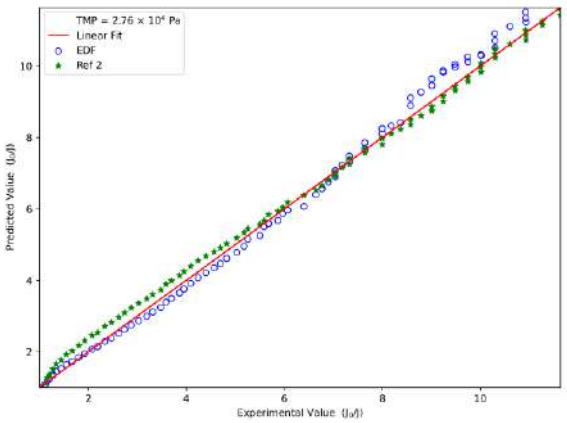
Figure S2 presents the linear regression of the result comparison between the EDF general model and Hermia's reference model from the literature for the same clogging mechanisms.



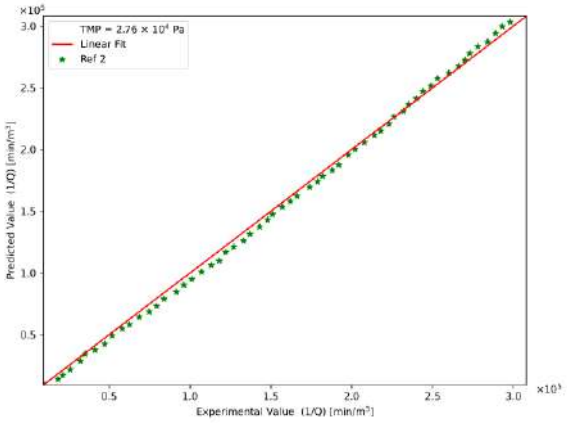
(a) (b)


TMP = 4.5 bar
Linear Fit
EDF
Ref 1
Predicted Value (1/J²) [m⁴·h²/L²]
Experimental Value (1/J²) [m⁴·h²/L²]

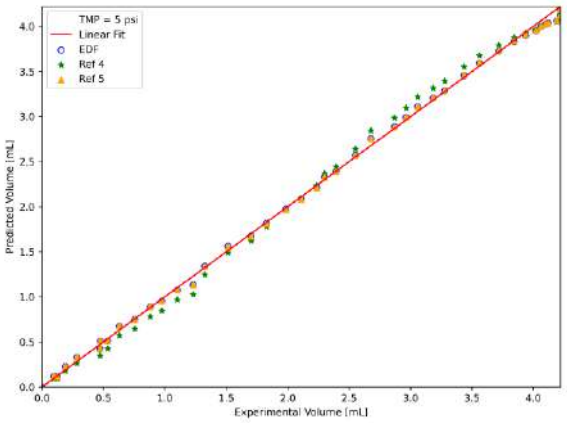
(c)


TMP = 2.76 × 10⁴ Pa
Linear Fit
EDF
Ref 2
Predicted Value (1/J)
Experimental Value (1/J)

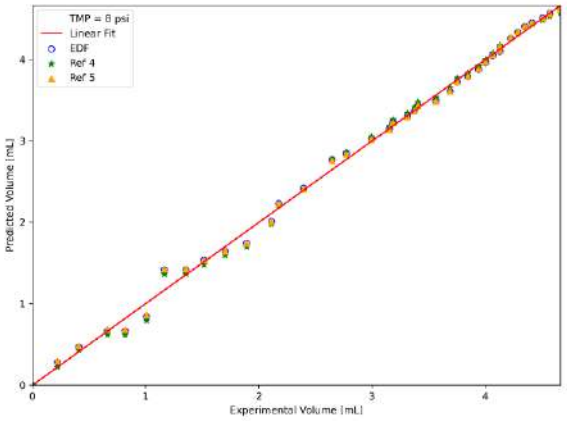
(d)


TMP = 2.76 × 10⁴ Pa
Linear Fit
Ref 2
Predicted Value (1/Q) [min/m³]
Experimental Value (1/Q) [min/m³]

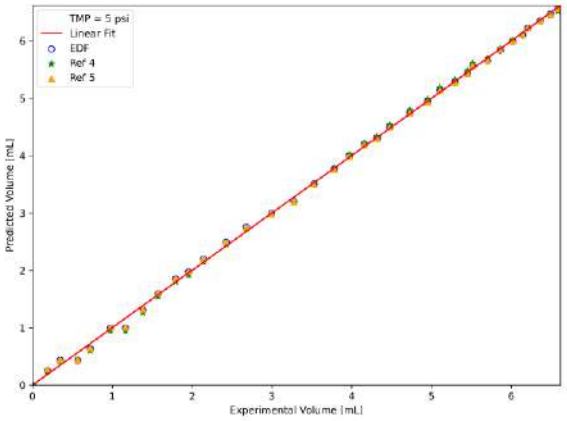
(e)


TMP = 5 psi
Linear Fit
EDF
Ref 4
Ref 5
Predicted Volume [mL]
Experimental Volume [mL]

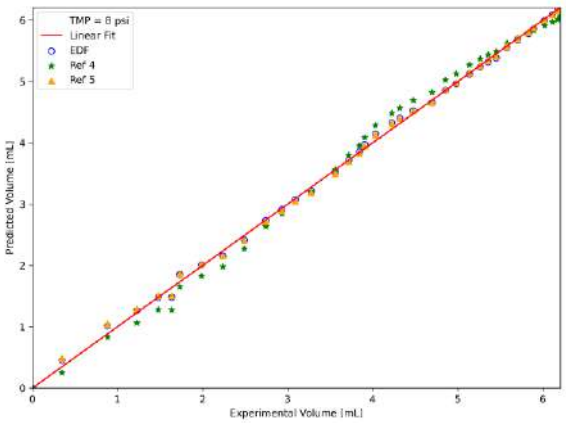
(f)


TMP = 8 psi
Linear Fit
EDF
Ref 4
Ref 5
Predicted Volume [mL]
Experimental Volume [mL]

(g)


TMP = 5 psi
Linear Fit
EDF
Ref 4
Ref 5
Predicted Volume [mL]
Experimental Volume [mL]

(h)



(I)

Figure annex 2. 2: Plot comparison of the linear regression between the EDF general model and Hermia's reference model from the literature for the same indicated clogging mechanisms. Results are shown for: DB III. 1: (A) at P = 1.5 bar, (B) at P = 3 bar, and (C) at P = 5 bar; DB III. 2: at P = 2.76 × 10⁴ Pa, as a function of permeate flux in (D), and as a function of rate in (E); DB III. 2, for the solution of pQR150 (kanamycin resistance, 20 kb): (F) at P = 5 psi and (G) at P = 8 psi; and for the solution of pGEc47 (tetracycline resistance, 56 kb): (H) at P = 5 psi and (I) at P = 8 psi.

Scientific production

Scientific production

Review papers:

Cherifi, L., Ammi, Y., Hanini, S., et al. (2025). A novel empirical fractional approach for modeling the clogging of membrane filtration during protein microfiltration. Membranes, 15(4), 99. https://doi.org/10.3390/membranes15040099

Belkacem, O., Rezrazi, A., Aizi, K., et al. (2025). Prediction of barite scale formation and inhibition in hydrocarbon reservoirs using AI modeling: Focus on different optimization algorithms. Results in Engineering, 105222. https://doi.org/10.1016/j.rineng.2025.105222

Cherifi, L., Ammi, Y., Hanini, S., et al. (2026). A generalized fractional model for one-step identification of membrane filtration clogging mechanisms. Scientific Reports. https://doi.org/10.1038/s41598-025-33755-4

International and national communications:

1. Cherifi, L., Ammi, Y., Hanini, S. *An Empirical Model Evaluation for Predicting Membrane filtration Clogging:* 3rd International Conference on Contemporary Academic Research ICCAR 2024, November 10 – 11 in 2024 at Konya/Turke
2. Cherifi, L., Ammi, Y., Hanini, S. Development the model of clogging of ultrafiltration membranes by neural networks: 1st international conference on physico-chemistry, materials sciences and applied mathematics (ICPMSAM'23), November 27-28, 2023 at *the 20 August 1955 University of Skikda, Algeria.*
3. Cherifi, L., Ammi, Y., Hanini, S. "Modeling the clogging of ultrafiltration membranes by neural networks ". Computational and Applied Physics Symposium 2023" (CAPS2023), May 10th 2023, at the University of Khemis Miliana (Algeria),
4. Cherifi, L., Ammi, Y., Hanini, S. 'Prediction of the clogging of ultrafiltration membranes by neural networks". 3rd National Conference on Applied Physics & Chemistry (3rdNCAPC23), March 12th &13th, 2023 in Laghouat (Algeria),